UNIVERSIDAD DE CHILE
FACULTAD DE CIENCIAS FÍSICAS Y MATEMÁTICAS
DEPARTAMENTO DE INGENIERIA DE MINAS

JOINT SIMULATION OF GRADES AND ROCK TYPES USING NON-STATIONARY GEOSTATISTICAL MODELS

TESIS PARA OPTAR AL GRADO DE DOCTOR EN INGENIERÍA DE MINAS

MOHAMMADALI MALEKITEHRANI

PROFESOR GUÍA:
XAVIER EMERY

MIEMBROS DE LA COMISIÓN
MARGARET ARMSTRONG
JOSÉ SAAVEDRA ROSAS

SANTIAGO DE CHILE
2016

Resumen

La simulación geoestadística se usa ampliamente en ingeniería de minas para cuantificar la incertidumbre geológica, al producir múltiples realizaciones alternativas de la distribución de los recursos in situ y/o reservas mineras en el subsuelo. Sin embargo, el modelamiento geoestadístico de propiedades de diferentes naturalezas, como las leyes de metales medidas en escalas cuantitativas continuas y los tipos de roca medidos en una escala categórica o nominal, sigue siendo un proceso engorroso y complejo. Tradicionalmente, se recurre a un enfoque jerárquico, donde se modela primero la extensión espacial de los tipos de roca, luego las leyes de metales dentro de cada tipo de roca por separado. Este enfoque tiende a producir discontinuidades en la distribución de las leyes al cruzar la frontera entre tipos de roca, lo que podría no ser deseable. Una alternativa para evitar tales discontinuidades es simular conjuntamente las leyes y los tipos de roca, enfoque que ha sido propuesto en años recientes, principalmente en un marco estacionario donde se supone que las distribuciones de leyes y de tipos de roca son invariantes al desplazarse en el espacio.

El modelamiento conjunto de leyes de metal y tipos de roca se torna más difícil cuando se busca reproducir tendencias espaciales y zonaciones en los tipos de roca, una característica que se encuentra comúnmente en la práctica y pone en duda el supuesto de estacionaridad para los tipos de roca. En este contexto, la tesis tiene como objetivo desarrollar propuestas metodológicas y prácticas para simular conjuntamente una ley de metal y un tipo de roca, al representar la primera por un campo aleatorio Gaussiano estacionario y el segundo por un campo aleatorio intrínseco de orden k con incrementos generalizados Gaussianos.

Las propuestas conciernen la inferencia de los parámetros del modelo y la construcción de realizaciones condicionadas a datos existentes. Por un lado, la principal dificultad en la inferencia radica en la identificación de la estructura de correlación espacial (covarianzas generalizadas directas y cruzada), para lo cual se diseña un algoritmo semi-automático basado en un ajuste de mínimos cuadrados de las covarianzas de indicadores de roca y covarianzas cruzadas de leyes e indicadores. Se define además varios modelos bivariables de covarianza para facilitar la elección de estructuras básicas en el modelamiento de las covarianzas generalizadas. Por otro lado, la simulación conjunta se basa en un algoritmo espectral para construir realizaciones no condicionales, y en un algoritmo iterativo y una variante de cokriging para condicionar las realizaciones a datos de leyes y tipos de roca.

Los modelos y algoritmos propuestos son aplicados a dos yacimientos cupríferos (Lince-Estefanía y Río Blanco-Los Bronces) para simular conjuntamente las leyes de cobre y la extensión de tipos de roca. Los resultados obtenidos muestran la capacidad de los modelos de reproducir las transiciones graduales de leyes al cambiar de tipo de roca, así como la zonación espacial de los tipos de roca en la región de estudio.

Abstract

Geostatistical simulation is widely used in mining engineering to quantify geological uncertainty, by producing multiple alternative outcomes of the mineral resources and/or ore reserves distribution in the subsurface. However, the geostatistical modeling of properties of different natures, such as metal grades measured on continuous quantitative scales and rock types measured on a categorical or nominal scale, is still a cumbersome and complex process. Traditionally, a hierarchical approach is adopted, where the layout of the rock type domains is modeled first, then the metal grades are modeled within each domain separately, but this approach tends to produce discontinuities in the grade distribution when crossing the boundary between rock type domains, which may not be desirable. An alternative to avoid such discontinuities is to jointly simulate the grade and the rock type, which has been proposed in the past years, mostly in a stationary setting where the distributions of grade and rock type are assumed to be invariant under a translation in space.

The joint modeling of a metal grade and a rock type is made much more difficult when one accounts for the spatial trends and zonations of the rock type domains, a feature that is commonly encountered in practice and makes the stationarity assumption questionable for the rock type. In this context, this thesis aims to make methodological and practical proposals for jointly simulating a metal grade and a rock type, when the former is represented by a stationary random field (transform of a Gaussian random field) and the latter is obtained by truncating an intrinsic random field of order k (shortly, IRF-k) with Gaussian generalized increments.

The proposals concern both the inference of the model parameters and the construction of realizations conditioned to existing data. On the one hand, the main difficulty for inference lies in the identification of the spatial correlation structure (generalized direct and cross covariances), for which a semi-automated algorithm is designed, based on a least squares fitting of the data-to-data indicator covariances and grade-indicator cross-covariances. A few bivariate covariance models are also presented to ease the choice of basic structures for the modeling of generalized covariances. On the other hand, the joint simulation relies on a spectral-turning bands algorithm for constructing non-conditional realizations, and on an iterative algorithm (Gibbs sampler) and a variant of cokriging (mixed simple/intrinsic) for conditioning the realizations to known data on the grade and rock type.

The proposed models and algorithms are applied to two copper deposits (Lince-Estefanía and Río Blanco-Los Bronces) to jointly simulate the copper grade and the rock type layout. The results show the ability of the proposed models to reproduce the gradual transitions of the grade when crossing a rock type boundary, as well as to reproduce the spatial zonation of the rock types in the region under study.

Acknowledgments

First, I would like to express my sincere gratitude to my advisor Professor Xavier Emery for the continuous support in my Ph.D. research, for his patience, motivation, and immense knowledge. His guidance helped me in all the time of research and writing of this thesis. I am also grateful to the commission members, Margaret Armstrong and José Saavedra, for their comments and advices to improve this thesis.

A special thanks to my family. Words cannot express how grateful I am to my mother and father for all the sacrifices they made on my behalf.

My sincere thanks also go to the Mining Engineering Department at University of Chile, which provided me an opportunity to join its Ph.D. program and gave me access to its laboratories and research facilities by its academic professionalism, and to Minera Michilla and Codelco-Chile for providing the data that have been used in the case studies presented in this thesis.

I finally would like to acknowledge the multiple funding sources that made my Ph.D. work possible. I was funded by the Advanced Mining Technology Center (AMTC) at University of Chile for the duration of my studies, and was honored to be an in-kind researcher of the CSIRO-Chile International Center of Excellence in Mining and Mineral Processing. My work was also partly supported by the Mining Engineering Department at University of Chile and by the Chilean Commission for Scientific and Technological Research, through Projects CONICYT/ FONDECYT / REGULAR / N°1130085 and CONICYT PIA Anillo ACT1407. I furthermore thank the International Association for Mathematical Geosciences (IAMG) for the Mathematical Geosciences Student Award that I was granted in the first year of my studies, as well as Codelco-Chile and the Center for Mathematical Modeling (CMM) at the University of Chile, organizers of the PiensaCobre competition of innovative theses in mining, for the student award I was granted in the last year of my studies.

Contents

Chapter 1: Introduction

1. Problem setting

In mineral resources evaluation, one often deals with two different kinds of variables. On the one hand, nominal or categorical variables such as rock types, lithofacies, alteration and mineralization domains. On the other hand, continuous quantitative variables (i.e., variables measured on continuous quantitative scales) such as metal grades, pollutant concentrations, rock density or rock porosity. Because all these variables are often inter-dependent, the evaluation of mineral resources aims to model the spatial distribution of continuous variables (say, metal grades), conditionally to the data on these variables and on a categorical variable (say, a rock type). However, because of their different natures, their joint modeling turns out to be quite complex. A hierarchical or cascade approach is the most common method in order to quantify the spatial uncertainty in these variables, which consists of two steps (Alabert and Massonnat, 1990; Roldão et al., 2012; Boucher and Dimitrakopoulos, 2012; Jones et al., 2013):

- First, the spatial layout of each rock type is delimited in the region under study. To this end, one can consider a deterministic model based on the available data and geological knowledge of the deposit, or a stochastic model based on simulating the occurrence of each rock type in the study region.

- Second, the grades are simulated in each rock type separately by using only the data that belong to this rock type.

This cascade approach is applicable when one has "hard" boundaries between the different rock types, i.e., when there is an abrupt transition or a discontinuity in the grade distribution when crossing the boundary between two rock types (Kim et al., 2005). Indeed, it ignores and neglects the spatial correlation of the continuous variable across the boundary (Wilde and Deutsch, 2012; Rossi and Deutsch, 2014). Therefore, in case of "soft" boundaries (i.e., a gradual change in the grade distribution when crossing the rock type boundaries), the cascade approach could be inappropriate. In addition, in deterministic modeling, one has a single interpretation of the layout of rock type domains, which precludes quantifying the uncertainty in the obtained rock type model.

To overcome the limitations of the aforementioned approach and to consider the spatial correlation of the continuous variables when crossing the rock type boundaries, a natural approach is to simulate the continuous and categorical variables simultaneously. So far, few

works have been done in this direction, mainly because of the difficulty in handling variables of different natures at the same time. As an exception, one can mention the works by Bahar and Kelkar (2000), Freulon et al. (1990), Dowd (1994, 1997), Emery and Silva (2009), Cáceres and Emery (2010) and Maleki and Emery (2015), which combine the multigaussian and truncated Gaussian or plurigaussian models to represent the continuous and categorical variables, respectively. However, one should notice that these works are based on a stationarity hypothesis. In other words, it is assumed that the probability of presence of each geological domain representing a category is constant throughout the region under study. But this assumption is often unrealistic because geological domains generally exhibit spatial trends, so their probability of occurrence is not constant in space. For instance, in porphyry copper deposits, one usually distinguishes two main mineral zones (hypogene and supergene) whose proportions vary along the vertical direction and control the variations in the copper grades. Likewise, one often observes variation of different alteration domains along the vertical direction. As an example, Figure 1.1 shows the so-called vertical proportion curves for four alteration domains in Sungun porphyry copper deposit, northwestern Iran. As can be seen, the proportion of each alteration domain varies along the vertical direction and even might vanish. In these situations, it is not logic and rational to use simulation models based on assumptions of stationarity and one should consider non-stationary simulation models.

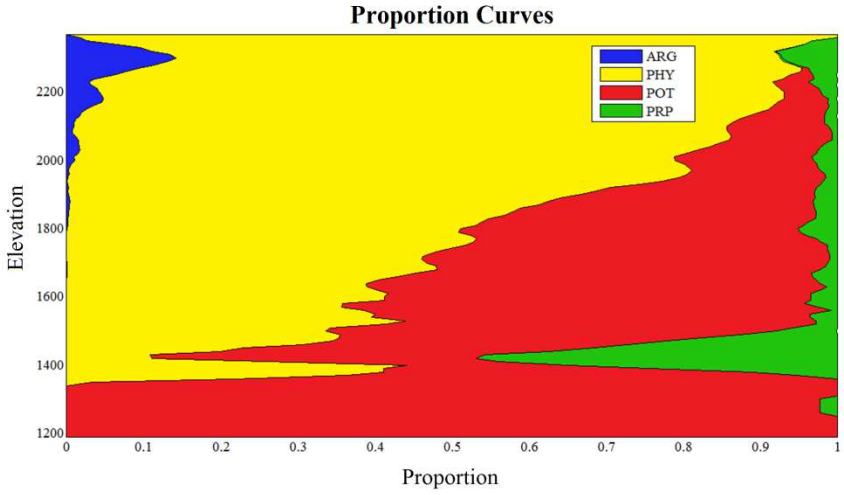

Figure 1.1: Vertical proportion curves for four alteration domains (argillic, phyllic, potassic and propylitic) in Sungun copper deposit, showing the variation of the domain proportions with the elevation. Modified from Talebi et al. (2013)

Consequently, in the process of joint simulation of grades and geological domains, if the domains are non-stationary, one cannot use the aforementioned stationary joint simulation methods.

2. Key idea of the thesis and objectives

To overcome this problem, one has to go one step further, assuming that the continuous variable may be represented by a stationary random field, but the categorical variable is represented by a non-stationary random field. So far, some approaches have been designed for dealing with non-stationary geological domains in plurigaussian simulation (Beucher et al., 1993; Ravenne et al., 2002). For instance, the first solution that comes to mind is to consider spatially varying parameters, such as local truncation thresholds (Armstrong et al., 2011). Although, this approach would be an interesting option, it does not offer a complete solution and suffers from some drawbacks. In particular, it does not allow managing the uncertainty on the true parameters (the local truncation thresholds), as one considers the domain proportions as if they were perfectly known, which is unrealistic (Biver et al., 2002); therefore an important source of uncertainty may be omitted.

The solution that will be discussed in this thesis is to look for a bivariate model, in which one random field is stationary (metal grade), while the other one is not stationary (rock type with a vertical or lateral trend) and can be represented by the truncation of an intrinsic random field of order k (IRF-k) with Gaussian generalized increments (Matheron, 1973; Chilès and Delfiner, 2012). Some bivariate models of this kind have already been designed for characterizing the joint spatial correlation structure of variables linked through partial differential equations, such as hydrogeological parameters (Kitanidis, 1999; Le Cointe, 2006). This work aims at extending these models to a more general framework.

The general objective of this work is to design geostatistical tools, models and algorithms for jointly simulating continuous (such as metal grades) and categorical (such as rock types) variables, represented by stationary and non-stationary random fields, respectively. The specific objectives include proposing guidelines and algorithms for the inference of the model parameter, especially for structural analysis, proposing guidelines and algorithms for the conditional joint simulation of grades and rock types, and applying the models and algorithms to case studies in ore body evaluation.

3. Novel aspects

The idea of simulating a non-stationary categorical random field (rock type) by truncating an intrinsic random field of order k with Gaussian generalized increments has been recently proposed by Madaniesfahani (2016). However, the latter work only considers the modeling of a categorical random field. The present work is concerned with a bivariate modeling of a non-stationary categorical random field (rock type) and a stationary continuous random field (metal grade), which implies extending the tools, models and algorithms to a bivariate

mixed (stationary/non-stationary) case. In particular, the following contributions that will be explained in Chapter 4 are novel:

- development of a methodology for inferring generalized direct and cross covariances from grade and rock type data;

- definition of coregionalization models that are mathematically valid;

- development of a spectral – turning bands algorithm for non-conditional simulation and of a mixed simple/intrinsic cokriging for conditioning to grade and rock type data.

Also, concerning the identification of the spatial correlation structure (generalized direct covariance) associated with the rock type, without considering the grade as a covariate, we will also modify the fitting procedure designed by Madaniesfahani (2016) in order to give more generality (see Chapter 4, Section 1.2).

4. Hypotheses

The proposed research relies on the following hypotheses:

- In ore deposits, regionalized variables such as metal grades or rock type indicators present an irregular behavior at a local scale, but a structured behavior at a more global scale. A description in terms of random fields is therefore suitable to characterize the spatial distribution of these variables.

- Variables representing geological domains, such as rock types, mineral or alteration domains, usually present regional trends and changes in their spatial continuity, so that a representation in term of stationary random fields is questionable. In other words, the probability of finding a particular domain is not constant in space and depends on the geological setting.

- Regionalized variables are known only partially, at a set of samples for which direct observations (chemical assays or geological loggings) have been made. The data associated with the observations are supposed to be representative of the actual values of the variables, i.e., sampling errors are neglected.

- Conditional simulation techniques allow constructing outcomes (called realizations) that reproduce the variability of the continuous and categorical regionalized variables at all spatial scales, and assessing the uncertainty in the domains and grades that may be found at unsampled locations.

Chapter 2: Literature review

In this chapter, some leading approaches that have received wide acceptance and are used for simulating continuous variables (such as grades) and categorical variables (such as geological domains) are reviewed. Then, the principal concept of the joint simulation of continuous and categorical variables is explained.

1. Multigaussian simulation of continuous variables (grades)

The multigaussian model is the most widely used for simulating continuous regionalized variables (Journel and Huijbregts, 1978; Verly, 1983; Rossi and Deutsch, 2014). As the name indicates, the principal assumption is that the parent random field associated with the variable under study has a multigaussian (multinormal) distribution. Since most variables are not normally distributed, a transformation – called anamorphosis – is needed to convert the original variable into a Gaussian one:

$$Z(x) = \phi[Y(x)],$$

where x indicates the spatial position, $Z(x)$ is the original variable (metal grade), ϕ is the transformation function (anamorphosis) and $Y(x)$ is the transformed (Gaussian) variable, with mean 0 and variance 1. Graphically, one associates each raw value with the Gaussian value having the same cumulative frequency (Figure 2.1) (Rivoirard, 1994).

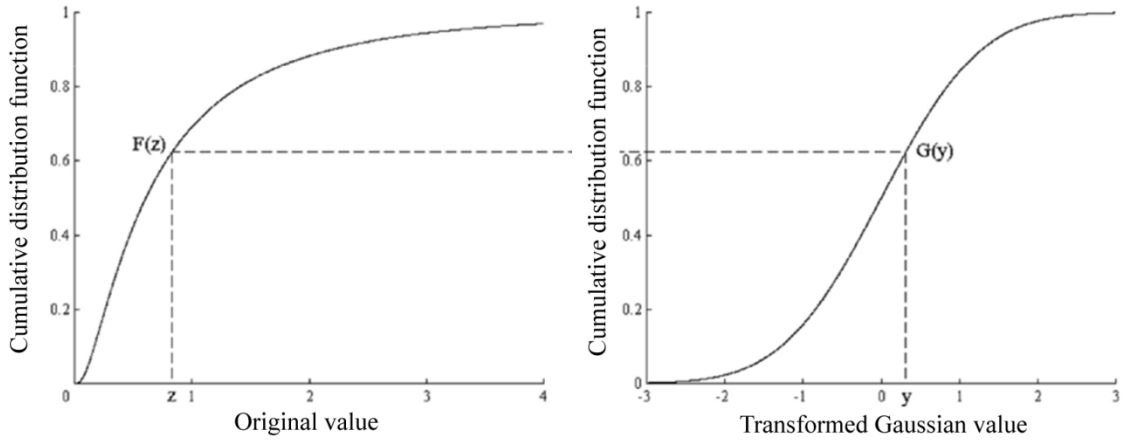

Figure 2.1: Anamorphosis of an original variable with cumulative distribution function F into a standard Gaussian variable with cumulative distribution function G

A variety of algorithms have been proposed to simulate a stationary multigaussian random field (or, for short, a Gaussian random field), which can broadly be classified into two families. The first family consists of algorithms that simulate random fields whose finite-dimensional distributions are exactly multivariate Gaussian. The most common simulation algorithms of this family are the covariance matrix decomposition method (Davis, 1987), sequential method (Ripley, 1987; Deutsch and Journel, 1998), convolution methods such as the auto-regressive and moving average (Box and Jenkins, 1976; Boulanger, 1990; Mignolet and Spanos, 1992; Spanos and Mignolet, 1992; Guyon, 1995; Chilès and Delfiner, 2012) and spectral approaches based on discrete and fast Fourier transforms (Pardo-Igúzquiza and Chica-Olmo, 1993; Dietrich, 1993; Chilès and Delfiner, 1997, 2012). The second family comprises algorithms that produce realizations of random fields whose spatial distribution is close to multigaussian. In practice, they are often the only alternative when dealing with large conditioning datasets or with simulation domains that contain several millions of target locations. Approximations take place because of algorithmic simplifications (e.g. moving neighborhood restrictions) or because the algorithm relies on the central limit theorem. In general, this is a minor concern for practical applications, but it may be a crucial issue in studies that aim to assess statistical procedures. To date, the most widespread approximate algorithms are continuous spectral (Shinozuka, 1972) and turning bands (Emery, 2006, 2008b; Lantuéjoul, 2002; Matheron, 1973) methods. In the following sections, the main simulation algorithms are described in more detail.

1.1. Matrix decomposition method

As mentioned before, this is an exact algorithm for simulating Gaussian random fields at a finite set of target locations. It can be applied to any spatial configuration of these target locations $\{x_1,\ldots, x_n\}$ and can also be adapted to produce realizations conditioned to a set of data (Davis, 1987).

Consider a Gaussian random field with mean 0 and covariance function *C*. The variance-covariance matrix of the variables at the target locations $x_1,\ldots, x_n$ is

$$\sum = [C(x_i - x_j)]_{i,j = 1\ldots n}$$

This is a real-valued, symmetric, positive semi-definite matrix. Provided that it is strictly positive definite, one can use the Cholesky decomposition of such a variance – covariance matrix:

$$\sum = AA^T$$

where A is a triangular matrix called the Cholesky factor of $\sum$.

Define a simulated vector as

$$Y = AX$$

where:

$X = [X_i]_{i = 1...n}$ is a vector of independent standard Gaussian random variables N(0,1)

$Y = [Y(x_i)]_{i = 1...n}$ is the simulated random field at the target locations $x_1,\ldots, x_n$.

This algorithm is straightforward and, once the matrix decomposition is obtained, one can generate many realizations very quickly. However, the Cholesky decomposition is difficult to obtain when the number *n* of target locations is large. In fact, the CPU time becomes prohibitive when more than a few thousands locations are considered (Deutsch and Journel, 1998; Chilès and Delfiner, 2012).

1.2. Sequential algorithm

Sequential simulation is one of the most widespread algorithms for simulating Gaussian random fields (Chilès and Delfiner, 2012; Deutsch and Journel 1998; Gómez-Hernández and Cassiraga, 1994; Ripley, 1987). Assume that the Gaussian random field has to be simulated at target locations $\{x_1,\ldots, x_n\}$. The sequential simulation algorithm comprises the following steps:

1- Simulate a standard Gaussian random variable (with mean 0 and variance 1) U_1 and put $Y(x_1) = U_1$

2- For $i \in \{2,\ldots n\}$, put

$$Y(x_i) = Y^{sk}(x_i) + \sigma_{sk}(x_i)U_i$$

where $Y^{sk}(x_i)$ is the simple kriging predictor of $Y(x_i)$ from the previously simulated variables $[Y(x_1), \ldots Y(x_{i-1})]$, $\sigma_{sk}(x_i)$ is the standard deviation of the simple kriging error, and U_i is a standard Gaussian random variable, independent of $[U_1, \ldots U_{i-1}]$.

At each step, one simulates the random field at one location and incorporates the simulated value to the set of conditioning data for simulating the random field at the next locations.

One of the main advantages of this algorithm is the direct conditioning of the simulations to a set of data, as it only requires considering these data as if they were previously simulated values and including them in all the kriging systems. Among the drawbacks of this algorithm, one can mention to the possibility to be confronted with numerical problems when the covariance function or the variogram is very regular near the origin and the target locations are very close (Lantuéjoul, 1994). Also, this method is slow in the sense that the kriging system becomes bigger and bigger when the simulation progresses (it involves not only the initial data but also all the previously simulated data). In practice, to overcome this drawback, one uses a moving neighborhood in order to restrict the conditioning variables (original data and previously simulated variables) to the ones located close to the target location (Deutsch and Journel, 1998), which makes the algorithm approximate (Emery and Peláez, 2011).

1.3. Turning bands

This method was originally formulated by Matheron (1973). Its advantage lies in the computational efficiency derived from the reduction in the dimension of space where the simulation is actually performed. In other words, the turning bands method is designed to reduce a multidimensional simulation into unidimensional ones. In a nutshell, one performs simulation along several lines; then at each point of the multidimensional space, a weighted sum of the corresponding values of the line processes is assigned. So, one first needs to define the direction of the lines and to determine the one dimensional fields to be simulated (Chilès and Delfiner, 2012; Emery and Lantuéjoul, 2006; Lantuéjoul, 2002). The whole process of generating a realization of a random field through the turning bands algorithm can be divided into three main steps.

1.3.1. Generating lines

The concept of turning bands simulation relies on generating one dimensional realizations along different lines turning around a center point and scanning the entire space. So, in the first step, one should define the directions of these lines. For isotropic random fields, one can choose random (uniformly distributed) directions, or directions distributed as regularly as possible rather than randomly. In the two-dimensional space, choosing regular directions is straightforward (Chilès, 1977), considering the following azimuths:

$$\theta_i = (i-1)\pi/n_D \qquad i = 1, \dots, n_D$$

However, in the 3D space, the maximum number of regularly spaced directions is reduced to n_D = 15, which does not lead to a good approximation (Chilès, 1977). In this case, it is advisable to choose equidistributed directions instead of regular ones (Freulon, 1991; Lantuéjoul, 1994). For instance, consider the binary and the ternary expansions of any integer $n = 1,2, \dots$

$$n = a_0 + 2a_1 + \cdots + 2^p a_p \qquad a_i = 0,1$$

$$n = b_0 + 3b_1 + \cdots + 2^q b_q \qquad b_j = 0,1$$

From these decompositions, two numbers between 0 and 1 are generated

$$u_n = \frac{a_0}{2} + \frac{a_1}{4} + \cdots + \frac{a_p}{2^{p+1}}$$

$$v_n = \frac{b_0}{3} + \frac{b_1}{6} + \cdots + \frac{b_q}{3^{q+1}}$$

Finally, the coordinates of the n^{th} point of the sequence are (Figure 2.2):

$$x_n = (\cos(2\pi u_n)\sqrt{1 - v_n^2}\,, \sin(2\pi u_n)\sqrt{1 - v_n^2}\,, v_n)$$

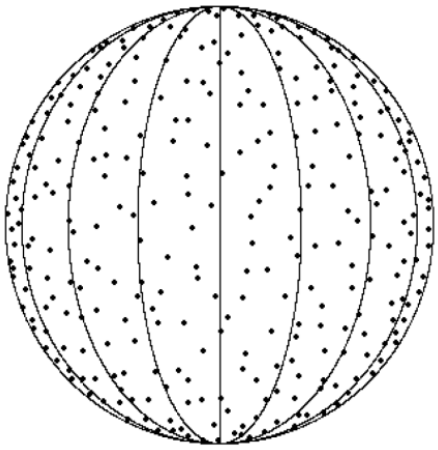

Figure 2.2: generation of 400 points according to an equidistributed sequence

For anisotropic random fields, the distribution of the line directions is no longer uniform (Matheron, 1973). However, the common cases of geometric and zonal anisotropies can be derived from the isotropic case (Emery and Lantuéjoul, 2006).

1.3.2. Deriving the covariance function of the one-dimensional random fields

For generating one-dimensional random fields, one needs to derive their covariance $C_1(r)$ from the dimensional covariance $C_d(h)$ of the desired field in the d-dimensional space (in general, d = 2 or 3). For simplicity, assume that the latter is isotropic (the case of geometric or zonal anisotropies can be obtained by a simple transformation of the spatial coordinates). For d = 3, the one-dimensional covariance can be obtained from the following equation (Matheron, 1973; Chilès and Delfiner, 2012):

$$C_1(r) = \frac{d}{dr}(rC_3(r)) \qquad (2.1)$$

In the same way, there is a one-to-one relationship between the one-dimensional and two-dimensional covariances (Brooker, 1985):

$$C_1(r) = \frac{d}{dr}\int_0^r \frac{t}{\sqrt{r^2 - t^2}}\, C_2(t)dt \qquad (2.2)$$

Table 2.1 and Figure 2.3 show the 1D covariance functions associated with the 3D isotropic spherical and exponential covariance models.

Table 2.1: 3D and 1D covariance functions

	3D Model	1D Model
Spherical model	$C_3(r) = \begin{cases} 1 - \frac{3r}{2a} + \frac{r^3}{2a^3} \; if \; r < a \\ 0 \; otherwise \end{cases}$	$C_1(r) = \begin{cases} 1 - \frac{3r}{a} + 2\frac{r^3}{a^3} \; if \; r < a \\ 0 \; otherwise \end{cases}$
Exponential model	$C_3(r) = \exp(-\frac{r}{a})$	$C_1(r) = \left(1 - \frac{r}{a}\right)\exp(-\frac{r}{a})$

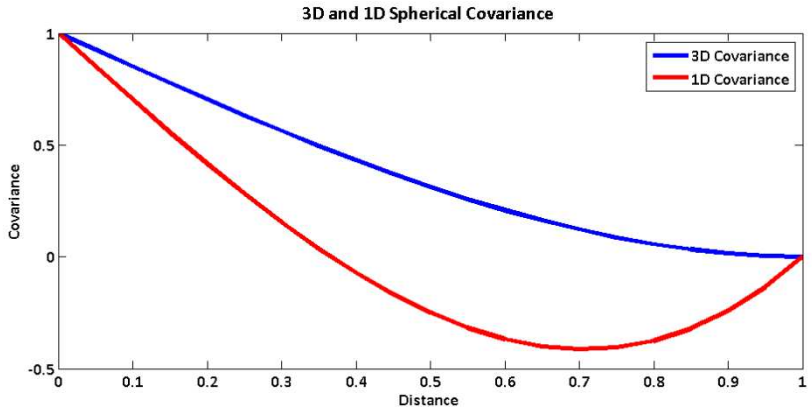

A

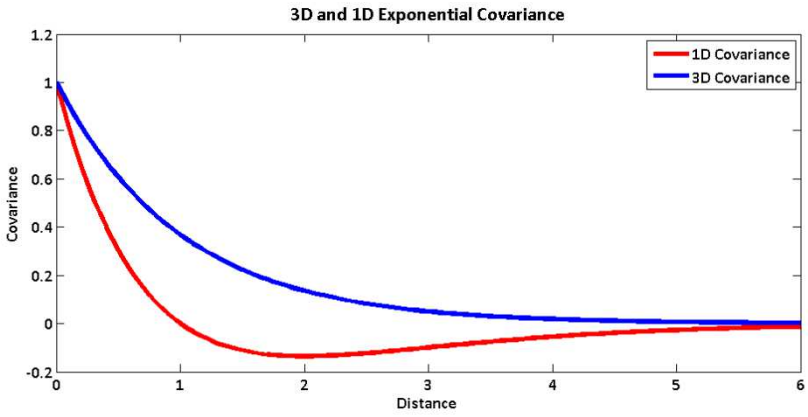

B

Figure 2.3: 3D and 1D covariance function for A) spherical and B) exponential models

1.3.3. Generating realizations along the lines

After defining the direction of the lines and obtaining the corresponding 1D covariance function, one can perform one dimensional simulation along each line. Different methods have been proposed for this purpose, for instance, spectral, partition and dilution methods (Lantuéjoul, 1994, 2002). Figure 2.4 shows the one dimensional simulation associated with a 3D isotropic spherical covariance model by using these three methods.

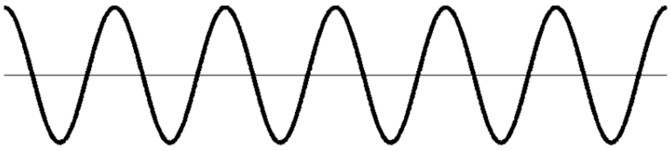

A

B

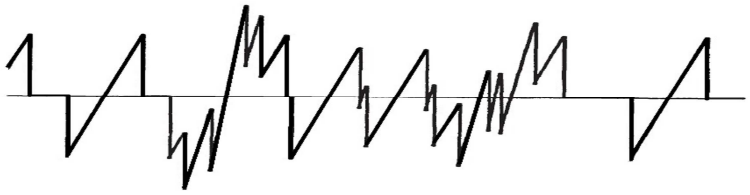

C

Figure 2.4: One dimensional simulation with A) spectral method
B) partition method C) dilution method. Modified from Lantuéjoul (2002)

Among all existing approaches for simulating along the lines, the spectral method will be amply used in this thesis, which yields a simulation algorithm known as the "spectral - turning bands" method (Mantoglou and Wilson, 1982; Mantoglou, 1987). This method and its variants are meticulously explained in the following sections.

1.4. Spectral - turning bands simulation

This method is a particular case of turning bands, for which the one-dimensional simulation is obtained by using a cosine wave. The required steps of this method are as follows:

1- Generating the lines

2- Simulating a random field along each line with the spectral method (Figure 2.4A).

The method is based on the spectral representation of a covariance function. According to Bochner's theorem (Bochner, 1933), every continuous covariance function in the *d*-dimensional space with a unit value at the origin (unit variance) is the Fourier transform of a positive integrable measure $F(d\omega)$ (Lantuéjoul, 2002; Shinozuka, 1971):

$$C(h) = \int e^{2\pi i(<\omega|h>)} F(d\omega) = \int e^{2\pi i(<\omega|h>)} f(\omega)\, d\omega \qquad (2.3)$$

where < | > is the usual scalar product and $F(d\omega)$ is the spectral measure (with an integral equal to 1, therefore this is a probability measure). If this measure is absolutely continuous, it is equal to $F(d\omega) = f(\omega)\, d\omega$ where $f(\omega)$ is a probability density function called the spectral density.

It can be shown (Lantuéjoul, 2002; Shinozuka, 1971) that the following random field:

$$Y(x) = \sqrt{2}\cos(< \omega | x > + \phi) \tag{2.4}$$

is stationary with mean zero and covariance function $C(h)$, where ω is a random frequency distributed according to the spectral density in the *d*-dimensional space, and ϕ is a random phase uniformly distributed in [0, 2π[. To obtain a simulation that is multigaussian, one has to sum and properly rescale many of such independent simulations, based on the central limit theorem (Lantuéjoul, 1994, 2002):

$$Y(x) = \sqrt{\frac{2}{n_D}} \sum_{i=1}^{n_D} \cos(< \omega_i | x > + \phi_i) \tag{2.5}$$

In a nutshell, for using the spectral method, one needs to know the spectral measure or the spectral density and the number of basic random fields (n_D) to be summed. For deriving the spectral density from a given covariance function in the *d*-dimensional space, the following formula can be used (Yaglom, 1987; Lantuéjoul, 2002; Chilès and Delfiner, 2012):

$$f(\omega) = \frac{1}{(2\pi)^d} \int e^{2\pi i(<\omega|\mathrm{h}>)}\, C(h) d(h) \tag{2.6}$$

where *d* is the dimension of the space where the target random field is defined.

Table 2.2 gives a list of isotropic covariance functions and their spectral densities (spectral measures) in $\mathbb{R}^d$ (Lantuéjoul, 2002; Chilès and Delfiner, 2012). For the sake of simplicity, the covariance functions in this table are assumed to have a unit sill and a unit scale factor; a proper rescaling of the spectral densities should be done if the sill or the scale factor differs from 1 (Marcotte, 2015).

3- The simulated value at each target point (*x*) of the *d*-dimensional space is the sum of the simulated values at the projections of this target point (*x*) on the different lines obtained from the previous step.

Table 2.2: Spectral densities of some basic isotropic covariance models

Model	**Spectral measure in $\mathbb{R}^d$**
Spherical	$\frac{3}{4\pi\|\|\omega\|\|^3}\left[Bessel_j\left(\frac{\|\|\omega\|\|}{2}\right)\right]^2$
Exponential	$\frac{1}{\pi^{\frac{d+1}{2}}}\frac{1}{(1+\|\|\omega\|\|^2)^{\frac{d+1}{2}}}$
Gaussian	$\frac{1}{(2\sqrt{\pi})^d}\exp\left(-\frac{\|\|\omega\|\|^2}{4}\right)$
Matérn (K-Bessel)	$\frac{\Gamma(\mu+\frac{d}{2})}{\Gamma(\mu)\pi^{\frac{d}{2}}}\frac{1}{(1+\|\|\omega\|\|^2)^{\mu+\frac{d}{2}}}$

As an illustration, consider Figure 2.5A, where θ_i is the angle of line D_i with the abscissa axis, u_i is the unit vector of line D_i with component $\cos\theta_i$ and $\sin\theta_i$, and s_i is the projection of the target point on line D_i. The simulation at point *x* is determined by:

$$Y(x) = \frac{1}{\sqrt{n_D}}\sum_{i=1}^{n_D} Y_i(s_i) \qquad (2.7)$$

where Y_i is a cosine wave as per Equation (2.4) (Figure 2.5B). This approach has been first proposed by Shinozuka (1971).

For instance, to simulate a Gaussian random field with a Gaussian covariance function with a unit sill and a unit scale factor in $\mathbb{R}^3$, one should first simulate a set of frequency vectors $\{\omega_i : i = 1, \dots, n_D\}$ with the Gaussian density given in Table 2.2 (these are vectors in $\mathbb{R}^3$ whose coordinates are independent Gaussian random variables with mean 0 and variance 2) and a set of independent phases $\{\phi_i : i = 1, \dots, n_D\}$ uniformly distributed in [0, 2π[. The simulated random field can then be obtained by calculating a sum of cosine waves as given in Equation (2.5).

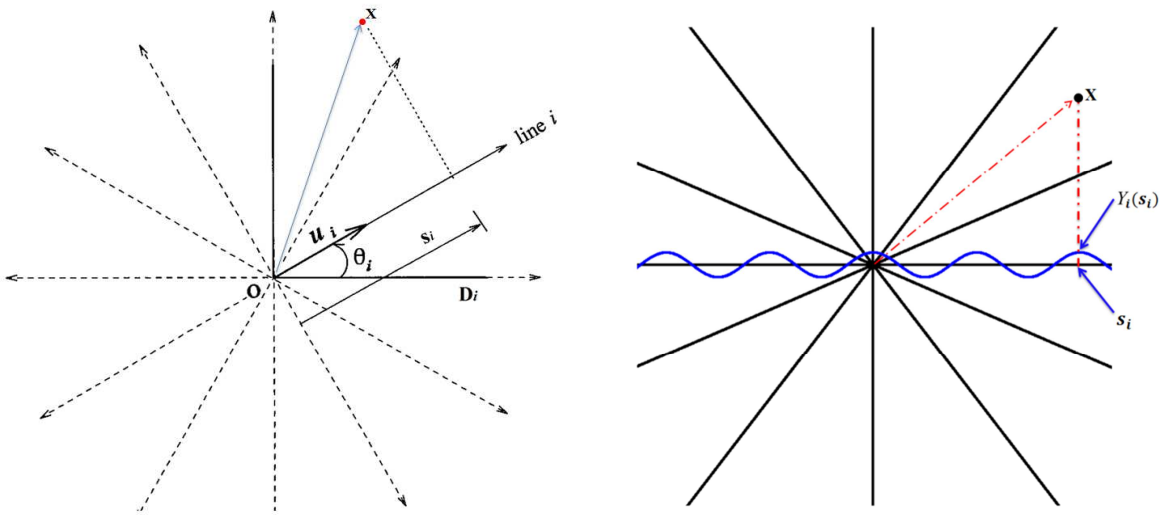

A B

Figure 2.5: Principles of spectral-turning bands simulation

1.5. Variants of spectral simulation

Shinozuka and Jan (1972) proposed a variant of the spectral simulation method, where the previous formula is combined with a coefficient (amplitude) to generate realizations of the random field:

$$Y(x) = \sqrt{\frac{2f(\omega)}{|D|}} \cos(< \omega | x > + \phi) \qquad (2.8)$$

where:

- f is the spectral density of the target covariance in the d-dimensional space
- ϕ is a random phase with uniform distribution in $[0, 2\pi]$
- ω is a random vector in the d-dimensional space uniformly distributed in a bounded domain D containing the support of f
- $|D|$ is the measure of D
- $f(\omega)$ is an amplitude depending on ω.

The inconvenient of this method is that it is applicable only to the simulation of random fields whose spectral densities have a bounded support, which is quite restrictive. Emery et al. (2016) removed this inconvenient by applying importance sampling for simulating vector ω, i.e., ω is simulated with a probability density g different from a uniform density:

$$Y(x) = \sqrt{\frac{2f(\omega)}{g(\omega)}}\cos(<\omega|x>+\phi) \tag{2.9}$$

where

- f is the target spectral density
- g is another density that must contain the support of the target spectral density
- ω is a random vector with probability density g in the *d*-dimensional space
- ϕ is an independent random variable (phase) uniformly distributed over the interval $[0, 2\pi]$.

Based on the central limit theorem, to obtain an approximately Gaussian random field, it suffices to sum up and properly normalized many of such independent random fields:

$$Y(x) = \sum_{i=1}^{n_D} \sqrt{\frac{2f(\omega_i)}{n_D g(\omega_i)}}\cos(<\omega_i|x>+\phi_i) \tag{2.10}$$

where

- n_D is a large integer
- ω_i are independent random vectors with probability density g
- ϕ_i are independent random variables (phases) uniformly distributed over $[0, 2\pi]$.

Interestingly, the previous variants can be generalized to the multivariate case, i.e., to the simulation of a vector random field instead of a scalar random field. In a nutshell, one has to replace the square root in Equations (2.9) and (2.10) by a Cholesky factor, insofar as the spectral density $f(\omega)$ is no longer a scalar, but a Hermitian, positive semi-definite matrix. Therefore, one can simulate any vector random field whose direct and cross covariance functions are continuous and absolutely integrable, provided one knows the analytical expression of their spectral densities, without the need for these spectral densities to have a bounded support. The only restriction is that the support of the density g from which the frequency vectors are simulated must contain the support of f. The reader is referred to Emery et al. (2016) for details.

2. Simulation of categorical variables (rock types)

Most often, the spatial distribution of metal grades in an ore deposit is related to geological characteristics, so that the modeling of geological domains is a critical step in mineral resource and ore reserve evaluation. Up to now, many approaches have been proposed in order to model the layout of geological domains and significant improvements have been achieved in the last decades. Generally, the existing approaches can be divided into two groups: deterministic and stochastic approaches.

Deterministic approaches, such as hand contouring, wireframing or implicit modeling, rely on an interpretation of the available data (typically, from drill hole samples) and on the geological knowledge of the deposit. The main drawback of these approaches is that they do not account for any uncertainty (possible misclassification) in the assumed geological model, insofar as they provide a single interpretation of the geology of the deposit without offering any measure of the uncertainty in the boundaries of the geological domains (Cáceres et al., 2011; Cown, 2003).

In contrast, stochastic approaches consist in simulating the layout of the geological domains in order to provide a set of alternative outcomes of the geology of the deposit and to allow quantifying the uncertainty in the domain boundaries. There exist many stochastic methods, such as object-based and Boolean simulation (Chessa and Martinius, 1992; Stoyan et al., 1996; Viseur, 1999; Lantuéjoul, 2002; Chilès and Delfiner, 2012), sequential indicator simulation (Journel, 1983; Journel and Isaaks, 1984; Alabert, 1987; Journel and Alabert, 1988; Journel, 1989), simulation based on multiple-point statistics (Guardiano and Srivastava, 1993; Strebelle and Journel, 2000; Ortiz, 2003; Ortiz and Deutsch, 2004; Daly and Caers, 2010; Mariethoz and Caers, 2014), truncated Gaussian and plurigaussian simulation (Matheron et al., 1987; Beucher et al., 1993; Galli et al., 1994; Le Loc'h et al., 1994; Le Loc'h and Galli, 1997; Armstrong et al., 2011). Since the truncated Gaussian and plurigaussian will play a key role in this thesis, these methods are detailed in the following section.

2.1. Truncated Gaussian model

The underlying idea in truncated Gaussian model is to simulate a Gaussian random field in the region of interest and to obtain the geological domain at each specific location depending on the simulated Gaussian value at this location (Matheron et al., 1987; Galli et al., 1994; Armstrong et al., 2011). For instance, to simulate two geological domains, each covering 50% of the study region, one defines a truncation threshold set to 0 (median of the standard Gaussian distribution) (Figure 2.6). In general, the values of the truncation thresholds define the proportion of space covered by each geological domain.

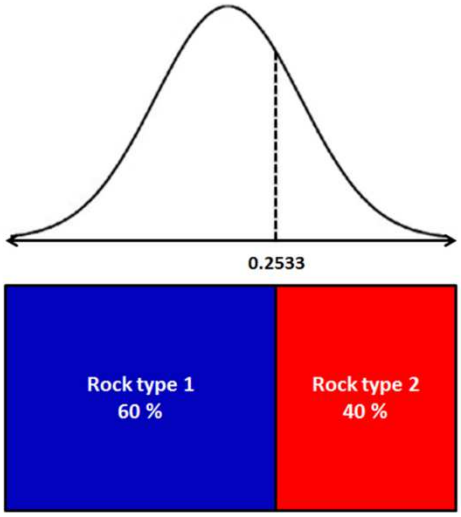

Figure 2.6: An example of truncation rule to convert a Gaussian field into two rock type domains

The design of the truncated Gaussian model is motivated by its simplicity of use and by the existence of numerous algorithms for simulating Gaussian random fields (at least, in the case of stationary random fields) and for conditioning the realizations to pre-existing categorical data (Lantuéjoul, 2002; Chilès and Delfiner, 2012). Along with the truncation threshold(s), one needs to determine the auto-covariance function of the underlying Gaussian random field in order to complete the determination of the model. This covariance function can be inferred from the covariance functions of the domain indicators, as there is a one-to-one relationship between Gaussian and indicator covariance functions (Armstrong et al., 2011). In practice, instead of covariance functions, one often works with variograms. If one denotes by y a truncation threshold, by G the cumulative distribution function of the standard normal distribution, and by γ_y and γ the indicator and Gaussian variograms, respectively, then the following relationship holds (Matheron, 1975; Kyriakidis et al., 1999; Chilès and Delfiner, 2012):

$$\gamma_y = G(y)[1 - G(y)] - \frac{1}{2\pi}\int_0^{\arcsin(1-\gamma)} \exp\left\{-\frac{y^2}{1+\sin(\theta)}\right\} d\theta \qquad (2.11)$$

As a matter of fact, the variogram of the Gaussian random field controls the regularity of the boundary between geological domains: if this variogram is smooth near the origin, then the boundary will be regular; otherwise the boundary will be erratic (Lantuéjoul, 2002).

The conditional simulation of a truncated Gaussian model can be performed in three steps. First, knowing the covariance function of the underlying Gaussian random field, one can generate a set of Gaussian values at the data locations in agreement with this covariance function and with the coding of geological domains (this step can be performed by Gibbs sampling, which will be explained later). Then one can perform a multigaussian simulation using the Gaussian values of the previous step as conditioning data. Finally, by truncating the Gaussian realizations according to the truncation rule, one obtains realizations of the geological domains (Figure 2.7).

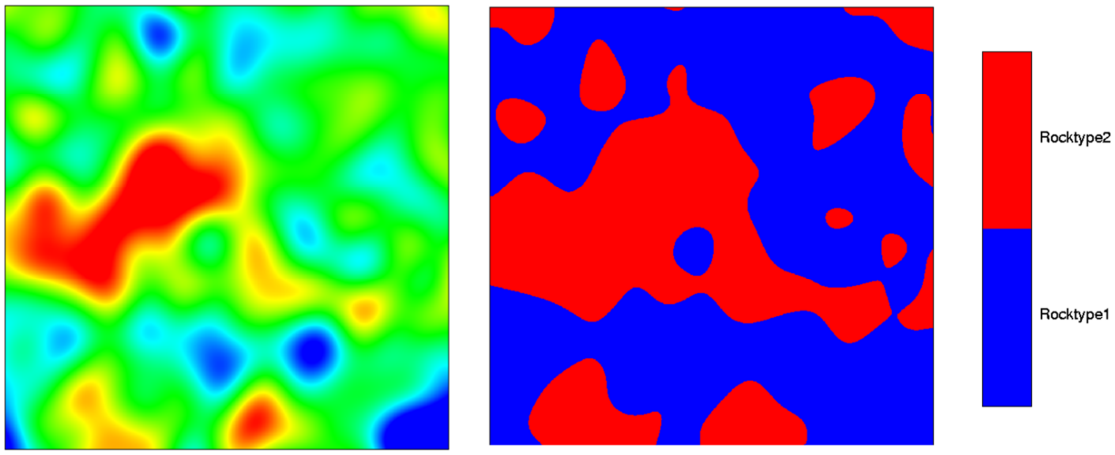

Figure 2.7: Simulated Gaussian random field and corresponding geological domains after truncation

2.2. Plurigaussian model

In many cases, the truncated Gaussian approach is restrictive. For instance, if there is no natural sequence in the rock types, or if a given rock type can be in contact with more than two other rock types, it is difficult to use truncated Gaussian approach (Galli et al., 1994; Armstrong et al., 2011). To overcome this restriction, one can use the plurigaussian model, which extends the truncated Gaussian model by considering two or more Gaussian random fields and using a truncation rule to convert these Gaussian fields into geological domains (Figures 2.8 and 2.9) (Le Loc'h et al., 1994; Le Loc'h and Galli, 1997).

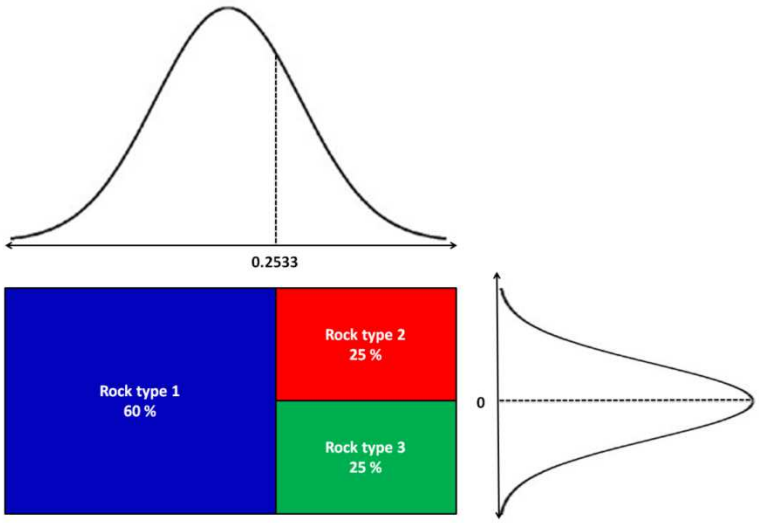

Figure 2.8 : An example of truncation rule with two Gaussian random fields and two different thresholds

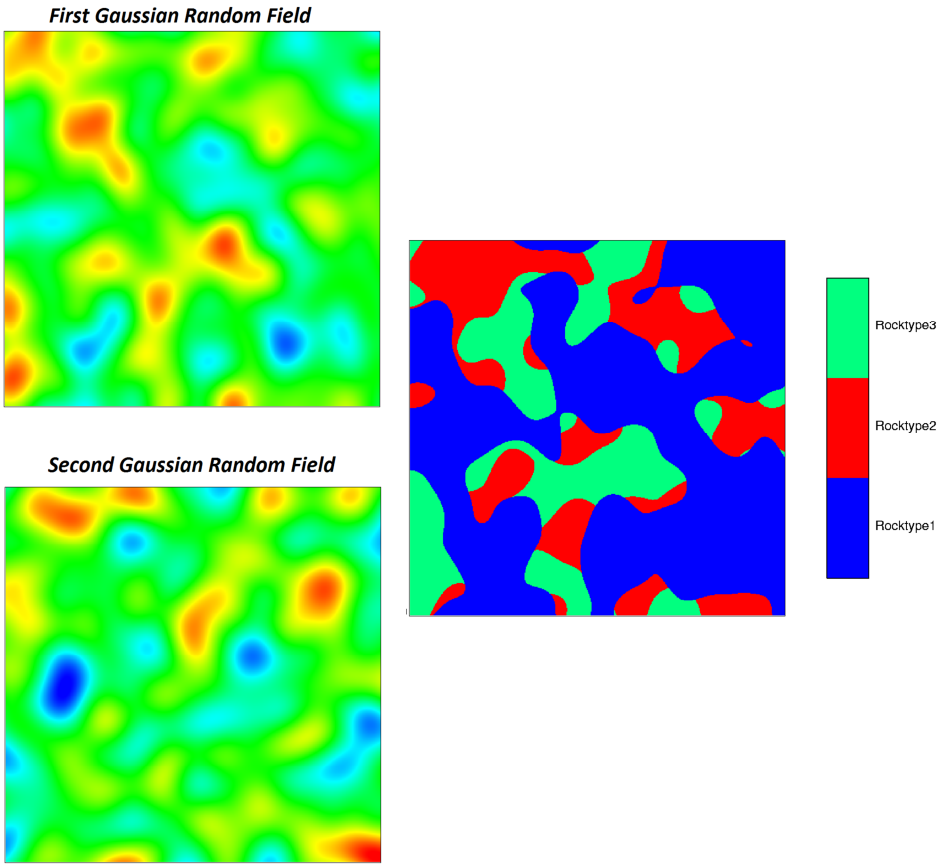

Figure 2.9: Simulated Gaussian random fields and corresponding geological domains obtained after truncation

The plurigaussian model thus gives more flexibility for defining geological domains, as the user has several free parameters such as the number of underlying Gaussian random fields, their direct and cross covariances or variograms, and the definition of truncation thresholds. The latter are related to the proportions of space covered by the different domains, while the former are related to their spatial continuity (indicator direct and cross variograms).The simulation of a plurigaussian model is similar to that of the truncated Gaussian model (Lantuéjoul, 2002; Armstrong et al., 2011):

- Gibbs sampling for simulating the Gaussian random fields at the conditioning data locations, conditionally to the categorical data.
- Multigaussian simulation for simulating the Gaussian random fields at the target locations.
- Truncation to convert the simulated Gaussian fields into geological domains.

2.3. Gibbs sampler

As mentioned before, in the process of truncated Gaussian and plurigaussian simulation, one needs to generate Gaussian values at the data locations and then, with the generated values, one can perform simulation at the desired target locations. As this last step can be done with any multigaussian simulation algorithm, it remains only to generate Gaussian values at the data locations, which can be done with a Monte Carlo Markov Chain (MCMC) algorithm known as the "Gibbs sampler" (Freulon, 1992; Chan, 1993; Le Loc'h and Galli, 1997; Emery, 2007a; Armstrong el al., 2011). Let us explain this algorithm through a simple example consisting of two rock type domains (coded as "1" or "2") that are defined by considering a single Gaussian random field $Y(x)$ and a single truncation threshold (y):

$$\begin{cases} Y(x) < y \text{ if rock type "1" prevails at } x \\ Y(x) \geq y \text{ if rock type "2" prevails at } x \end{cases}$$

2.3.1. First stage: Initialization

At this stage, one defines an arbitrary value for $Y(x)$ at each data location that fulfills the conditions imposed by the geological domain prevailing at this location (i.e., the value should be smaller than y if the location corresponds to rock type 1, larger than y otherwise). The generated values are obtained independently between one location and another, so that they do not reproduce the desired spatial continuity for $Y(x)$.

2.3.2. Second stage: Iteration

(a) Select a data location, say x_α. The selection can be done in a regular or a random order, provided that each data location would be selected infinitely many times if the number of iterations gets infinite.
(b) Calculate the distribution of $Y(x_\alpha)$ conditional to all the other data $\{Y(x_\alpha): \beta \neq a\}$. This is a Gaussian distribution, with mean equal to the simple kriging prediction of $Y(x_\alpha)$ and variance equal to the simple kriging variance.
(c) Simulate a random variable Y_a according to the previous conditional distribution.
(d) If Y_a is compatible with the rock type prevailing at location x_α (i.e., Y_a is smaller than y if x_α corresponds to rock type 1, or it is larger than y if x_α corresponds to rock type 2), replace the current value of $Y(x_\alpha)$ by Y_a. If it is not compatible, one can go back to step (c) until obtaining a compatible value, or go back to step (a).
(e) Go back to step (a) and loop many times.

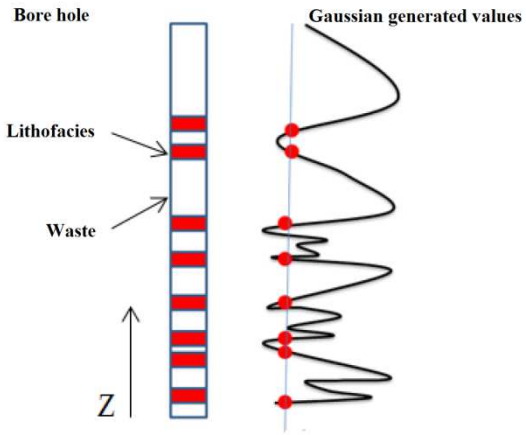

Figure 2.10: Generating a set of Gaussian values by Gibbs sampling

The practice of the Gibbs sampler requires some care in two aspects: the calculation of kriging predictions and kriging variances at step (b) and the number of iterations required before stopping the algorithm. Regarding the first aspect, Emery et al. (2014) proved that the successive vectors simulated in the iterative phase do not converge in distribution to the desired distribution unless kriging is performed in a unique neighborhood. Some variations of the Gibbs sampler have been proposed to avoid solving a large kriging system (Arroyo et al., 2012; Lantuéjoul and Desassis, 2012), but so far these are restricted to the simulation of stationary Gaussian random fields (thus not directly applicable in this thesis). As for the number of required iterations, it can be determined through statistical testing (Emery, 2008a) or through an empirical assessment of the convergence of the Gibbs sampler (Lantuéjoul, 2002; Armstrong et al., 2011).

3. Joint simulation of grade and rock types

In the multigaussian simulation approach, one simulates a continuous variable (say, a metal grade) by means of a Gaussian random field in order to construct the grade realizations. In the truncated Gaussian and plurigaussian approaches for simulating categorical variables, one uses auxiliary Gaussian random fields to construct realizations of geological domains (rock type domains). As a consequence, by introducing spatial cross-correlations between the Gaussian random field associated with the grade and the Gaussian random field(s) associated with the rock type, one can take account of the dependency between rock types and grades and impose this dependency by jointly simulating all these Gaussian random fields. Finally, when obtaining the results of the Gaussian joint simulation, one can transform the simulated Gaussian random fields into simulated grades and rock types by using the anamorphosis function and the truncation rule, respectively. This idea and variants of it have been explored by a few authors in the past decades (Dowd, 1994, 1997; Bahar and Kelkar, 2002; Emery and Silva, 2009; Cáceres and Emery, 2010).

Specifically, in order to perform joint simulation of grades and rock types, the following steps should be taken (Emery and Silva, 2009):

1- At the first step, one has to codify the rock type information into indicators

$$\forall\, x \in \mathbb{R}^d,\quad \forall \mathrm{i} \in \{1,\dots,n\},\quad \Theta_{\mathrm{i}}(x) = \begin{cases} 1 & \text{if } x \text{ belong to rock type i} \\ 0 & \text{otherwise} \end{cases}$$

2- Then one has to transform the continuous variable (grade, denoted as Z_0) into a Gaussian variable (Y_0) and model the corresponding anamorphosis function ϕ.

$$\forall\, x \in \mathbb{R}^d,\ Z_0(x) = \phi\big(Y_0(x)\big),$$

3- After obtaining the Gaussian and indicator data, one has to calculate their direct and cross covariances or variograms.

4- According to the spatial relationships and contacts between rock types, one has to determine a truncation rule and the number (N) of Gaussian random fields $\{Y_1,\dots, Y_N\}$ needed to model the rock type layout with plurigaussian simulation (or truncated Gaussian simulation if N = 1). By determining the truncation rule, one specifies the number of thresholds. The threshold values can be determined according to the proportion of each rock type.

5- The most important step is then to propose a coregionalization model for the previously defined Gaussian random fields $\{Y_0, Y_1,\ldots, Y_N\}$. The model should be defined so as to fit the experimental direct and cross covariances or variograms of the Gaussian random field Y_0 and rock type indicators $\Theta_1 \ldots, \Theta_n$. This step will be explained in detail through the real case study presented in Chapter 5.

Finally, after determining the coregionalization model, one jointly simulates the Gaussian random fields, by means of multigaussian simulation algorithms and Gibbs sampling. The realization of the categorical variable (rock type) is obtained by truncating the simulated Gaussian values of $Y_1,\ldots, Y_N$ according to the truncation rule, while the realization of the continuous variable (grade) is obtained by transforming the simulated Gaussian values of Y_0 according to the anamorphosis function. Figure 2.11 illustrates the different steps of joint simulation.

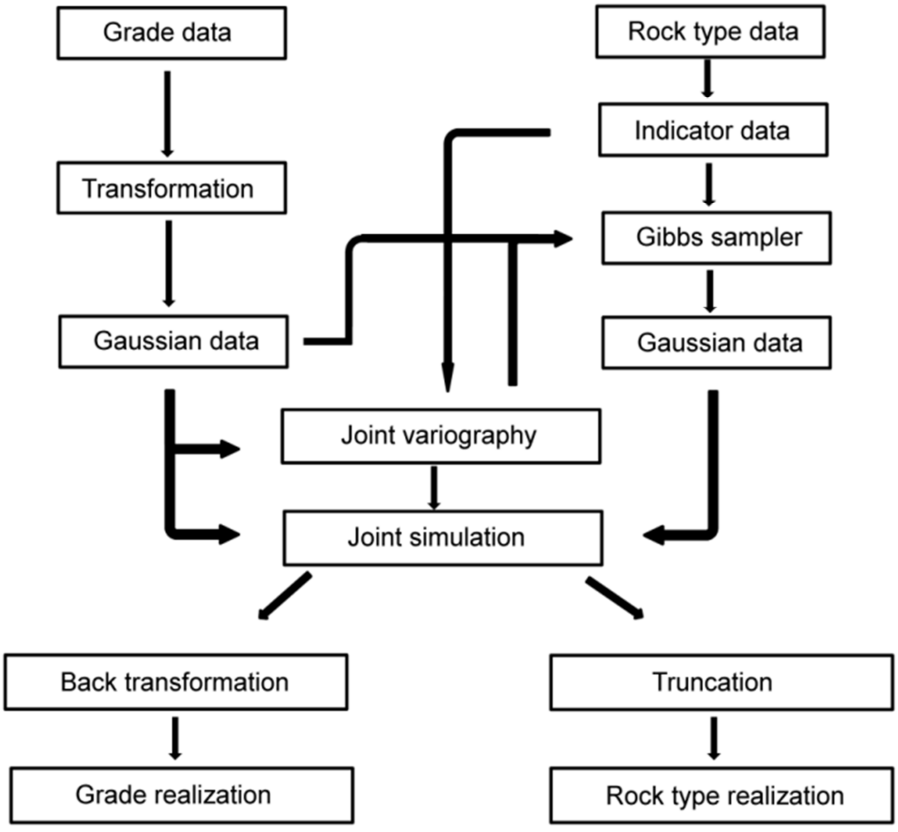

Figure 2.11: The process of stationary joint simulation (Maleki and Emery, 2015)

Joint simulation accounts for the uncertainty in the spatial layout of the boundaries between rock type domains, which is ignored when using a deterministic geological model. Also it considers the spatial correlation of the continuous variable across the boundaries, which is ignored when performing a cascade simulation of the categorical and continuous variables. In addition, joint simulation accounts for the spatial dependencies between the continuous and categorical variables. For more information on the advantages of this approach compared with other methods and for application case studies, the interested readers can consult Emery and Silva (2009) and Maleki and Emery (2015); the latter reference is reproduced in Chapter 5.

Chapter 3: From stationary to intrinsic random fields of order *k*

1. Non-stationary geological domains

As mentioned in the previous chapter, many models and algorithms have been designed for simulating categorical regionalized variables such as rock types. However, most of these are based on a stationarity hypothesis. In other words, it is assumed that the probability of presence of each rock type is constant throughout the region under study. This assumption is unrealistic, insofar as the probability of occurrence of different rock types is generally not constant under translation. Under these circumstances, one should think of using non-stationary simulation methods. For instance, in the process of truncated Gaussian or plurigaussian simulation, one may introduce local proportions of rock types for determining the truncation thresholds.

One solution for dealing with non-stationary geological domains is using local proportions instead of global proportions. It means that one should define the local proportion (viewed as the probability of occurrence) of each rock type in different parts of the region under study. When performing simulation, instead of global proportions, the local proportions of rock types will be used.

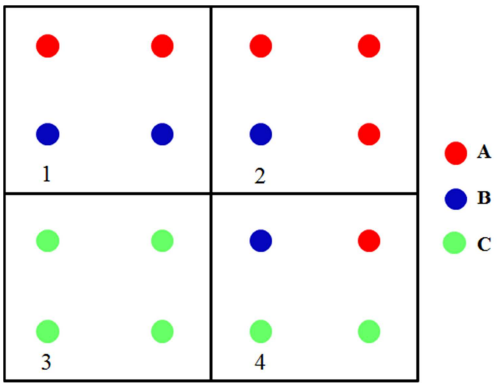

Figure 3.1: Deducing the proportion of each rock type in specific blocks from available data

For instance, in Figure 3.1, one has four blocks to simulate. From the available data one can deduce that, in block number 2, the proportion of rock type A is seventy five percent and the proportion of rock type B is twenty five percent. So, if one generates one hundred

realizations in this block, approximately seventy five realizations should correspond to rock type A and twenty five realizations should correspond to rock type B. In the same way, if one generates one hundred realizations in block number 3, all the realizations would be rock type C.

The idea of using local proportions is interesting and seems logical. However, in practice there are some difficulties:

- The first problem is how to calculate the local proportions in all parts of the region under study. The simplest response that comes to mind is calculating the local proportion with the available drill hole data, but the calculations may be unreliable when these data are scarce or non-evenly distributed.

- One may use an interpreted block model that is provided by geologists for deducing the local proportion of each rock type across the region under study. However, there is also a level of uncertainty in the interpreted block model and the accuracy of this model may be questionable.

Other methods can be used for modeling non-stationary geological domains. In this thesis, in order to model non-stationary geological domains and to avoid these disadvantages of using the local proportions approach, we will resort to models based on intrinsic random fields of order k or IRF-k, for short (Matheron, 1973). Briefly, in order to generate a realization of non-stationary geological domains, the idea is to consider the truncation of such an IRF-k with Gaussian generalized increments (Matheron, 1973; Dimitrakopoulos, 1990; Chilès and Delfiner, 2012), following the recent work by Madaniesfahani (2016).

In the following sections, the stationarity hypothesis will be reviewed. Then, the concepts, methods and tools that will be used in this thesis for modeling non-stationary geological domains will be explained.

2. Review of stationarity hypotheses

The possibility of statistical inference (inference of the model parameters such as the mean, variance or variogram) often relies on a stationarity assumption, which allows substituting a repetition over different realizations of a random field at a given location, by a repetition over a single realization of the random field within a sufficiently large domain (Matheron, 1989; Chilès and Delfiner, 2012).

2.1. Stationary random fields (strict stationarity)

In geostatistical simulation it is common to assume that the random field $Z = \{Z(x): x \in \mathbb{R}^d\}$ under study is (strictly) stationary, i.e. that its finite-dimensional distributions are invariant under translation (Chilès and Delfiner, 2012, Matheron, 1971). So, for any vector h and any set of locations $\{x_1,\ldots, x_k\}$ and thresholds $\{z_1,\ldots, z_k\}$:

$$\text{Prob}[Z(x_1) < z_1, \ldots, Z(x_k) < z_k] = \text{Prob}[Z(x_1 + h) < z_1, \ldots, Z(x_k + h) < z_k] \quad (3.1)$$

Physically this means that the random field is homogeneous in space and, so to speak, repeats itself in the whole space. This makes statistical inference possible on a single realization.

2.2. Second-order stationarity

Strict stationarity requires all the moments of the finite-dimensional distributions to be invariant under translation, but since this cannot be verified from the limited experimental data, one usually restricts it to the first two moments (the mean and the covariance function). This is called "weak" or second-order stationarity. In other words, the expected value (or mean) of $Z(x)$ must be constant for all points x. Secondly, the covariance function between any two points x and $x+h$ depends on the vector h but not on x. In summary, the first and second moments should exist and be invariant under translation (Chilès and Delfiner, 2012, Matheron, 1971):

$$\begin{cases} \text{E}[Z(x)] = m \\ \text{E}\{[Z(x) - m][Z(x + h) - m]\} = C(h) \end{cases} \quad (3.2)$$

Note that, provided its first and second order moments exist, a strictly stationary random field is also second-order stationary. Conversely, a second-order stationary random field is not necessarily strictly stationary, because its higher order moments may not be invariant through a translation (Chilès and Delfiner, 2012).

2.3. Intrinsic stationarity (IRF-Order 0)

In practice the previous assumptions may still be questionable for representing regionalized variables with non-homogeneous spatial variations. Therefore, for dealing with this kind of

situations, one can privilege the stationarity of the increments over the stationarity of the random field itself. This milder hypothesis assumes that for every vector h the increment $Y(x) = Z(x+h) - Z(x)$ is a second-order stationary random field. Then $Z(x)$ is called an intrinsic random field (of order 0) and is characterized by the following properties (Matheron, 1971):

$$\begin{cases} \mathrm{E}[Z(x+h) - Z(x)] = 0 \\ \mathrm{E}\{[Z(x+h) - Z(x)]^2\} = 2\gamma(h) \end{cases} \tag{3.3}$$

with $\gamma(h)$ the (semi)variogram.

For instance, as can be seen in Figure 3.2, the (realization of the) random field shows a clear trend along the x direction. However, by calculating the increments of this random field one can obtain a new field that does not exhibit trend anymore. So, one can model the original field as an intrinsic random field.

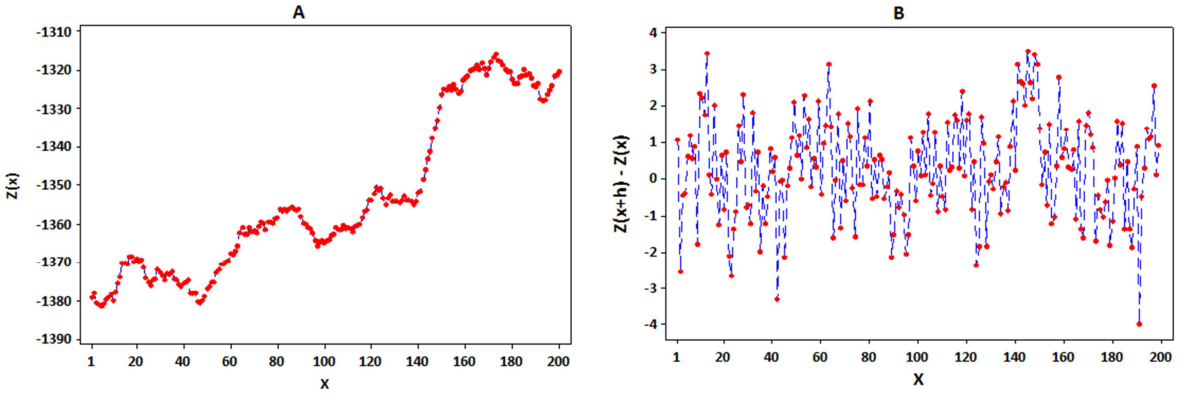

Figure 3.2: (A) a random field with trend (B) increments of the random field with a stationary behavior

There are some main changes when passing from stationary to intrinsic random fields (Chilès and Delfiner, 2012, Matheron, 1971):

- The basic working tool of the stationary case, the covariance function $C(h)$ is replaced by the variogram $\gamma(h)$. This is more general, since the class of valid variogram functions is broader than the class of covariance functions, as $C(h)$ must be positive semi-definite whereas it is only required that $-\gamma(h)$ be conditionally positive semi-definite (Armstrong and Jabin, 1981). In contrast to the covariance function, the variogram may be unbounded, and this enables the description of phenomena with a potentially unlimited dispersion (theoretically infinite variance).

- In the stationary case there exists a mean value (m) around which the random field fluctuates. The phenomenon remains "controlled" in the sense that the deviations from the mean are never too large nor last too long. In the case of an intrinsic random field (of order 0) with an unbounded variogram, no such regulation exists. There is no constant mean value (m). Such a random field is defined up to an arbitrary constant and is generally studied only through its increments.

- In the case of a second-order stationary random field, any linear combination

$$Z = \sum_{\mathrm{i}} \lambda_{\mathrm{i}} Z(x_{\mathrm{i}}) \tag{3.4}$$

has the variance:

$$\mathrm{Var}\left[\sum \lambda_{\mathrm{i}}\, Z(x_{\mathrm{i}})\right] = \sum_{\mathrm{i}} \sum_{\mathrm{i}} \lambda_{\mathrm{i}} \lambda_{\mathrm{j}}\, C(x_{\mathrm{i}} - x_{\mathrm{j}}) \tag{3.5}$$

where $C(h)$ is the covariance function. In the case of an intrinsic random field, only special linear combinations have a finite variance, the allowable ones, satisfying the condition $\sum \lambda_{\mathrm{i}} = 0$. The variance is then calculated by using $-\gamma(h)$ as if it were a covariance function:

$$\mathrm{Var}\left[\sum \lambda_{\mathrm{i}}\, Z(x_{\mathrm{i}})\right] = -\sum_{\mathrm{i}} \sum_{\mathrm{i}} \lambda_{\mathrm{i}} \lambda_{\mathrm{j}}\, \gamma(x_{\mathrm{i}} - x_{\mathrm{j}}) \tag{3.6}$$

Other linear combinations do not, in general, have a finite variance. Thus, at the cost of a relatively minor operating restriction (only use linear combinations whose weights sum up to zero), one gains the possibility of dealing with a larger class of phenomena that cannot be represented by stationary random fields. In fact, the intrinsic hypothesis allows using a wider range of variograms but the weights must sum to zero (in the intrinsic model, one can only calculate the expectation and the variance of linear combinations with weights adding to zero). In contrast, the range of admissible variogram models is more restricted for the stationary hypothesis but any weighting factors may be used (Chilès and Delfiner, 2012).

3. Non-stationary modeling

The use of stationary or intrinsic models may still be questionable in some circumstances, as it may not allow accounting for local changes of the phenomenon under study, in particular, local changes in the mean value (trends), in the dispersion (proportional effects) and in the spatial continuity (e.g., local anisotropies or local ranges of correlation). In fact, many natural parameters do not fulfill the second-order or intrinsic stationarity hypothesis, because of known systematic changes in the parameter values. Therefore, many approaches have been proposed to alleviate even more these stationary assumptions. In the following section some well-known methods that are used in this thesis for modeling non-stationary random fields will be explained.

3.1. Universal kriging

In the universal kriging model, the random field is split into two components (Matheron, 1971; Chilès, 1977; Goovaerts, 1997; Deutsch and Journel, 1998; Chilès and Delfiner, 2012):

- $f(x)$ a deterministic drift that accounts for the spatial trend
- $Y(x)$ a random residual that is assumed second-order stationary or intrinsic

such that:

$$Z(x) = Y(x) + f(x) \tag{3.7}$$

where $Z(x)$ is the random field under study, $f(x)$ is the drift, and $Y(x)$ is the fluctuation, or residual, about this drift (Figure 3.3). In fact, the residual represents the variations in the small scale and reflects local anomalies, whereas the drift represents the variations in the large scale.

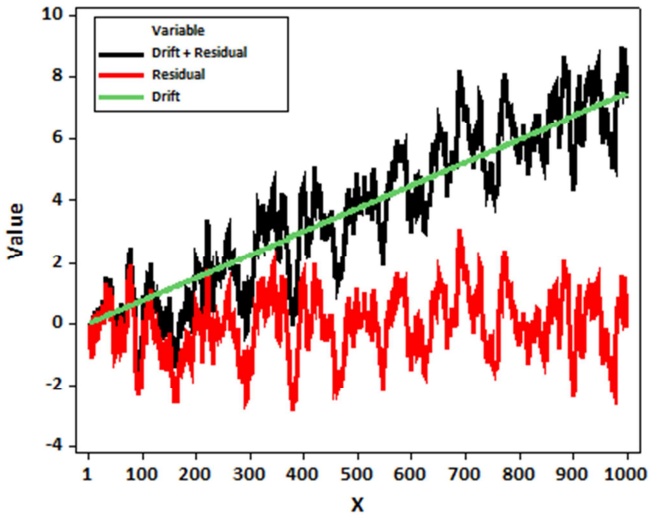

Figure 3.3 : Dichotomy into drift and residual

Obviously, if the drift is removed from the regionalized variable, the residual is stationary or intrinsic and ordinary kriging can be applied to it. So, one can do the following three steps:

- The drift is estimated and removed to form stationary residuals at the data points
- The stationary residuals are kriged to obtain a prediction of the residuals at un-sampled locations
- The predicted residuals are combined with the drift to obtain a prediction of the actual regionalized variable.

The drawback of this approach (residual kriging) is that it relies on an estimate of the drift, which is actually uncertain. So, instead of performing this complicated series of operations, one can generalize the kriging system of equations in order to incorporate additional Lagrange multipliers that represent the constraints imposed by the addition of a drift. Then the kriging weights are estimated as thought the drift effect had been removed from the regionalized variable. By having a set of data at locations $x_1, \dots, x_n$ and a location x_0 targeted for prediction, the universal kriging predictor is of the form:

$$Z^*(x_0) = \sum_{\alpha=1}^{n} \lambda_\alpha Z(x_\alpha) \tag{3.8}$$

In this approach, one assumes that the drift is a linear combination of known basis functions, but with unknown coefficients (Matheron, 1971; Chilès, 1977):

$$f(x) = \sum_{s=0}^{k} b_s f^s(x) \tag{3.9}$$

where f^s is a basis function defined according to the nature of the drift or trend, and b_s is an unknown coefficient. Usually the first basis function is the constant function identically equal to 1, which guarantees that the constant-mean case is included in the model. In the universal kriging approach, the remaining functions are usually chosen as polynomials of the coordinates (Matheron, 1971, 1973; Chilès, 1977; Chilès and Delfiner, 2012). For instance, in the presence of a quadratic trend in the *x* direction, $f(x)$ is equal to:

$$f(x) = b_0 + b_1 x + b_2 x^2$$

Similarly, if one has a quadratic trend in the *x* and *y* directions, $f(x, y)$ is equal to:

$$f(x, y) = b_0 + b_1 x + b_2 y + b_3 x^2 + b_4 y^2 + b_5 xy$$

Finally, by imposing the restrictions of linearity, authorization, unbiasedness and optimality one can obtain the following universal kriging equations, depending on whether the residual is second-order stationary or intrinsic (Matheron, 1971; Goovaerts, 1997; Chilès and Delfiner, 2012):

- universal kriging with second-order stationary residual

$$\begin{bmatrix} C\,(x_\alpha - x_\beta) & f^s(x_\alpha) \\ f^s(x_\beta) & 0 \end{bmatrix} \times \begin{bmatrix} \lambda_\beta \\ \mu_l \end{bmatrix} = \begin{bmatrix} C\,(x_\alpha - x_0) \\ f^s(x_0) \end{bmatrix} \tag{3.10}$$

- universal kriging with intrinsic residual

$$\begin{bmatrix} \gamma\,(x_\alpha - x_\beta) & f^s(x_\alpha) \\ f^s(x_\beta) & 0 \end{bmatrix} \times \begin{bmatrix} \lambda_\beta \\ -\mu_l \end{bmatrix} = \begin{bmatrix} \gamma\,(x_\alpha - x_0) \\ f^s(x_0) \end{bmatrix} \tag{3.11}$$

Using universal kriging is not always straightforward. In fact, one of the main difficulties in the separation into drift and residual relates with variogram analysis. Indeed, due to the presence of the drift, the sample variogram of the original data is a biased estimator of the underlying variogram (Matheron, 1971; Chilès, 1977; Chilès and Delfiner, 2012).

In addition, even if one considers the variogram analysis of the residual instead of the original data, since this residual is unknown, one has to estimate it at the data locations. However, supposing that one estimates the drift and removes it from the data, the sample variogram of the estimated residual remains biased, especially at medium and large distances (Matheron, 1971; Chilès, 1977; Chilès and Delfiner, 2012). The inference of the variogram without bias can only be done in a few specific cases, such as having no drift along one direction of space (Journel and Huijbregts, 1978). The formalism of intrinsic random fields of order *k* explained in the next section is aimed at solving this inference problem while dealing with a more general class of non-stationary random fields.

3.2. Intrinsic random fields of order *k* (IRF-*k*)

3.2.1. Introduction

As mentioned in the previous section, if the assumption of second-order stationarity is not satisfied, one can work with the increments of the random field. In this case the increments fulfill the assumptions of second-order stationarity. However, there exist many natural phenomena with a clear trend, for which even the increments are not stationary. For instance, one can mention the following phenomena:

- In the geothermal reservoir modeling, temperature and pressure tend to increase with depth, whereas porosity and permeability tend to decrease (Chilès and Gable, 1984; Suárez Arriaga and Samaniego, 1998).
- In petroleum reservoir modeling, geometrical characteristics or petrophysical properties such as rock porosity present trends that cannot be dealt with stationary hypotheses (Chilès and Gable, 1984; Dimitrakopoulos, 1990).
- In groundwater hydrology, the hydraulic gradient is often responsible for a trend in the parameters that characterize an aquifer system (de Marsily, 1986; Dong, 1990; Kitanidis, 1983; Kitanidis, 1999; Le Cointe, 2006).

To overcome this problem, Matheron (1973) proposed the theory of intrinsic random fields of order *k*. The key idea of intrinsic random fields of order *k* is to work with higher order increments ("generalized increments") that can filter out the trend and be stationary. As an example, consider a non-stationary random field that presents a quadratic drift. In order to obtain a stationary random field one can calculate the increment of the initial random field. However, as can be seen in Figure 3.4A, even after calculating the increments, these are not stationary. So, one can go one step further and calculate the increments of the previous

increments in order to obtain stationary generalized increments. As shown in Figure 3.4B the results do not present drift and agree with an assumption of stationarity. In other words, by calculating twice the increments one obtains a stationary random field. Therefore, one can conclude that the original field is an intrinsic random field of order 1.

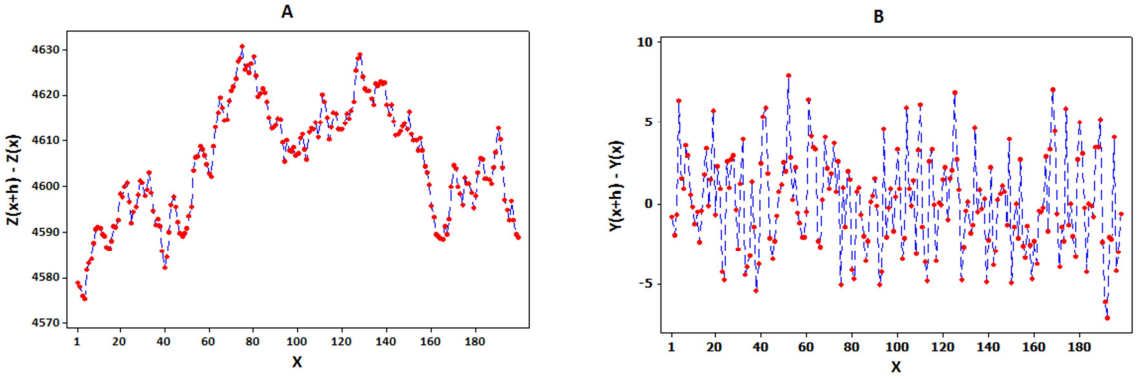

First increments $Y(x) = Z(x+h) - Z(x)$ Second increments $G(x) = Y(x+h) - Y(x)$

Figure 3.4: calculating first and second increments in order to obtain stationary generalized increments

3.2.2. Generalized increments of order k (authorized linear combinations of order k)

Under the standard intrinsic hypothesis, instead of dealing with the original random field, one deals with its increments. This procedure filters out the constant values and the modeling is done with the variogram instead of the covariance function. Intrinsic random fields of order *k* go one step further and try to filter out not only the constant value, but also all probable drift in the region under study, by working with higher – order increments (Matheron, 1973; Chilès, 1977; Chilès and Delfiner, 2012). In this respect, first of all, such an increment, also called a "generalized increment of order *k*" or an "authorized linear combination of order *k*" (ALC-*k*, for short), is defined as a system of weights and locations $\lambda = \{\lambda_i, x_i\}$, such that, for any monomial f^s of degree less than or equal to *k*, one has:

$$\sum_i \lambda_i f^s(x_i) = 0 \tag{3.12}$$

In other words, the authorized linear combinations of order 0 are increments that filter out the constant values and the authorized linear combinations of order *k* are generalized increments that filter out the polynomials of degree *k* or less.

In the following, it is shown that how authorized linear combinations of order *k* are formed in order to filter out the drift. As mentioned in the universal kriging model, suppose that, instead of a complete knowledge of the drift, its functional form is given:

$$f(x) = \sum_{s=0}^{S} b_s f^s(x) \tag{3.13}$$

where coefficients b_s are unknown.

The generalized increments are formed in such a way that the unknown drift coefficients b_s do not influence them. $\mathsf{Z}(\lambda)$ is such an increment if it is of the form:

$$\mathsf{Z}(\lambda) = \sum_{i=1}^{n} \lambda_i Z(x_i) \tag{3.14}$$

Here λ stands for the vector of weights (λ_1 ... λ_n), such that the value of the increment is independent of the drift. According to the concepts of IRF-*k*, the increment is independent of the unknown coefficients b_s of the drift if:

$$\sum_{i=1}^{n} \lambda_i f^s(x_i) = 0 \tag{3.15}$$

As a result, for all $p \leq k$ in the one-dimensional space:

$$\sum_{i=1}^{n} \lambda_i x_i^p = 0 \tag{3.16}$$

For all *p*, *q* such that $p + q \leq k$ in the two-dimensional space:

$$\sum_{i=1}^{n} \lambda_i x_i^p y_i^q = 0 \tag{3.17}$$

$$\sum_{i=1}^{n} \lambda_i x_i^p y_i^q = 0 \tag{3.18}$$

For all p, q, r such that $p + q + w \leq k$ in the three-dimensional space:

$$\sum_{i=1}^{n} \lambda_i x_i^p y_i^q z_i^r = 0 \tag{3.19}$$

There exists a criterion about the minimal number of locations that should be used for constructing a generalized increment of order k, which depends on the order k and on the workspace dimension (d). According to Chilès and Delfiner (2012), this minimal number of locations can be obtained from the following formula:

$$1 + \frac{(k+d)!}{k!\,d!} \tag{3.20}$$

Since the unbiasedness constraint of universal kriging is the same as the constraint of generalized increments of order k, one can use universal kriging for calculating weights of generalized increments. For this purpose, one just needs to predict the random field at a location from the values at the remaining locations, by universal kriging with any arbitrary covariance function. For instance, Figure 3.5 shows a configuration of eight locations. By performing universal kriging one can assign a weight for each location in order to construct a generalized increment of order k.

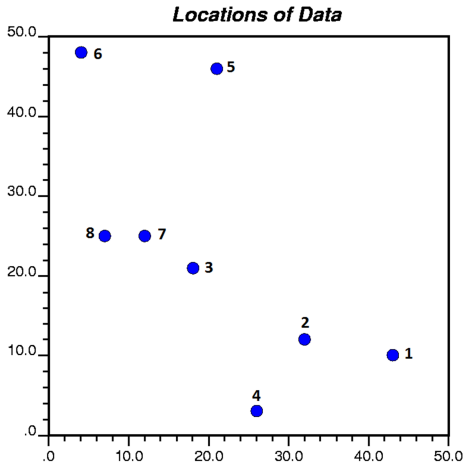

Figure 3.5: configuration of eight data

As can be seen in the next tables, the weight assigned to each data location varies from order to order (Tables 3.1 and 3.2).

Table 3.1: weights assigned to eight locations (order 1)

Location	**1**	**2**	**3**	**4**	**5**	**6**	**7**	**8**
Weights for order 1	-1	0.2942	0.2615	0.3838	0.8881	0.6786	0.4846	0.6318
	0.6062	-1	0.1612	0.2645	0.0743	0.3991	0.2184	0.1755
	0.1367	0.4378	-1	0.3373	0.0489	0.2644	0.0282	0.258
	0.012	0.1503	0.1314	-1	-0.2474	0.2296	0.047	-0.1222
	0.0672	0.0644	0.226	0.1942	-1	-0.1001	0.1311	0.0155
	0.1189	0.0163	0.0222	0.3614	0.2022	-1	0.1086	0.2636
	0.0221	0.105	0.0615	-0.3778	0.5916	-0.1844	-1	-0.2222
	0.0369	-0.068	0.1363	-0.1635	-0.5578	-0.2873	-0.0178	-1
Sum	**0**	**0**	**0**	**0**	**0**	**0**	**0**	**0**

Table 3.2: weights assigned to eight locations (order 2)

Location	**1**	**2**	**3**	**4**	**5**	**6**	**7**	**8**
Weights for order 2	-1	0.187	0.7322	4.5963	0.704	0.4443	0.4546	1.5609
	0.8025	-1	-0.0423	-1.7688	-1.0572	-4.0994	0.4771	-0.0946
	-0.0726	0.372	-1	-1.3284	14.5969	14.7234	-0.0023	-0.0475
	0.2611	0.6338	0.5618	-1	-5.8135	-12.8335	0.2238	-0.0425
	-0.0078	0.3875	-0.0479	-4.1194	-1	3.1834	0.0497	-1.0746
	0.099	-0.5419	0.0477	3.344	-15.4828	-1	-0.0968	0.2698
	0.0138	-0.0571	-0.1851	0.2239	5.5825	0.3647	-1	0.4286
	-0.0959	0.0186	-0.0665	0.0524	2.4702	-0.7829	-0.1062	-1
Sum	**0**	**0**	**0**	**0**	**0**	**0**	**0**	**0**

3.2.3. Definition of intrinsic random fields of order k (IRF-k)

From a mathematical viewpoint, a random field $Z = \{Z(x): x \in \mathbb{R}^d\}$ is an intrinsic random field of order k (shortly IRF-k) if its generalized increments of order k or authorized linear combinations of order k (ALC-k) have a zero expectation and a variance that is invariant under a spatial translation (Matheron, 1973; Chilès, 1977; Chilès and Delfiner, 2012).

If $\{\lambda_i, x_i\}$ is an ALC-k, then:

$$\forall h, \begin{cases} \mathrm{E}[\sum_i \lambda_i Z(x_i + h)] = 0 \\ \mathrm{var}\,[\sum_i \lambda_i Z(x_i + h)] \quad \text{does not depend on } h \end{cases}$$

In addition, according to the above definition, if Z_1 is an IRF-k, then for each random field Z_2 that differs from Z_1 by a polynomial of degree $\leq k$ and for each ALC-k $\lambda = \{\lambda_i, x_i\}$, one has:

$$\sum_i \lambda_i Z_1(x_i) = \sum_i \lambda_i Z_2(x_i) \tag{3.21}$$

This identity is due to the fact that the authorized linear combinations of order k filter out the polynomials of degree less than or equal to k, therefore Z_1 and Z_2 are indistinguishable if one only works with ALC-k.

One can therefore extend the definition of an IRF-k to an equivalence class of random fields that differ by a (deterministic or random) polynomial of degree less than or equal to k, and from which one member of the class is an IRF-k in the sense of the first definition. This amount to defining an IRF-k as an application Z on the class Λ_k of ALC-k such that:

$$\forall \lambda \in \Lambda_k,\ \mathsf{Z}(\lambda) = \textstyle\sum_i \lambda_i Z(x_i)$$

So, we can say that:

- $\mathsf{Z} = \{\mathsf{Z}(\lambda): \lambda \in \Lambda_k\}$ is an intrinsic random field of order k
- $Z = \{Z(x): x \in \mathbb{R}^d\}$ is a *representation* of this intrinsic random field.

In summary, the regionalized variable is viewed as one realization of one representation of an intrinsic random field of order *k*, which is a class of random fields defined up to a polynomial of degree less than or equal to *k*. Each element of the class generates the same generalized increments or authorized linear combinations of order *k*.

3.2.4. Generalized covariance

The spatial structure of a stationary random field $Z(x)$ is defined by its ordinary covariance function $C(h)$. In addition, the variogram $\gamma(h)$ can also be used as a structural analysis tool if only the increments of the random field are assumed stationary (intrinsic stationarity assumption). However, $\gamma(h)$ only allows calculating the variance of a linear combination whose weights sum up to zero, which are ALC-0. In the same manner when the stationary assumptions are limited to the generalized increments of order *k*, what characterizes the correlation structure of $Z(x)$ is a new function called the *generalized covariance* function and usually denoted by $K(h)$. For second-order stationary random fields, the generalized covariance is the usual covariance. For an IRF-0, the generalized covariance is minus the variogram, which is broader than the class of ordinary covariances (Chilès and Delfiner, 2012; Matheron, 1973). Just as there were more models for variograms than for covariance, there are more models for generalized covariances than for both ordinary covariances and variograms. In fact, the class of generalized covariances becomes broader and broader when *k* increases.

Let Z be an IRF-*k* and *Z* be one of its representations. From a mathematical point of view, a symmetric function $K(h)$ defined on $\mathbb{R}^d$ is called a generalized covariance of Z if:

$$\forall \lambda = \{\lambda_i, x_i\}_i \in \Lambda_k, \forall \mu = \left\{\mu_j, x_i'\right\}_i \in \Lambda_k$$

$$\mathrm{E}[\mathsf{Z}(\lambda)\mathsf{Z}(\mu)] = \mathrm{Cov}\left[\sum_i \lambda_i Z(x_i), \sum_j \mu_j Z(x_i')\right] = \sum_i \sum_j \lambda_i \mu_j K(x_i - x_i') \tag{3.22}$$

The variance of any ALC-*k* is:

$$\mathrm{E}[\mathsf{Z}(\lambda)^2] = \mathrm{var}\{\sum_i \lambda_i Z(x_i)\} = \sum_i \sum_j \lambda_i \lambda_j K(x_i - x_j) \tag{3.23}$$

In other words, one can calculate the variance of any linear combination of order *k* as if there exists an ordinary covariance function, but by replacing this hypothetical covariance by the generalized covariance $K(h)$.

In addition to all the ordinary covariances, which are also generalized covariances, specific generalized covariance models have been developed, such as (Figure 3.6):

- Power model $K(h) = (-1)^{k+1}|h|^{\alpha}$
  with $\alpha \in \mathbb{R}_+$ and $k \in \mathbb{N}$ such that $2k < \alpha < 2k + 2$

- Spline model $K(h) = (-1)^{k+1}|h|^{2k} \ln(|h|)$ with $k \in \mathbb{N}$

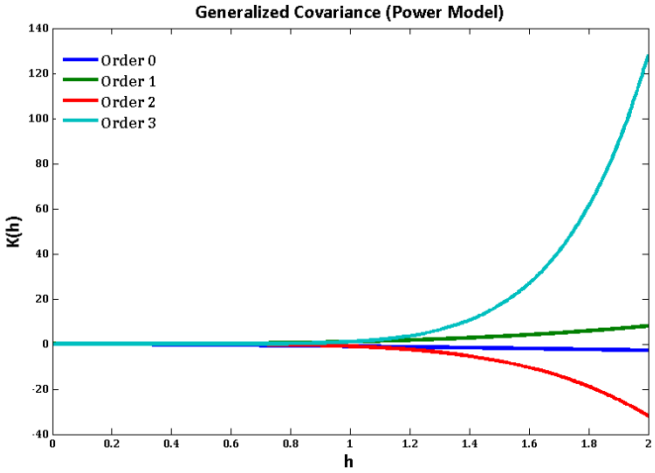

A

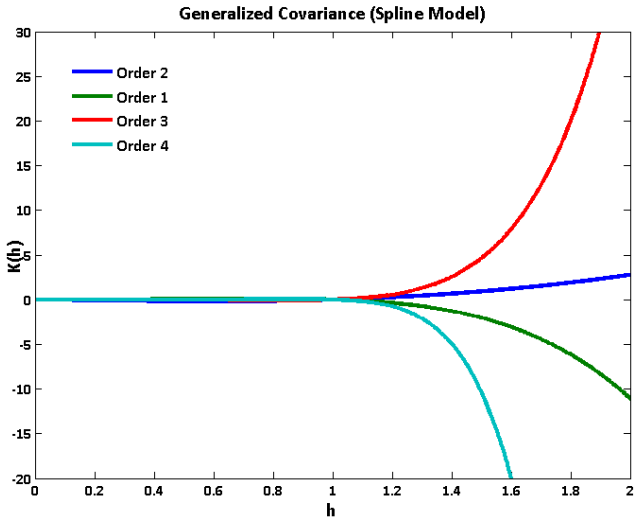

B

Figure 3.6: Generalized covariance of differents orders for the Power model (A) and Spline model (B)

Figure 3.7 shows realizations of (representations of) IRF-*k* with power or spline generalized covariance of different orders.

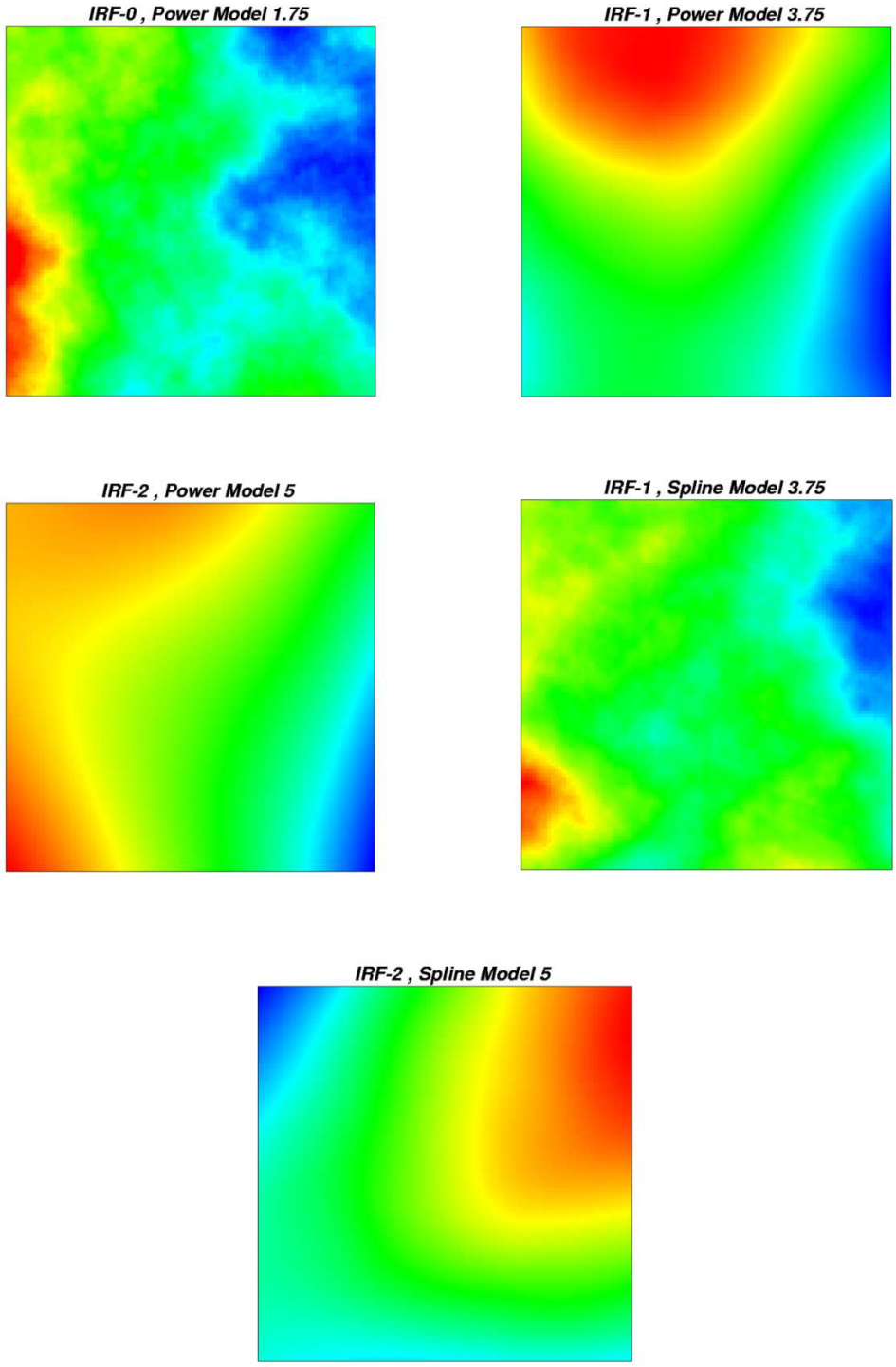

Figure 3.7: Examples of realizations of intrinsic random fields with power or spline generalized covariance

Several approaches have been proposed for identifying the generalized covariance function from a set of data on (a representation of) the intrinsic random field. Some of these approaches are non-parametric, i.e., do not presume that the generalized covariance belongs to a parametric family of functions (Cressie, 1987; Chilès and Gentier, 1993; Chiasson and Soulie, 1997; Huang et al., 2009), while others are essentially parametric and are often applicable only within the scope of automatic or semi-automatic structure identification (Delfiner, 1976; Chilès, 1977; Kitanidis, 1983, 1985; Marshall and Mardia, 1985; Stein, 1986; Renard, 1989; Zimmerman, 1989; Bruno and Raspa, 1993; Pardo-Igúzquiza, 1997; Kunsch et al., 1997; Cassiani and Christakos, 1998).

3.2.5. Generalized variogram

An important drawback of the generalized covariance is that one cannot calculate an experimental covariance and, as a result, one cannot choose and fit a model graphically. So, structure identification is not as straightforward or intuitive as in the stationary case. As a solution, one can use and work with the so-called generalized variogram instead of the generalized covariance (Chilès and Delfiner, 2012). The generalized variogram can be calculated experimentally and can be displayed and fitted graphically. The generalized variogram for different orders is presented in the following formulae:

$$k = 0 : \Gamma(h) = \frac{1}{2} Var[Z(x+h) - Z(x)] \tag{3.24}$$

$$k = 1 : \Gamma(h) = \frac{1}{6} Var[Z(x+2h) - 2\,Z(x+h) + Z(x)] \tag{3.25}$$

$$k = 2 : \Gamma(h) = \frac{1}{20} Var[Z(x+3h) - 3\,Z(x+2h) + 3\,Z(x+h) - Z(x)] \tag{3.26}$$

where $\Gamma(h)$ is the generalized variogram. The variance can be estimated experimentally by the mean squared value.

Also there is a relation between generalized covariance and generalized variograms through the following formulae (Chilès and Delfiner, 2012):

$$k = 1 : \Gamma(h) = K(0) - \frac{4}{3}K(h) + \frac{1}{3}K(2h) \tag{3.27}$$

$$k = 2 : \Gamma(h) = K(0) - \frac{3}{2}K(h) + \frac{3}{5}K(2h) - \frac{1}{10}K(3h) \tag{3.28}$$

3.2.6. Internal representation

Some representations of an IRF-*k* may be written as authorized linear combinations of order *k*, therefore they have a finite expectation, a finite variance and a finite covariance function (in general, this covariance is not stationary and is a function $C(x, x')$ rather than $C(x - x')$). Such representations are called internal representations.

For example, if $Z = \{Z(x): x \in \mathbb{R}^d\}$ is a representation of an IRF-0, then one can define another representation $Y = \{Y(x): x \in \mathbb{R}^d\}$ that differs by a constant value, by putting:

$$Y(x) = Z(x) - Z(x_0) \tag{3.29}$$

This second representation Y is an increment; therefore it has a finite expectation and a finite variance. Generally, if Z is a representation of an intrinsic random field of order *k* and $\lambda = \{\{\lambda_i, x_i\}_i; (-1, x)\} \in \Lambda_k$, , then an internal representation can be defined by putting:

$$Y(x) = Z(x) - \sum_i \lambda_i \, Z(x_i) \tag{3.30}$$

The covariance function of the internal representation $Y = \{Y(x): x \in \mathbb{R}^d\}$ can be expressed as if Z had a stationary covariance function, but replacing this hypothetical covariance by the generalized covariance. One finds:

$$\text{cov}\{Y(x), Y(\text{x}')\} = K(x - x') - \sum_i \lambda_i K(x_i - x) - \sum_i \lambda_i K(x_i - x') - \sum_i \sum_j \lambda_i \lambda_j \, K(x_i - x_j) \tag{3.31}$$

3.2.7. Intrinsic kriging

Consider that the regionalized variable under study is a representation of an IRF-*k* with known generalized covariance $K(h)$. Denote by $f^s(x)$ the basic functions (monomials of degree less than or equal to *k*) and by $K(x_a - x_\beta)$ the generalized covariance for the vector separating locations x_a and x_β. Also, let $x_1,\ldots, x_n$ be the data locations and x_0 the location targeted for prediction. According to the general rules of kriging (Matheron, 1971; Chilès and Delfiner, 2012), four restrictions should be fulfilled in order to deduce the final kriging system:

- Linearity
  The predictor at location x_0 is of the form:

$$Z^*(x_0) = \sum_{\alpha=1}^{n} \lambda_i Z(x_\alpha) \tag{3.32}$$

  where $\{\lambda_\alpha : \alpha = 1 \ldots n\}$ are weights to be defined later.

- Authorization
  One has to be sure that the prediction error has a finite expectation and a finite variance. Therefore, the error must be an ALC-*k*, which entails the following conditions:

$$\sum_{\alpha=1}^{n} \lambda_\alpha f^s(x_\alpha) = f^s(x_0) \tag{3.33}$$

- Unbiasedness
  The prediction error should have a zero expectation. As any ALC-*k* has a zero expectation, this constraint is automatically fulfilled.

- Optimality
  One wants that the prediction error has a minimal variance. Because the variance of an ALC-*k* can be calculated as if there exists a covariance, by replacing this covariance by the generalized covariance, one has:

$$\text{var}\{Z(x_0), Z(x_0')\} = K(0) + \sum_{\alpha=1}^{n}\sum_{\beta=1}^{n}\lambda_\alpha\lambda_\beta\, K(x_\alpha - x_\beta) - 2\sum_{\alpha}\lambda_\alpha K(x_\alpha - x_0) \qquad (3.34)$$

To minimize this variance under the authorization constraint (3.33), one has to introduce Lagrange multipliers. One finds:

$$\forall\alpha = 1 \ldots n, \sum_{\beta=1}^{n}\lambda_\beta K(x_\alpha - x_\beta) + \sum_{l}\mu_l f^l(x_\alpha) = K(x_\alpha - x_0) \qquad (3.35)$$

Therefore, the system of equations to determine the kriging weights is as follows (Chauvet, 1999; Wackernagel, 2003; Chilès and Delfiner, 2012):

$$\begin{bmatrix} K(x_\alpha - x_\beta) & f^s(x_\alpha) \\ f^s(x_\beta) & 0 \end{bmatrix} \times \begin{bmatrix} \lambda_\beta \\ \mu_l \end{bmatrix} = \begin{bmatrix} K(x_\alpha - x_0) \\ f^s(x_0) \end{bmatrix} \qquad (3.36)$$

where μ_l are Lagrange multipliers. As can be seen, the system of intrinsic kriging is the same as the one of universal kriging, with the difference that one should substitute the generalized covariance for the ordinary covariance or the variogram.

3.2.8. Simulation of an IRF-k with Gaussian generalized increments

Several approaches have been developed for simulating intrinsic random fields of order *k* with Gaussian generalized increments (i.e., such that the finite-dimensional distributions of the generalized increments are multivariate Gaussian). Among these, let us mention:

- Sequential approaches (Chilès, 1995)
- Dilution approaches (Chilès, 1995; Chilès and Delfiner, 2012)
- Discrete spectral approaches (Chilès, 1995; Stein, 2001, 2002)
- Continuous spectral approaches (Emery and Lantuéjoul, 2008; Arroyo and Emery, 2016a, 2016b)
- Turning bands (Chilès, 1977; Dimitrakopoulos, 1990; Emery and Lantuéjoul, 2006)
- Gibbs sampling (Arroyo and Emery, 2015).

Continuous spectral approaches will be used in this thesis, insofar as they have proven to be computationally efficient, applicable to large-scale problems and to multivariate simulation, and accurate in the reproduction of the desired generalized covariance structure. The reader is referred to the next chapter for deeper algorithmic details.

Apart from the Gibbs sampler, the aforementioned approaches produce non-conditional realizations. To condition the realizations to existing data, a post-processing stage is needed (Delfiner, 1976; Chilès and Delfiner, 2012), based on the kriging of the residuals between the conditioning data values and the simulated values at the data locations. This is similar to the procedure used for conditioning realizations of stationary Gaussian random fields, except that here intrinsic kriging has to be used instead of simple kriging in the residual kriging stage.

Chapter 4: Methodology

In this chapter we explain the proposed method for the joint simulation of continuous and categorical variables when the categorical variable is represented by a non-stationary random field. To this end, this chapter is divided into two main parts. In the first part, it is explained how to infer the model parameters. The second part is dedicated to explain the algorithm used to simulate the continuous and categorical variables.

1. Inference of model parameters

The inference of model parameters consists of three steps: inference of the grade model, inference of the rock type model, and inference of the cross-correlation structure.

1.1. Inference of the grade model

As the grade (continuous variable) is viewed as a realization of a stationary random field, there is no difficulty in the process of determining the parameters of this variable, based on the multigaussian model explained in Chapter 2. First, one has to transform the grade data into standard Gaussian data and then calculate the experimental variogram (or covariance) of the transformed Gaussian data. Then, one fits a theoretical model to the experimental variogram (covariance) and obtains the parameters for the grade model.

In the following, we will denote by Y_0 the stationary Gaussian random field associated with the grade and by $K_0(h)$ its stationary covariance function.

1.2. Inference of the rock type model

The following presentation is limited to the case of two rock types obtained by truncating a single intrinsic random field of order k, but the formalism could be extended to more rock types by considering the truncation of several intrinsic random fields (plurigaussian model) instead of a single one.

In the stationary case, there exists a one-to-one relation between the covariance function $\rho(h)$ of a Gaussian random field and the covariance function $C_y(h)$ of an indicator random field obtained by truncation (Equation 2.11). This relation can be expressed by means of an expansion using Hermite polynomials (Matheron, 1975; Chilès and Delfiner, 2012):

$$C_y(h) = g(y)^2 \sum_{p=1}^{+\infty} \frac{1}{p} H_{p-1}^2(y)[\rho(h)]^p \tag{4.1}$$

where $\{H_p: p \in \mathbb{N}\}$ are Hermite polynomials, y is the truncation threshold, and g is the standard Gaussian probability density function.

When one considers a non-stationary random field (namely, an IRF-*k* with Gaussian generalized increments) instead of a stationary one, the spatial structure is no longer described by an ordinary covariance function and one should work with a generalized covariance that has no any clear relation with the indicator covariance.

To overcome this difficulty, one can take advantage of an interesting characteristic of an intrinsic random field of order *k*, which is the concept of internal representation that was explained in the previous chapter. Such an internal representation of an intrinsic random field of order *k* will play a key role in the inference of the rock type model. As a matter of fact, because an internal representation is written as an authorized linear combination of order *k*, it has a finite covariance function that can be associated with the covariance function of the indicator random field obtained by truncation. In the following, let $Z = \{Z(x): x \in \mathbb{R}^d\}$ be a representation of an intrinsic random field of order *k*, $\mathsf{Z} = \{\mathsf{Z}(\lambda): \lambda \in \Lambda_k\}$, with generalized covariance $K_1(h)$ and Gaussian generalized increments, and truncate it at a given threshold *z*:

$$I_z(x) = \begin{cases} 1 & \text{if } Z(x) < z \\ 0 & \text{otherwise} \end{cases} \tag{4.2}$$

An internal representation of the same IRF-*k* can be obtained by putting:

$$Y_1(x) = Z(x) - \sum_{\mathrm{i}=1}^{\mathrm{n}} \lambda_i(x) Z(x_\mathrm{i}) \tag{4.3}$$

where $\{x_\mathrm{i}: \mathrm{i} = 1, \ldots, \mathrm{n}\}$ are given (fixed) locations, while $\lambda_\mathrm{i}(x)$ is the universal kriging weight assigned to location x_i when predicting location x with a pure nugget effect model (Equation 3.10):

$$\begin{pmatrix} \mathrm{I}_n & \mathrm{F}_0^T \\ \mathrm{F}_0 & 0_{L,L} \end{pmatrix} \begin{pmatrix} \Lambda(x) \\ \mathrm{M}(x) \end{pmatrix} = \begin{pmatrix} 0_{n,1} \\ \mathrm{F}(x) \end{pmatrix} \tag{4.4}$$

where $L = \frac{(k+d)!}{k!d!}$ is the total number of basic drift functions $\{\mathrm{f}_l: l = 1 \ldots L\}$ associated with the chosen order *k* and workspace dimension *d*, I_n is the identity matrix with size $n \times n$, $0_{p,q}$ is the zero matrix with size $p \times q$, F_0 is the $L \times n$ matrix with $\mathrm{f}^l(x_\mathrm{i})$ as the entry at

row l and column i, $\mathrm{F}(x)$ is the $L \times 1$ vector with entry $\mathrm{f}^l(x)$ at row l, $\Lambda(x)$ is the $n \times 1$ vector of universal kriging weights, and $\mathrm{M}(x)$ is a $L \times 1$ vector of Lagrange multipliers. Using the formula giving the inverse of a 2 × 2 block matrix (Bernstein, 2005), one finds:

$$\Lambda(x) = \mathrm{F}_0^T(\mathrm{F}_0\mathrm{F}_0^T)^{-1}\,\mathrm{F}(x) \tag{4.5}$$

Denoting by Z_0 the $n \times 1$ vector with entry $Z(x_\mathrm{i})$ at row i, one therefore has:

$$Y_1(x) = Z(x) - Z_0^T\mathrm{F}_0^T(\mathrm{F}_0\mathrm{F}_0^T)^{-1}\mathrm{F}(x) \tag{4.6}$$

As can be seen, $Y_1(x)$ differs from $Z(x)$ by a combination of the components of $\mathrm{F}(x)$, i.e., by a polynomial function of the coordinates of x, so that Y_1 is a representation of the same IRF-k Z as Z. Furthermore, the expression of $Y_1(x)$ is equal to a universal kriging error, which is an authorized linear combination of order k, which means that Y_1 has zero mean, finite variance and ordinary covariance function. Hence $Y_1 = \{Y_1(x)\colon x \in \mathbb{R}^d\}$ is an internal representation of Z.

Recall that the minimal number of locations $\{x_\mathrm{i}\colon \mathrm{i} = 1, \ldots, \mathrm{n}\}$ necessary for constructing an internal representation depends on the workspace dimension (d) and order of intrinsic random field of order k and can be calculated from the following equation (Chilès and Delfiner, 2012):

$$n \geq L = \frac{(k+d)!}{k!\,d!} \tag{4.7}$$

Now, the indicator (Equation 4.2) can be rewritten as:

$$I_z(x) = \begin{cases} 1 & \text{if} \quad Y_1(x) < z - p(x) \\ 0 & \text{otherwise} \end{cases} \tag{4.8}$$

where $p(x) = Z_0^T\mathrm{F}_0^T(\mathrm{F}_0\mathrm{F}_0^T)^{-1}\mathrm{F}(x)$ is a polynomial with random coefficients of the coordinates of x. The internal representation Y_1 is a Gaussian random field, with zero mean and with a (non-stationary) covariance function $C_1(x, x')$ that can be expressed as a function of the generalized covariance $K_1(h)$ of Z:

$$\begin{aligned} C_1(x, x') = {} & K_1(x - x') \\ & - \sum\nolimits_i \lambda_i K_1(x_i - x) - \sum\nolimits_i \lambda_i K_1(x_i - x') - \sum\nolimits_i \sum\nolimits_j \lambda_i \lambda_j K_1(x_i - x_j) \end{aligned} \tag{4.9}$$

The internal representation Y_1 can now be standardized to a unit variance by putting:

$$\tilde{Y}_1(x) = \frac{Y_1(x)}{\sqrt{C_1(x,x)}} \tag{4.10}$$

The covariance function of $\tilde{Y}_1$ is:

$$\rho_1(x,x') = \frac{C_1(x,x')}{\sqrt{C_1(x,x)}\sqrt{C_1(x',x')}} \tag{4.11}$$

Now Equation (4.8) can be rewritten as follows:

$$I_z(x) = \begin{cases} 1 & \text{if} \quad \tilde{Y}_1(x) < y(x) \\ 0 & \text{otherwise} \end{cases} \tag{4.12}$$

with

$$y(x) = \frac{z - p(x)}{\sqrt{C_1(x,x)}} \tag{4.13}$$

Recalling the relationship between the covariance function of a standard Gaussian random field ($\tilde{Y}_1$) and its indicator (Equation 4.1) one obtains:

$$C_z(x,x') = \sum_{p=1}^{+\infty} H_{p-1}\big(y(x)\big) H_{p-1}\big(y(x')\big)\, g\big(y(x)\big) g(y(x'))[\rho_1(x,x')]^p \tag{4.14}$$

Finally, the non-centered indicator covariance between any two locations x and x' can be expressed as:

$$E\{I_z(x)\, I_z(x')\} = C_z(x,x') + G(y(x))G(y(x')) \tag{4.15}$$

where G is the standard Gaussian cumulative distribution function.

The right-hand side of Equation (4.15) depends on the generalized covariance function K_1, the locations $\{x_\mathrm{i}: \mathrm{i} = 1 \ldots \mathrm{n}\}$ and weights $\{\lambda_\mathrm{i}(x): \mathrm{i} = 1, \ldots, \mathrm{n}\}$ used to construct the internal representation (known), as well as the truncation threshold z and vector Z_0 (through the difference $z - p(x)$ that defines the numerator of $y(x)$ in Equation (4.13)), while the left-

hand side can be calculated experimentally for each pair of data locations, for which the indicator (0 or 1) is known.

Accordingly, if the generalized covariance K_1 can be parameterized through a few parameters (e.g., by considering a set of known basic nested models weighted by unknown nonnegative coefficients), one can estimate these parameters jointly with the truncation threshold z and vector Z_0 by least squares fitting, in order to find the parameters that minimize the sum of squared errors between the theoretical covariances (Equation 4.15) and their experimental estimates.

The following table summarizes the main tools that have been used in this subsection for rock type modeling.

Table 4.1: Random fields, covariance tools and truncation thresholds used for rock type modeling

Random field	**Notation**	**Spatial correlation structure**	**Truncation threshold**
Representation of IRF-*k*	$Z(x)$	$K_1(x-x')$	z
Internal representation	$Y_1(x)$	$C_1(x,x')$	$z-p(x)$
Standardized internal representation	$\tilde{Y}_1(x)$	$\rho_1(x,x')$	$\frac{z-p(x)}{\sqrt{C_1(x,x)}}$
Indicator	$I_z(x)$	$C_z(x,x')$	

The above approach for inferring $K_1(h)$ slightly differs from the one recently proposed by Madaniesfahani (2016), although both approaches rely on the passage from the initial representation of the intrinsic random field of order *k* to an internal representation of it, in order to establish a link between the generalized covariance $K_1(h)$ and the indicator covariance $C_z(x,x')$. In the approach by Madaniesfahani (2016), the internal representation Y_1 is constructed by choosing $\{x_i: i = 1, \dots, n\}$ among the data locations and the values of the truncation threshold *z* and of vector Z_0 are fixed, so that $z - p(x) = -1$. The approach proposed here does not make such assumptions and is more general.

1.3. Inference of the cross-correlation structure

The key assumption in the inference of the cross-correlation structure is that the joint distribution of the stationary random field Y_0 associated with the grade and the generalized increments of the IRF-k Z (in particular, the internal representation Y_1 and its standardized version $\tilde{Y}_1$) are multivariate Gaussian.

Let $K_{10}(h)$ be the generalized cross-covariance between Z and Y_0. The cross covariance C_{10} between the internal representation Y_1 and Y_0 can be expressed as a function of K_{10} and of the locations $\{x_i : i = 1, \dots, n\}$ and weights $\{\lambda_i(x) : i = 1, \dots, n\}$ used to construct the internal representation:

$$\begin{aligned} C_{10}(x, x') &= \operatorname{cov}\left\{Z(x) - \sum_{i=1}^{n} \lambda_i(x) Z(x_i), Y_0(x')\right\} \\ &= K_{10}(x - x') - \sum_{i=1}^{n} \lambda_i(x) K_{10}(x_i - x') \end{aligned} \tag{4.16}$$

Likewise, the cross covariance between the standardized internal representation $\tilde{Y}_1$ and Y_0 is:

$$\rho_{10}(x, x') = \frac{C_{10}(x, x')}{\sqrt{C_1(x, x)}} \tag{4.17}$$

Now, there exists a relationship linking this cross covariance ρ_{10} and the cross covariance between Y_0 and the indicator random field defined in Equations (4.2) and (4.12). To establish this relationship, let us expand the indicator into Hermite polynomials:

$$\begin{aligned} &\operatorname{cov}\{1_{\tilde{Y}_1(x) < y(x)}, Y_0(x')\} \\ &= \operatorname{cov}\left\{G(y) + \sum_{p=1}^{\infty} \frac{1}{\sqrt{p}} H_{p-1}(y(x)) g(y(x)) H_p(\tilde{Y}_1(x)),\ Y_0(x')\right\} \end{aligned}$$

Since the Hermite polynomial of degree 1 is equal to minus the identity function, one has:

$$Y_0(x') = -H_1(Y_0(x'))$$

Accounting for the fact that the Hermite polynomials applied to jointly Gaussian random fields do not have any cross-correlation unless they have the same degree (Rivoirard, 1994) and that H_0 is identically equal to 1, it comes:

$$\begin{aligned} C_{z,0}(x,x') &= \mathrm{cov}\{1_{\tilde{Y}_1(x)<y(x)}, Y_0(x')\} \\ &= -\,g\big(y(x)\big)\,\mathrm{cov}\{H_1(\tilde{Y}_1(x)), H_1(Y_0(x'))\} \\ &= -\,g\big(y(x)\big)\,\mathrm{cov}\{\tilde{Y}_1(x), Y_0(x')\} \end{aligned}$$

Using Equation (4.17), one finally has:

$$C_{z,0}(x,x') = -\,g\big(y(x)\big)\,\rho_{10}(x,x') \qquad (4.18)$$

The right-hand side of Equation (4.18) depends on the generalized cross covariance K_{10}, the locations $\{x_i: i = 1 \ldots n\}$ and weights $\{\lambda_i(x): i = 1, \ldots, n\}$ used to construct the internal representation, as well as the truncation threshold z and vector Z_0 (through the difference $z - p(x)$ that defines the numerator of $y(x)$ in Equation (4.13)), while the left-hand side can be calculated experimentally for each pair of data locations by knowing the values of the indicator (0 or 1) and the Gaussian transforms of the grade data.

Therefore, as in the previous subsection, if the generalized cross covariance K_{10} can be parameterized through a few parameters, one can estimate these parameters jointly with the truncation threshold z and vector Z_0 by least squares fitting, in order to find the parameters that minimize the sum of squared errors between the theoretical cross covariances (Equation 4.18) and their experimental estimates.

The following table summarizes the main tools that have been used in this subsection for modeling the cross-correlation structure between grade and rock type.

Table 4.2: Random fields, covariance tools and truncation thresholds used for modeling the cross-correlation between grade and rock type

Gaussian random field associated with grade	**Notation**	**Random field associated with rock type**	**Notation**	**Spatial cross-correlation structure**
Stationary Gaussian random field	$Y_0(x)$	Representation of IRF-*k*	$Z(x)$	$K_{10}(x-x')$
		Internal representation	$Y_1(x)$	$C_{10}(x,x')$
		Standardized internal representation	$\tilde{Y}_1(x)$	$\rho_{10}(x,x')$
		Indicator	$I_z(x)$	$C_{z,0}(x,x')$

1.4. Summary

Because they involve some common parameters (truncation threshold *z* and vector Z_0), the inference of the rock type model (generalized direct covariance K_1) and the inference of the cross-correlation model (generalized cross-covariance K_{10}) should be performed jointly in a single least squares fitting process.

In summary, the steps to follow in order to infer both generalized covariances are:

- Choose an order *k* for the intrinsic random field Z that will yield the rock type after truncation.

- Choose a set of locations $\{x_i: i = 1 \ldots n\}$ on which to construct the internal representation Y_1.

- Choose basic nested structures for the direct and cross covariance models, including the ordinary direct covariance $K_0(h)$ (associated with grade), the generalized direct covariance $K_1(h)$ (associated with rock type) and the generalized cross covariance $K_{10}(h)$. The unknowns are all or part of the parameters of these nested structures: sills, slopes, scale parameters, shape parameters or exponents.

- Calculate the experimental non-centered covariance matrix of the indicator data (the matrix entries are 1 or 0) and experimental cross covariance of the indicator data and transformed grade data.

- Calculate the theoretical covariance matrix of the indicator data and the theoretical cross covariance of indicator and transformed grade data, as per Equations (4.15) and (4.18). The entries of these two matrices depend on the parameters to be fitted.

- Find the covariance parameters, truncation threshold z and vector Z_0 that minimize the total sum of squared errors between the experimental and theoretical direct and cross covariance matrices.

Note that vector Z_0 varies from one realization to another, as it depends on the values of the initial representation of the intrinsic random field Z at the chosen locations $\{x_{\mathrm{i}}: \mathrm{i} = 1, \dots, \mathrm{n}\}$, while the parameters of the generalized direct and cross covariances $K_1(h)$ and $K_{10}(h)$ are the same for all the realizations of this intrinsic random field. Therefore, it is convenient to keep only the latter parameters for the simulation stage and "forget" the value of Z_0 delivered by the least-squares fitting algorithm.

Also, as the truncation threshold z and vector Z_0 are not fitted independently, but through the difference $z - p(x)$ that defines the numerator of $y(x)$ in Equation (4.13), the value of the truncation threshold z remains undetermined. This indetermination is actually not an issue, as it has no relevance on the model. Indeed, instead of truncating the initial representation Z at threshold z (Equation 4.2), one can use another representation of the same intrinsic random field of order k equal to $Z - z$ with a truncation threshold equal to zero. Put in other words, up to a change in the representation of the intrinsic random field of order k, Z, the truncation threshold can be set to zero without any loss of generality.

1.5. Examples of bivariate covariance models

In this thesis, we will suppose that the stationary random Gaussian field Y_0 associated with the grade has a Matérn (K-Bessel) covariance function $K_0(h)$, the non-stationary random field Z to truncate (representation of the IRF-k associated with rock type) has a power generalized covariance $K_1(h)$, and the generalized cross-covariance between both fields $K_{10}(h)$ is a Matérn (K-Bessel) model. The Matérn model is chosen because of its versatility (it depends on a shape parameter that controls the behavior of the covariance at the origin; also, the well-known exponential and Gaussian covariance models are particular cases of the Matérn model). In this section, all these covariances are further assumed to have a unit scale parameter, but this parameter can be modified to any other value, possibly depending on the direction of space in order to model geometric or zonal anisotropies.

So, the matrix of generalized direct and cross covariances has the following form:

$$C(h) = \begin{pmatrix} K_0(h) & K_{10}(h) \\ K_{01}(h) & K_1(h) \end{pmatrix} = \begin{pmatrix} K_{Bessel_{00}} & K_{Bessel_{10}} \\ K_{Bessel_{01}} & K_{Power_{11}} \end{pmatrix} \tag{4.19}$$

Since the spectral - turning bands method will be used for simulating the random fields, one needs to determine the spectral density corresponding to each covariance or generalized covariance function. The corresponding spectral density matrix of the above covariance matrix is:

$$\mathrm{f}(\omega) = \begin{pmatrix} f_{B_{00}} & f_{B_{10}} \\ f_{B_{01}} & f_{P_{11}} \end{pmatrix} \tag{4.20}$$

where:

$f_{B_{00}}$ is the spectral density for the Matérn direct covariance

$f_{P_{11}}$ is the spectral density for the power generalized direct covariance

$f_{B_{01}}$ and $f_{B_{10}}$ are the spectral densities for the Matérn generalized cross covariance.

For having an admissible model, the only restriction is to define the elements of the matrix in order to meet the positive semi-definiteness condition for the spectral density matrix. It means that one should fulfill the following condition:

$$f_{B_{00}} \times f_{P_{11}} \geq f_{B_{10}} \times f_{B_{01}} \tag{4.21}$$

The spectral densities of the Matérn model with sill c_{00} and shape parameter μ_{00} and of the power model with slope c_{11} and exponent α_{11} have the following expressions (Lantuéjoul, 2002; Chilès and Delfiner, 2012; Arroyo and Emery, 2016a):

$$f_{Bessel}(\omega) = c_{00} \frac{\Gamma(\mu_{00} + 1.5)}{\Gamma(\mu_{00})\pi^{1.5}} \frac{1}{(1 + ||\omega||^2)^{\mu_{00}+1.5}} \tag{4.22}$$

$$f_{Power}(\omega) = c_{11} \frac{\Gamma(\frac{\alpha_{11}}{2} + 1)\Gamma(\frac{\alpha_{11}+3}{2})}{\Gamma\left(\frac{\alpha_{11}}{2} - k\right)\Gamma\left(1 - \frac{\alpha_{11}}{2} + k\right)\pi^{\alpha_{11}+1.5}} \frac{1}{\left(\frac{||\omega||}{2\pi}\right)^{\alpha_{11}+3}(2\pi)^3} \tag{4.23}$$

where k is the integer part of $\frac{\alpha_{11}}{2}$.

Therefore, in order to fulfill condition (4.21), one must have:

$$c_{00}\frac{\Gamma(\mu_{00}+1.5)}{\Gamma(\mu_{00})\pi^{1.5}}c_{11}\frac{\Gamma(\frac{\alpha_{11}}{2}+1)\Gamma(\frac{\alpha_{11}+3}{2})}{\Gamma\left(\frac{\alpha_{11}}{2}-k\right)\Gamma\left(1-\frac{\alpha_{11}}{2}+k\right)\pi^{\alpha_{11}+1.5}}\frac{1}{(1+||\omega||^2)^{\mu_{00}+1.5}\left(\frac{||\omega||}{2\pi}\right)^{\alpha_{11}+3}(2\pi)^3}$$
$$\geq {c_{10}}^2\frac{\Gamma^2(\mu_{10}+1.5)}{\Gamma^2(\mu_{10})\pi^3}\frac{1}{(1+||\omega||^2)^{2\mu_{10}+3}}$$

where c_{10} and μ_{10} represent the sill and shape parameter of the Matérn cross-covariance.

After simplification, one reaches the following two constraints:

- First condition

$$4\mu_{10}-2\mu_{00}\geq\alpha_{11} \tag{4.24}$$

- Second condition

$${c_{10}}^2\leq c_{00}\,c_{11}\frac{\Gamma(\mu_{00}+1.5)}{\Gamma(\mu_{00})}\frac{\Gamma\left(\frac{\alpha_{11}}{2}+1\right)\Gamma\left(\frac{\alpha_{11}+3}{2}\right)}{\Gamma\left(\frac{\alpha_{11}}{2}-k\right)\Gamma\left(1-\frac{\alpha_{11}}{2}+k\right)}\frac{\Gamma^2(\mu_{10})}{\Gamma^2(\mu_{10}+1.5)}\,2^{\alpha_{11}} \tag{4.25}$$

where

c_{00} and c_{10} are the sills of the Matérn direct and cross covariances

c_{11} is the slope of the power direct covariance

μ_{00} is the shape parameter of the Matérn direct covariance

μ_{10} is the shape parameter of the Matérn cross covariance

α_{11} is the exponent of the power direct covariance.

In a nutshell, one first needs to know the analytical expression of the spectral densities of the direct and cross covariance matrix and then, by considering conditions (4.24) and (4.25), find suitable covariance parameters (c_{00}, c_{11}, c_{10}, μ_{00}, μ_{10}, α_{11}). The parameters associated with the grade (c_{00} and μ_{00}) can be fitted on the basis of the experimental covariance or variogram of the transformed grade data, whereas the remaining parameters are unknown and should be fitted by least squares optimization based on Equations (4.15) and (4.18) (see previous subsections for details).

2. Joint simulation

2.1. Non-conditional simulation

After determining the model parameters, one can jointly simulate the two random fields Y_0 and Z based on the spectral - turning bands algorithm. This algorithm has been chosen in this thesis because it is very computationally fast, flexible (simulation can be performed at as many locations as desired, irrespective of their spatial configuration) and accurate, in the sense that the simulated fields have the desired covariances or generalized covariances.

To this end, the algorithm proposed by Emery et al. (2016) and presented in Chapter 2 can be generalized to the multivariate case, i.e., to the simulation of a vector random field instead of a scalar random field: one has to replace the square root in Equation (2.9) by a Cholesky factor, insofar as the spectral density $f(\omega)$ is no longer a scalar, but a positive semi-definite matrix. Therefore, one can simulate any vector random field whose direct and cross covariance functions are continuous and absolutely integrable, provided that one knows the analytical expression of their spectral densities, without the need for these spectral densities to have a bounded support. The only restriction is that the support of the density g of the simulated frequency vectors contains the support of f.

An extension of this method has recently been proposed by Arroyo and Emery (2016a) for simulating intrinsic random fields of order 0, which uses the spectral densities associated with their variograms (generalized covariance of order 0) instead of that of the ordinary covariances. We can furthermore extend this method for simulating an intrinsic random field of order k (with $k > 0$) by considering the spectral representation of their generalized covariances, as introduced in Matheron (1973) and Chilès and Delfiner (2012). First, let us explain in more detail the method of Arroyo and Emery (2016a).

For any $x \in \mathbb{R}^d$, let us define a multivariate random field with P scalar components in the d-dimensional Euclidean space as follows:

$$Y(x) = \sum_{p=1}^{P} \alpha_p(\omega_p)\,(\cos(2\pi < x, \omega_p > + \phi_p) - \cos(\phi_p)) \tag{4.26}$$

where

- $<,>$ represents the inner product in $\mathbb{R}^d$
- $\omega_p : p = 1, \dots, P$ are independent random vectors (frequencies) with probability density g in $\mathbb{R}^d$

- $\phi_p : p = 1, \dots, P$ are independent random variables (phases) uniformly distributed over $[0, 2\pi]$
- $\alpha_p : p = 1, \dots, P$ are vector-valued mappings with P real-valued components.

In order to characterize the simulated vector random field Y, let us calculate its matrix of direct and cross variograms. In the following, let define $\Upsilon(h)$ the $P \times P$ matrix of direct (diagonal terms) and cross (off-diagonal terms) variograms of Y:

$$\Upsilon(h) = \frac{1}{2} E\{[Y(x+h) - Y(x)][Y(x+h) - Y(x)]^T \tag{4.27}$$

where ^{T} indicates vector transposition (one should actually write Υ as a function of x and $x+h$, but we will see later that it actually depends only on the separation vector h, therefore the simulated field is intrinsic of order 0).

By elementary calculations, one obtains:

$$\Upsilon(h) = 2E\{[\sum_{p=1}^{P} \alpha_p(\omega_p) \sin(\pi < 2x + h, \omega_p > + \phi_p) \sin(\pi < h, \omega_p >)]$$

$$\times [\sum_{q=1}^{P} \alpha_q(\omega_q) \sin(\pi < 2x + h, \omega_q > + \phi_q) \sin(\pi < h, \omega_q >)]^T\}$$

$$= 2E\{\sum_{p=1}^{P} \sum_{q=1}^{P} \alpha_p(\omega_p) \alpha_q(\omega_q)^T \sin(\pi < h, \omega_p >) \sin(\pi < h, \omega_q >)$$

$$\times \sin(\pi < 2x + h, \omega_p > + \phi_p) \sin(\pi < 2x + h, \omega_q > + \phi_q)\}$$

Since $\phi_p : p = 1, \dots, P$ are independent and uniformly distributed in $[0, 2\pi]$, the only terms that do not vanish in the previous sums are found when $p = q$. Therefore, the previous equation can be simplified into:

$$\Upsilon(h) = 2E\{\sum_{p=1}^{P} \alpha_p(\omega_p)\alpha_p(\omega_p)^T \sin^2(\pi < h, \omega_p >) \sin^2(\pi < 2x + h, \omega_p > + \phi_p)\}$$

$$= \sum_{p=1}^{P} E\{\alpha_p(\omega_p)\alpha_p(\omega_p)^T\} \sin^2(\pi < h, \omega_p >)$$

$$= \int \sum_{p=1}^{P} \alpha_p(\omega)\alpha_p(\omega)^T \frac{1 - \cos(2\pi < h, \omega >)}{2} \mathrm{g}(\omega)\mathrm{d}\omega$$

So, the $P \times P$ matrix of direct and cross variograms $\Upsilon(h)$ becomes:

$$\Upsilon(h) = \int A(\omega)A^T(\omega) \frac{1 - \cos(2\pi < h, \omega >)}{2} \mathrm{g}(\omega)\mathrm{d}(\omega) \tag{4.28}$$

where $A(\omega)$ is the $P \times P$ matrix whose p-th column is $\alpha_p(\omega)$.

Now let us compare this expression with the spectral representation of a variogram (Matheron, 1973; Chilès and Delfiner, 2012):

$$\gamma(h) = \int \frac{1 - \cos(2\pi < \mathrm{h}, \omega >)}{4\pi^2 \parallel \omega \parallel^2} \chi(\mathrm{d}\omega)$$

where χ is a positive symmetric measure with no atom at the origin such that:

$$\int \frac{\chi(\mathrm{d}\omega)}{1 + 4\pi^2 \parallel \omega \parallel^2} < \infty$$

If $\chi(\mathrm{d}\omega)$ is absolutely continuous, then the previous representation can be written as:

$$\gamma(h) = \int [1 - \cos(2\pi < h, \omega >)] f(\omega)\mathrm{d}\omega$$

with

$$f(\omega)\mathrm{d}\omega = \frac{\chi(\mathrm{d}\omega)}{1 + 4\pi^2 \parallel \omega \parallel^2}$$

f is the spectral density associated with the variogram $\gamma(h)$. In the multivariate case, this spectral density becomes a $P \times P$ matrix. For the simulated vector random field Y to have direct and cross variograms associated with a given spectral density matrix f, based on Equation (4.28), the following condition must be satisfied:

$$\frac{\mathrm{A}(\omega)\mathrm{A}(\omega)^{\mathrm{T}}}{2} g(\omega) = f(\omega)$$

Or:

$$\mathrm{A}(\omega)\mathrm{A}(\omega)^{\mathrm{T}} = \frac{2f(\omega)}{g(\omega)} \tag{4.29}$$

The only necessary condition to find a matrix $\mathrm{A}(\omega)$ fulfilling the above equation is that $f(\omega)$ is a real-valued symmetric positive semi-definite matrix for every $\omega \in \mathbb{R}^d$ and that the support of g contains the support of f. In such a case, $\mathrm{A}(\omega)$ can be obtained by taking the Cholesky factor of $\frac{2f(\omega)}{g(\omega)}$:

$$\mathrm{A}(\omega) = \mathrm{chol}\left(\frac{2f(\omega)}{g(\omega)}\right) \tag{4.30}$$

Finally, based on the central limit theorem, to obtain a random field with (approximately) multivariate-Gaussian increments, it suffices to sum up and properly normalize many of such independent random fields:

$\forall\, x \in \mathbb{R}^d$,

$$Y(x) = \frac{1}{\sqrt{n_D}} \sum_{i=1}^{n_D} \sum_{p=1}^{P} \alpha_p(\omega_{i,p}) \cos(2\pi < x, \omega_{i,p} > + \phi_{i,p}) \tag{4.31}$$

with $n_D \in \mathbb{N}$.

The simulated vector random field is therefore a mixture of basic random fields made of weighted cosine waves associated with random frequencies and random phases.

As we want to simulate intrinsic random fields of order *k* greater than 0, the ordinary covariances or variograms may no longer exist. Instead, we have to use generalized covariances and cross covariances (Arroyo and Emery, 2016b), which have a spectral representation similar to that of ordinary covariances and variograms (Matheron, 1973; Chilès and Delfiner, 2012). In the particular case of the Matérn and power covariance models, the spectral densities have been presented in the previous section (Equations 4.22 and 4.23).

For practical implementation, the random frequencies $\omega_{i,p}$ are simulated with a density g different from the target spectral density f. To make sure that the support of g contains that of f, it is convenient to choose g as the spectral density of a Matérn covariance with shape parameter μ, as the support of this density is the entire space $\mathbb{R}^d$ (Lantuéjoul, 2002):

$$g(\omega,\mu) = \frac{\Gamma(\mu+\frac{d}{2})}{\Gamma(\mu)\pi^{\frac{d}{2}}} \frac{1}{(1+||\omega||^2)^{\mu+\frac{d}{2}}} \tag{4.32}$$

A random vector with such a density can be obtained by computing the ratio of a Gaussian random vector and the square root of gamma random variable with shape parameter μ (Emery and Lantuéjoul, 2006).

In summary, the steps for jointly simulating *P* intrinsic random fields of order *k* are:

- Identify the spectral density matrix *f* associated with the generalized direct and cross covariances of the random fields. In our case, we will use combinations of Matérn and power generalized covariances, for which the spectral densities have already been explicited.

- Choose a probability density *g*, with support containing the support of *f*

- Choose a number of turning lines n_D (a large integer).

- For $p = 1, \dots, P$ and $i = 1, \dots, n_D$:
  - Generate a random phase $\phi_{i,p}$ uniformly distributed on $[0, 2\pi[$.
  - Generate a random vector $\omega_{i,p}$ with density g.
  - Calculate the Cholesky decomposition of matrix $\frac{2f(\omega_{i,p})}{g(\omega_{i,p})}$

- Identify $\alpha_p(\omega_{i,p})$ as the p-th column of the Cholesky decomposition matrix calculated in the previous step.

- Calculate the simulated vector random field Y by using Equation (4.31).

2.2. Conditioning to data

The simulation is said to be conditional when it restitutes the data values at the sampling locations. In the stationary case, it is possible to convert a non-conditional simulation into a conditional simulation thanks to an additional step based on simple kriging (kriging with a known mean value). The conditional simulation can be obtained by putting (Journel and Huijbregts, 1978; Chilès and Delfiner 2012):

$$Y_{\mathrm{CS}}(x) = Y^{\mathrm{SK}}(x) + [Y_{\mathrm{S}}(x) - Y_{\mathrm{S}}^{\mathrm{SK}}(x)] \tag{4.33}$$

where:

$Y(x)$ is the true Gaussian random field (unknown except at the data locations)
$Y^{\mathrm{SK}}(x)$ is the simple kriging of $Y(x)$ from the conditioning data.
$Y_{\mathrm{S}}(x)$ is a non-conditional simulation at location x
$Y_{\mathrm{S}}^{\mathrm{SK}}(x)$ is the simple kriging of the non-conditional simulation from its values at the data locations.

In case of having two or more random fields, one should use simple cokriging instead of simple kriging in order to obtain conditional realizations of these random fields.

In the present thesis however, one has two random fields, only one of which is stationary, but the other one is an IRF-*k* (non-stationary), so that simple cokriging can no longer be used to condition the realizations.

We know that, in case of having a stationary Gaussian random field, the distribution at a given location conditional to observations at surrounding locations is Gaussian, with mean value equal to the simple kriging prediction and variance equal to the simple kriging variance. In the same manner, for an intrinsic random field of order *k* with Gaussian generalized increments, a similar result holds, but simple kriging has to be replaced by intrinsic kriging (Delfiner, 1976; Chilès and Delfiner, 2012). Therefore, in order to obtain joint conditional realizations of both the stationary and non-stationary random fields, we have to design a specific version of cokriging, which we will call mixed simple / intrinsic cokriging, to account for the stationarity and known mean value of the first random field

and the non-stationarity of the second one. The elements of the right hand and left hand side kriging matrices will be filled by considering the generalized direct and cross covariances and also the basis drift functions associated with the non-stationary field.

This mixed cokriging has actually to be used in two instances:

1) In the Gibbs sampler necessary to construct Gaussian data from known categorical data (stage required in truncated Gaussian and plurigaussian simulation).

2) In the post-conditioning step used to convert the non-conditional realizations into conditional ones (Equation (4.33) and its extension to a vector random field).

Chapter 5: First case study

This chapter presents an application of the joint simulation of grades and rock types to a stratabound copper deposit (Lince-Estefanía, northern Chile). In the region of interest, there exist three main rock types (intrusive, andesite and breccia bodies), therefore three auxiliary Gaussian random fields will be considered: one associated with the copper grade and two that will be used for simulating the rock types according to a two-dimensional plurigaussian truncation rule. The spatial dependence between the copper grade and the rock types will be reproduced by considering cross correlations between these three Gaussian random fields.

Because there are no obvious trends in the spatial distribution of the rock types, but rather occurrences that alternate throughout the region under study, here a stationary model can be elaborated for both the rock type and the grade. Accordingly, we will not resort to intrinsic random fields of order k and the proposed model will rely on the calculation and fitting of ordinary covariances and variograms. A non-stationary case study will be presented in the next chapter, where the rock type distribution exhibits a clear trend between the inner and the outer parts of the region under study.

Up to some minor edits, the remaining of this chapter reproduces a paper that has been published in Mathematical Geosciences. The information of the paper is the following:

Title: Joint simulation of grade and rock type in a stratabound copper deposit

Authors: Mohammad Maleki, Xavier Emery

Journal: Mathematical Geosciences

Issue: Vol. 47, pp. 471-495.

Abstract:
This work deals with the joint simulation of copper grade (as a continuous regionalized variable) and rock type (as a categorical variable) in Lince-Estefanía deposit, located in northern Chile. The region under study is heterogeneous, containing three main rock types (intrusive, andesite and breccia bodies) with different copper grade distributions. In order to perform joint simulation, the multigaussian and plurigaussian models are used in a combined form. To this end, three auxiliary Gaussian random fields are considered, one for simulating copper grade, up to a monotonic transformation, and two for simulating rock types according to a given truncation rule. Furthermore, the dependence between copper grade and rock types is reproduced by considering cross correlations between these Gaussian random fields.

In order to investigate the benefits of the joint simulation algorithm, copper grade and rock types are also simulated by the traditional cascade approach and the results are compared. It is shown that the cascade approach produces hard boundaries, i.e., abrupt transitions of copper grades when crossing rock type boundaries, a condition that does not exist in the study area according to the contact analysis held on the available data. In contrast, the joint simulation approach produces gradual transitions of the copper grade near the rock type boundaries and is more suited to the actual data.

Key words: contact analysis; multigaussian model; plurigaussian model; joint modeling; geological heterogeneity.

1. Introduction

In ore body modeling, it is often of interest to assess the spatial variability of geological parameters such as rock types and grades of elements of interest, which is a key factor in downstream processes, such as mine planning and management, and provides information on geological heterogeneity at multiple scales. Because the spatial distributions of grades and rock types are often interdependent, a separate modeling of these two parameters is inadequate. Instead, it is more natural to consider a joint modeling of grades and rock types.

Nowadays, a hierarchical approach (or cascade approach) is usually applied for this purpose. It means that, first of all, the layout of each rock type is delimited in the study area. In this respect, one can use a deterministic model based on geological knowledge and available exploration data (Duke and Hanna, 2001; Mackenzie and Wilson, 2001), or a stochastic model based on simulating the occurrence of each rock type in the study area (Journel and Alabert, 1990; Armstrong et al., 2011; Chilès and Delfiner, 2012; Strebelle, 2002, to name a few). After delimitating the rock type layouts, the grades are simulated in each rock type separately by using only the data that belong to this rock type, leading to a piecewise grade model (Alabert and Massonnat, 1990; Roldão et al., 2012; Boucher and Dimitrakopoulos, 2012; Jones et al., 2013). Although this cascade approach is simple, it has some substantial drawbacks. For instance, it does not take into account the dependence between the grades across rock-type boundaries, therefore, except for the case of a “hard boundary” for which there exists a sudden change in the grade distribution when crossing the boundary (Kim et al., 2005), it does not properly reflect the spatial relationship between the grades and the occurrence of given rock types (Wilde and Deutsch, 2012; Rossi and Deutsch, 2014). In addition, when using a deterministic rock type model, one works with a single interpretation of the deposit and does not account for any uncertainty in the rock type layout.

To account for the spatial dependence of grade across rock-type boundaries, Larrondo et al. (2004) and Ortiz and Emery (2006) suggest modeling not only the direct, but also the cross-

correlation functions of the grades variables defined separately within each rock type, while Vargas-Guzmán (2008) proposes a stepwise modeling of these grade variables using successive conditional covariance functions. In all cases, a piecewise grade model is still considered, insofar as the grade is split into as many variables as rock types, which does not allow for smooth transitions across rock types. An alternative approach that avoids such a piecewise modeling is to jointly simulate the grades and rock types. This approach is more complex because of the different natures of these two parameters: grades are measured on a continuous quantitative scale, whereas rock types are measured on a nominal scale. To overcome this difficulty, one can integrate two well-known geostatistical models, as proposed by Emery and Silva (2009) and Cáceres and Emery (2010): the multi-Gaussian model for simulating grades and the truncated plurigaussian model for simulating rock types. This approach allows a flexible modeling of the contact relationships between rock types and the dependence relationships between grades and rock types, but, to the best of the authors' knowledge, so far it has been applied only to disseminated deposits.

The objective of this paper is to apply the joint simulation approach to a stratabound copper deposit, in order to quantify the uncertainty in the copper grades and prevailing rock types, and to compare this approach with the aforementioned cascade approach. The outline is as follows: after a brief recall on the methodology, the case study will be presented, consisting of exploratory data analysis, contact analysis, joint modeling of grade and rock type, joint simulation and analysis of results.

2. Methodology

2.1. Multi-Gaussian simulation of grades

The multi-Gaussian model is widespread for simulating mineral grades (Journel and Huijbregts, 1978). The implementation consists of the following steps. First, one has to transform the grade data into normal scores and fit a variogram to the transformed data. Then, a Gaussian random field is simulated by use of algorithms such as the turning bands, sequential or spectral simulation (Deutsch and Journel, 1998; Lantuéjoul, 2002; Chilès and Delfiner, 2012). Finally, the simulated Gaussian values are back-transformed to grade values.

2.2. Plurigaussian simulation of rock types

Plurigaussian simulation aims at constructing realizations of a categorical variable (a rock type in the present case), represented by the truncation of one or more Gaussian random fields. First, according to the spatial relationships and contacts between rock types, one has to define a number of Gaussian random fields and a truncation rule (Lantuéjoul, 2002;

Dowd et al., 2003; Armstrong et al., 2011). Afterwards, the spatial correlation structure of the Gaussian random fields is modeled, in order to fit the rock type indicator variograms. With respect to simulation, a set of Gaussian values are first generated at the data locations, conditionally to the rock type data, by Gibbs sampling. Then, multi-Gaussian simulation is performed over the study area. Finally, using the truncation rule, the simulated Gaussian values are converted into rock types.

2.3. Joint simulation of grade and rock type

The joint simulation approach uses the multi-Gaussian model to simulate the grades and the plurigaussian model to simulate the rock types. The novelty is that the underlying Gaussian random fields are supposed to be spatially cross-correlated, which allows introducing a spatial dependence between rock types and grades. When all the Gaussian random fields have been jointly simulated, by using the back-transformation and truncation rule, one can obtain the simulated grades and rock types. Details of the approach can be found in Emery and Silva (2009). Figure 5.1 illustrates the main steps of the approach.

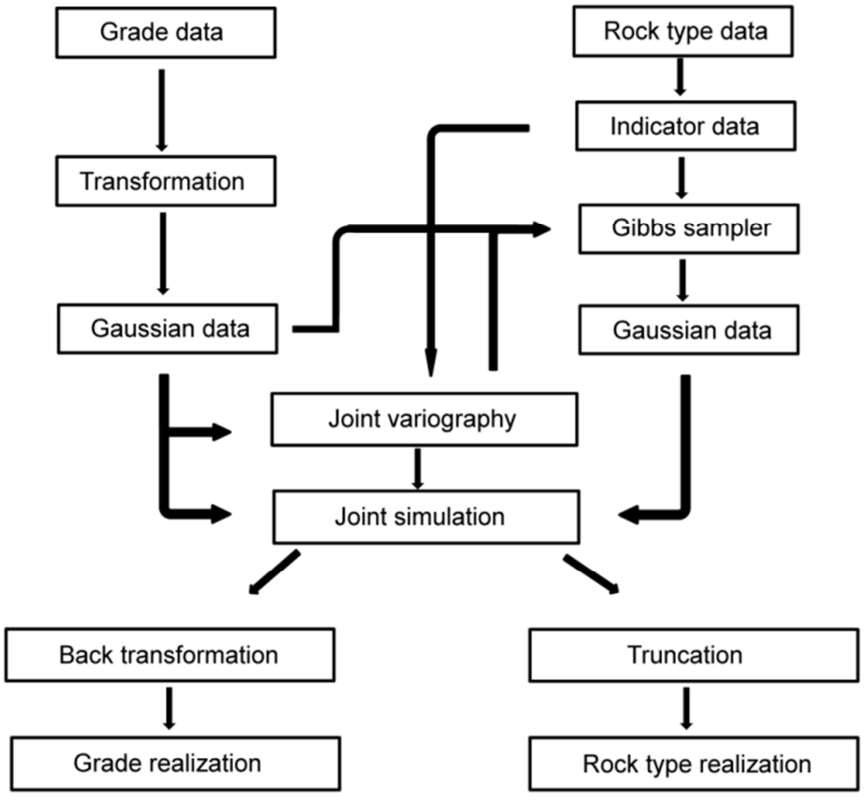

Figure 5.1: Steps of joint simulation approach

3. Case study: Lince-Estefanía deposit

The case study under consideration corresponds to a stratabound manto type copper deposit located in northern Chile and operated by Minera Michilla. Mining is done through underground (Estefanía) and open pit (Lince) operations.

3.1. Geological description

The Lince-Estefanía deposit Michilla is located 130 km north-northeast of Antofagasta city, Chile. The host sequence comprises andesitic basaltic lava flows of the La Negra Formation (Oliveros et al., 2008). This sequence has been intruded by diorite to granite bodies, dykes, as well as breccia bodies with volcanic clasts and an intrusive matrix. Breccia bodies are generally located around the dioritic intrusions and extend laterally from the intrusions into stratabound manto bodies. Breccias with high copper content are believed to be pre- or syn-mineralization.

The main ore minerals are copper oxides (predominantly atacamite and chrysocolla), which dominate near the surface (above elevation 500 m), and copper sulfides (chalcocite, bornite, covellite and chalcopyrite), which dominate at elevations below elevation 250 m. From elevations 250 to 500 m, a mixed sulfide-oxide transition is found. Chemical analyses of the ores, as well as field and petrographic observations, indicate that copper sulfides in stratabound-manto and breccia ore bodies were formed by the same processes, which suggests that one may observe a correlation of copper grades across these rock types.

3.2. Presentation of the data set

The case study will be developed on the basis of an exploration data set from diamond and reversed-circulation drill holes. For the sake of simplicity, the data have been restricted to a small portion of the deposit and the grade values have been multiplied by a constant factor in order to preserve data confidentiality. Concerning rock types, three main types will be considered for modeling:

- **Intrusive bodies (code 1)**, consisting of dioritic bodies with thicknesses from 20 to 450 m, associated with small dykes that crosscut all the other rock types. Their boundary with the surrounding rocks is irregular.

- **Andesite (code 2)**, composed of aphanitic andesites, porphyritic andesites, ocoites and metandesites that are unlikely to contain economic copper mineralization due to their low permeability. It is widely distributed in the deposit, with a monoclinal structure that strikes at N65°E and dips at 35-40° NW, and is part of the volcanic sequence known as La Negra Formation.

- **Volcanic breccias bodies (code 3)**, composed of amigdaloidal andesites and volcanic breccias that are likely to hold copper mineralization due to their high porosity. As for andesites, it is part of the La Negra Formation. It extends into stratabound manto bodies and occupies a monoclinal structure that strikes at N65°E and dips at 35-40° NW.

A cross section showing the data is presented in Figure 5.2, which uses local coordinates (abscissa axis oriented along the direction N65°E). A summary of descriptive statistics and a visualization of the copper grade distribution is given in Table 5.1 and Figure 5.3, showing a dependence between grade and rock type, with volcanic breccias (rock type 3) having the highest average copper grade and intrusive bodies (rock type 1) the lowest average copper grade. To better understand the dependence relationships between grade and rock type, a contact analysis is performed next.

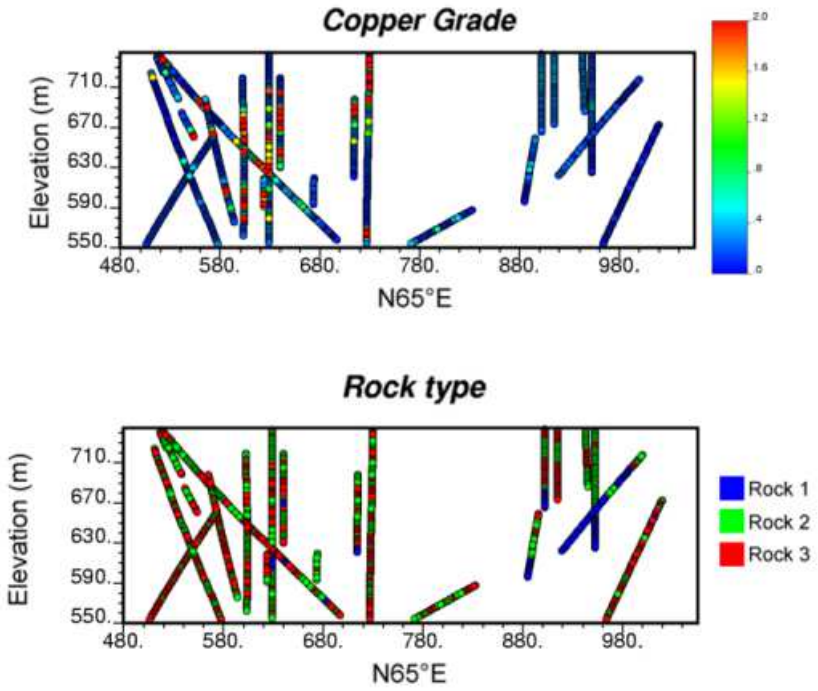

Figure 5.2: Location of copper grade and rock type data over a cross section of the deposit

	Global	Rock type 1	Rock type 2	Rock type 3
Count	7173	619	3680	2874
Minimum	0.00	0.00	0.00	0.00
Maximum	17.07	2.38	14.51	17.07
Mean	0.49	0.136	0.352	0.746
Standard deviation	1.14	0.187	0.709	1.576
Median	0.18	0.09	0.18	0.2

Table 5.1: Statistics of grade data (in percent), globally and per rock type

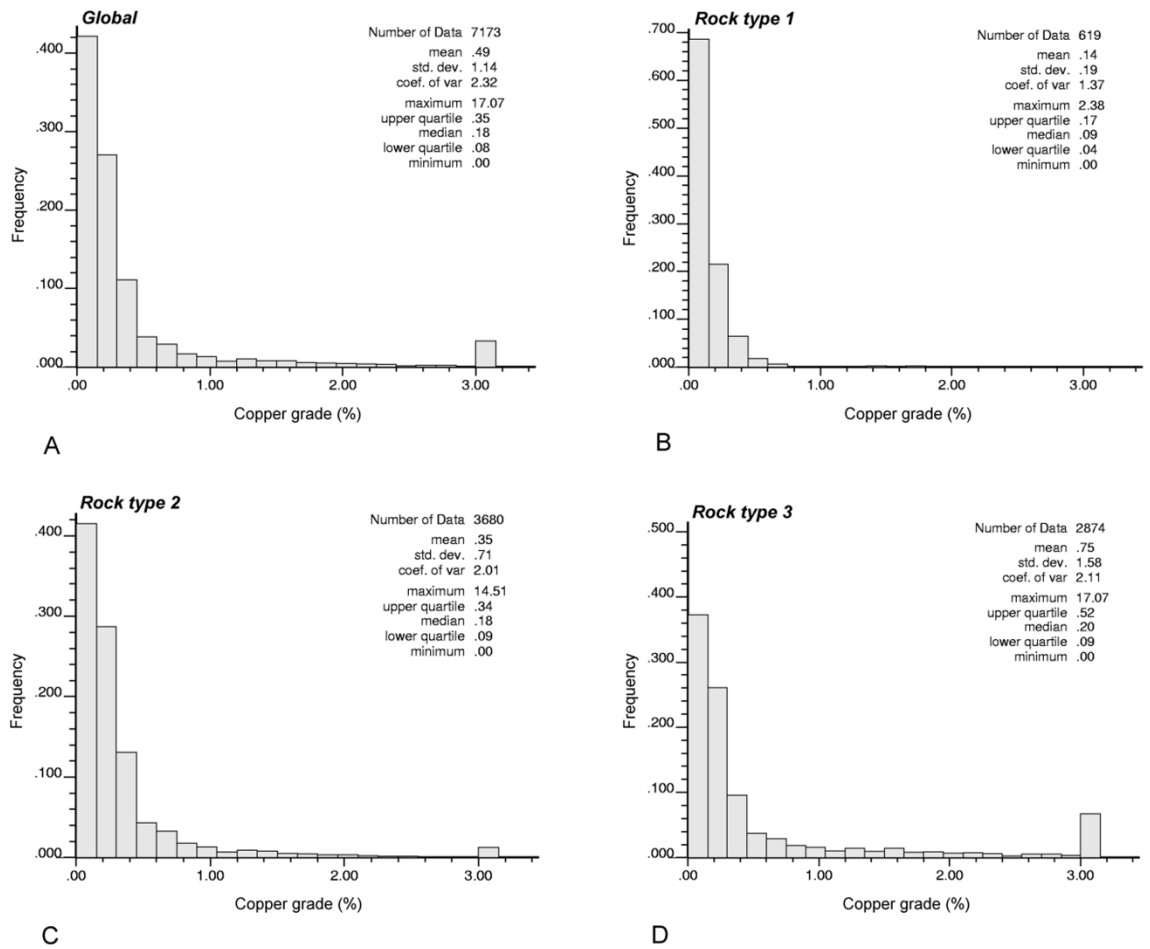

Figure 5.3: Histograms of copper grade data, overall (A) and per rock type (B, C, D)

3.3. Contact analysis

The analysis aims at determining the behavior of the copper grade in the neighborhood of the boundary between two rock types (Glacken and Snowden, 2001; Wilde and Deutsch, 2012). In practice, two kinds of analysis can be performed. The first one is a mean value contact analysis, consisting in grouping the data of one rock type into distance classes from the boundary with another rock type (as an approximation, one often considers the distance to the closest data of this second rock type in the same drill hole), then plotting the mean grade of each group as a function of the distance to the boundary (Rossi and Deutsch, 2014). The resulting plot shows how the mean grade varies when getting closer to or farther from a boundary. The second analysis is a cross correlation contact analysis, which consists in identifying pairs of data with a given lag separation distance that belong to two different rock types and plotting the correlation coefficient between such data pairs as a function of the lag separation distance. The plot indicates how correlated the grade values are between both sides of the boundary. As a result, one observes a soft contact between all rock types, characterized by a rather smooth transition of the mean grade (Figures 5.4A, 5.4C, 5.4E) and a correlation that does not vanish at small lag separation distances (Figures 5.4B,5. 4D, 5.4F). The width of the transition zone is limited to 10 to 20 meters, which makes a difference between this deposit (a high-variability stratabound deposit) and disseminated porphyry copper deposits with thicker transition zones.

3.4. Copper grade modeling

The grade data are transformed into normal scores (associated with a Gaussian random field Y_0) prior to performing variogram analysis. The modeled variogram (denoted as g_{00}) consists of a nugget effect and four nested anisotropic spherical structures (Figure 5.5)

$$g_{00} = 0.1\,\text{nugget} + 0.29\,sph(20,10,5) + 0.26\,sph(175,95,60) + 0.17\,sph(195,\infty,195) + 0.18\,sph(500,\infty,\infty). \quad (5.1)$$

In the above formula, the distances into brackets indicate the ranges (expressed in meters) along the main anisotropy directions.

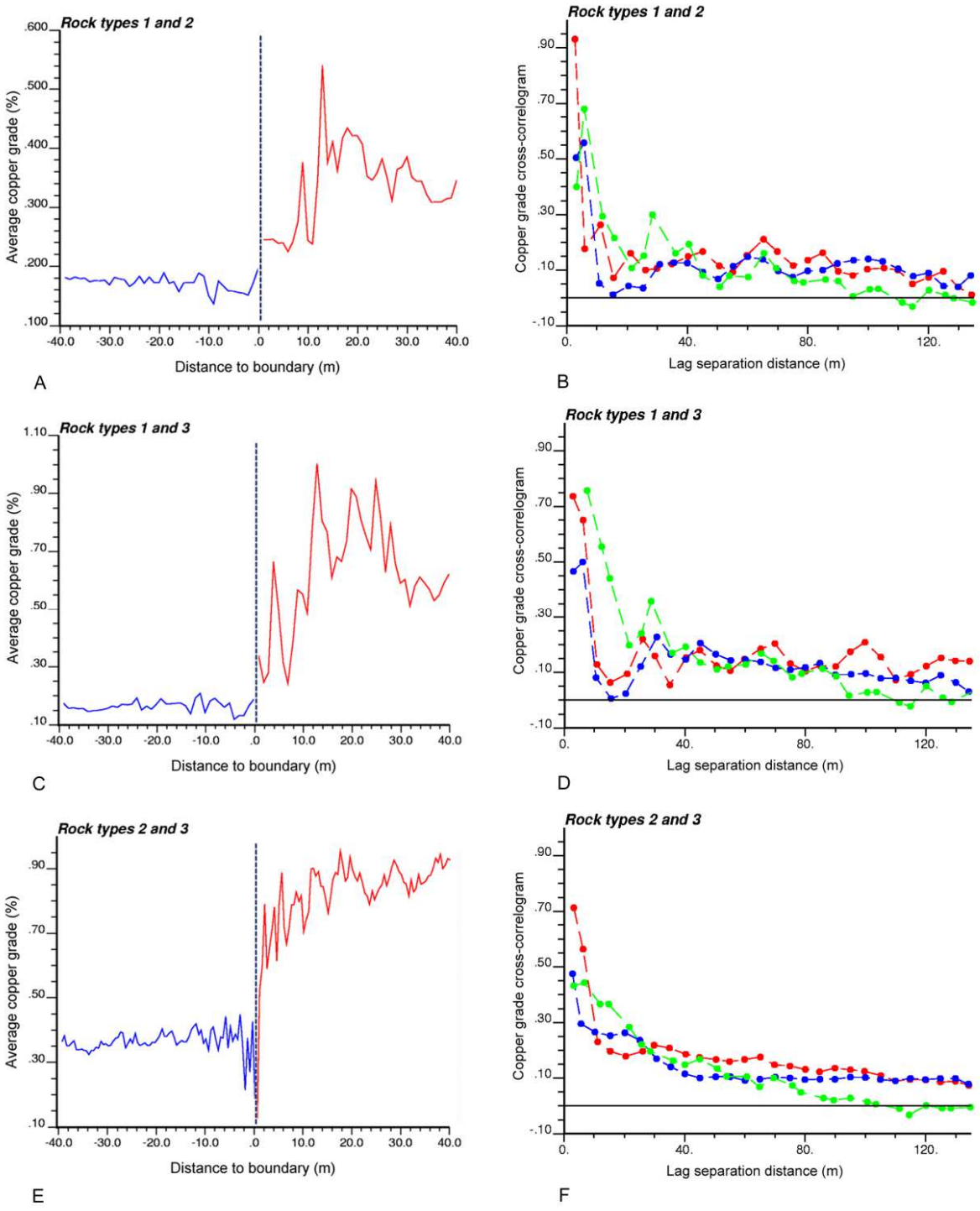

Figure 5.4: Contact analysis between rock types: (A, C, E) mean grade graphs; (B, D, F) cross-correlation functions calculated along main anisotropy directions (green: N25°W; red: N115°E dip -60°; blue: N25°W dip -30°)

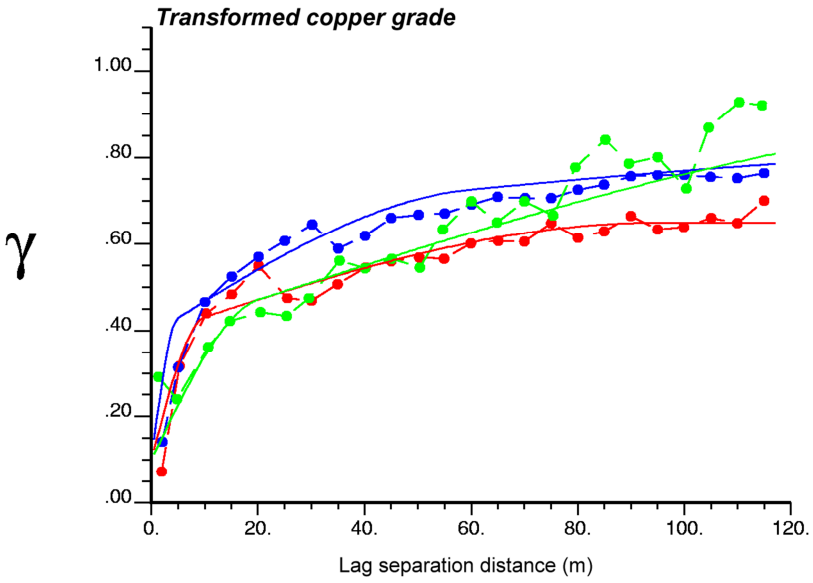

Figure 5.5: Sample (dashed lines) and modeled (solid lines) variograms of normal scores data associated with grade, calculated along main anisotropy directions (green: N25°W; red: N115°E dip -60°; blue: N25°W dip -30°)

3.5. Rock type modeling

3.5.1. Truncation rule

The examination of the drill hole data indicates that all the rock types are in contact. If one considers two independent Gaussian random fields (Y_1 and Y_2) for plurigaussian simulation, then three simple truncation rules can be considered in order to reproduce the contacts between rock types (Figure 5.6). A simple way to determine which of these truncation rules is best suited to the data is to examine the direct and cross variograms of rock type indicators. More specifically, if γ_{ij} represents the cross variogram between the indicators of rock types *i* and *j*, then (proof in Appendix A)

- $\frac{\gamma_{12}}{\gamma_{11}}$ and $\frac{\gamma_{13}}{\gamma_{11}}$ do not vary with the lag separation vector in the model of Fig. 5.6A
- $\frac{\gamma_{12}}{\gamma_{22}}$ and $\frac{\gamma_{23}}{\gamma_{22}}$ do not vary with the lag separation vector in the model of Fig. 5.6B
- $\frac{\gamma_{13}}{\gamma_{33}}$ and $\frac{\gamma_{23}}{\gamma_{33}}$ do not vary with the lag separation vector in the model of Fig. 5.6C.

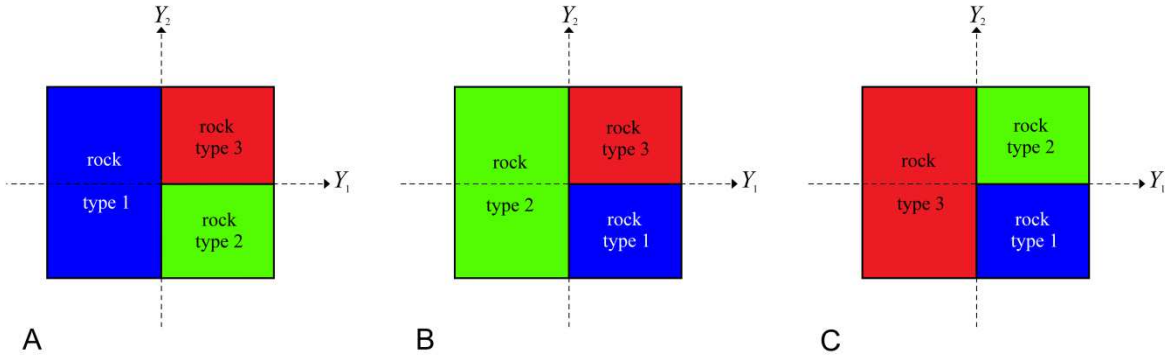

Figure 5.6: Possible truncation rules for plurigaussian modeling

Experimentally, one observes that γ_{12} and γ_{13} are practically proportional to γ_{11} (Figure 5.7A, 5.7B), but not to γ_{22} (Figure 5.7C) or γ_{33} (Figure 5.7E). Accordingly, the ratios γ_{12}/γ_{11} and γ_{13}/γ_{11} can be considered as independent of the lag separation vector, whereas the ratios γ_{12}/γ_{22} and γ_{13}/γ_{33} cannot. This suggests that Figure 5.6A is the best truncation rule to describe the contact relationships between rock types. Such a truncation rule, in which rock type 1 (intrusive bodies) appears to crosscut the other two rock types, furthermore agrees with the geology of the deposit, insofar as rock type 1 is the youngest one (dated between 168 and 112 Ma) and intruded both andesite and breccia bodies, which pertain to the Jurassic La Negra Formation (Oliveros et al., 2008).

The truncation rule will therefore be defined on the basis of two thresholds, associated with two independent Gaussian random fields Y_1 and Y_2, as follows:

- Location $\mathbf{x}$ belongs to the rock type 1 if $Y_1(\mathbf{x}) \leq y_1$
- Location $\mathbf{x}$ belongs to rock type 2 if $Y_1(\mathbf{x}) > y_1$ and $Y_2(\mathbf{x}) \leq y_2$
- Location $\mathbf{x}$ belongs to rock type 3 if $Y_1(\mathbf{x}) > y_1$ and $Y_2(\mathbf{x}) > y_2$.

The truncation thresholds y_1 and y_2 can be defined according to the rock type proportions (Armstrong et al., 2011). This leads to the following threshold values: y_1 = -1.405 and y_2 = 0.137.

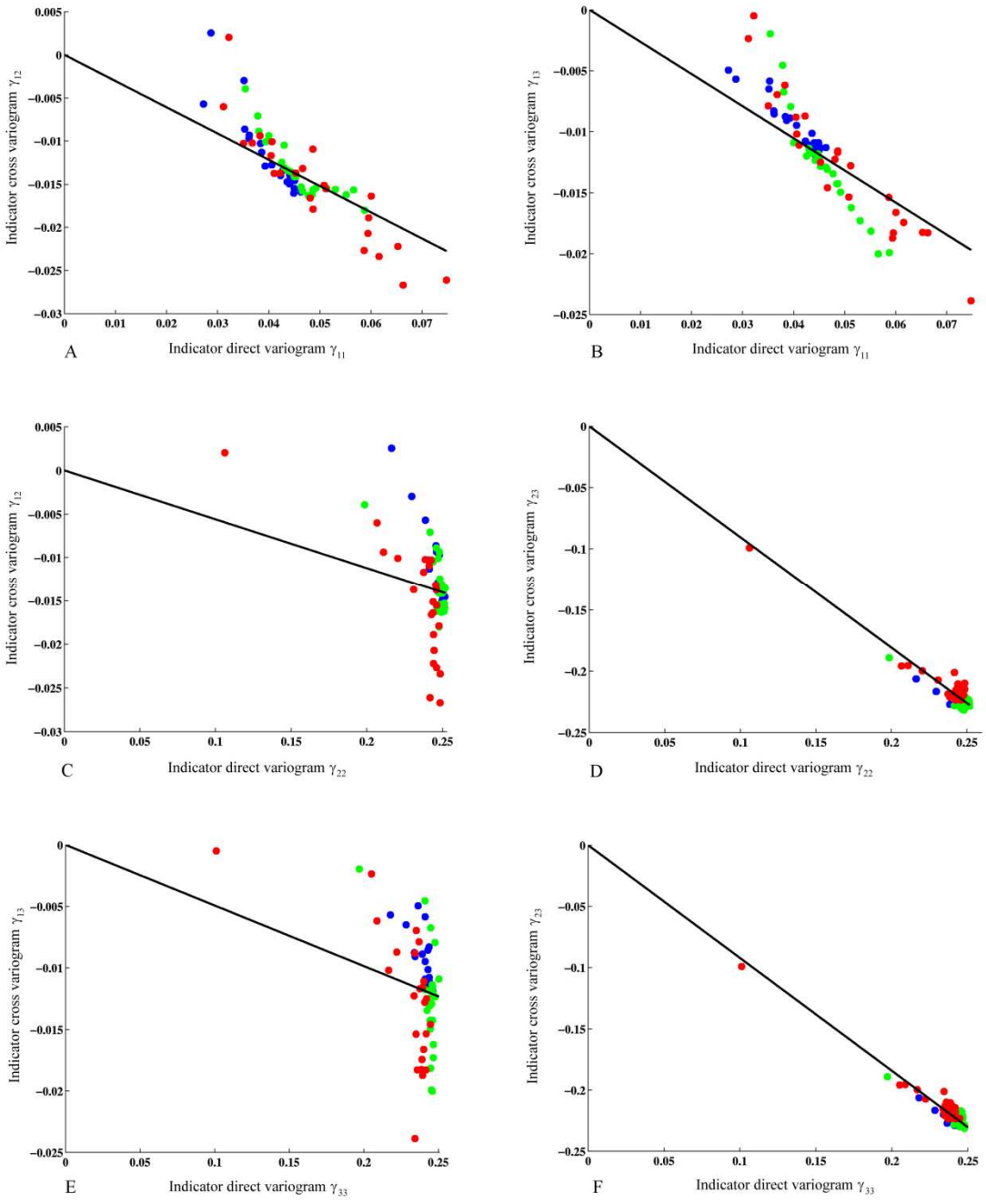

Figure 5.7: Cross versus direct variograms of rock type indicators, calculated along main anisotropy directions (green: N25°W; red: N115°E dip -60°; blue: N25°W dip -30°). Straight lines indicating perfect proportionality are superimposed

3.5.2. Variogram analysis

To complete the plurigaussian model, it remains to fit the variograms of the two underlying Gaussian random fields Y_1 and Y_2. Because these random fields are assumed independent, their cross-variogram is zero. As for the direct variograms, a trial-and-error procedure is used, in order to fit the variograms of rock type indicators (Emery, 2007b; Emery and Silva, 2009). At this stage, an important practical aspect to consider is that, in the following section, we will be interested in cross-correlating the two Gaussian random fields used in the plurigaussian model with the Gaussian random field already used in the multi-Gaussian model (Equation 5.1). Therefore, it is advisable to consider all or part of the basic nested structures used for grade modeling (Section 3.4). Following this recommendation, the variograms of Gaussian random fields associated with the plurigaussian model (denoted by g_{11} and g_{22}) are found to be

$$\begin{aligned} g_{11} &= 0.07\, sph(20,10,5) + 0.161 sph(175,95,60) \\ &\quad + 0.197 sph(195,\infty,195) + 0.572 sph(500,\infty,\infty) \end{aligned} \tag{5.2}$$

$$g_{22} = 0.50\, sph(20,10,5) + 0.50 sph(30,20,10). \tag{5.3}$$

In these formulae, the distances into brackets indicate the ranges along the same directions as for the grade data. The sample and modeled indicator direct and cross variograms are shown in Figure 5.8. The cross-variograms are negative due to the compositional nature of the rock type indicators: the increase of an indicator (from 0 to 1) is necessarily associated with the decrease of another indicator (from 1 to 0).

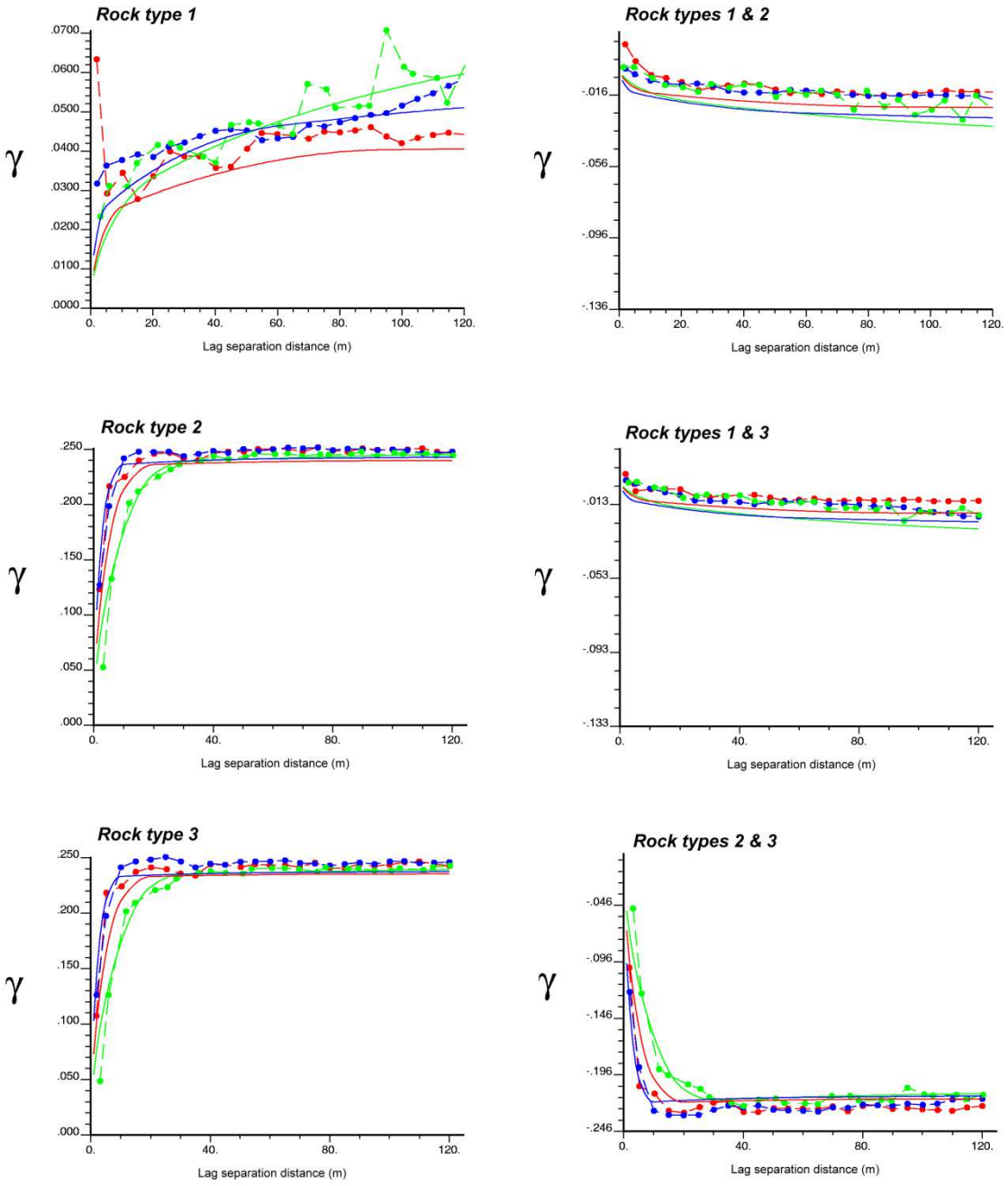

Figure 5.8: Sample (dashed lines) and modeled (solid lines) direct and cross variograms of indicator data associated with rock types, calculated along main anisotropy directions (green: N25°W; red: N115°E dip -60°; blue: N25°W dip -30°)

3.6. Modeling the spatial dependence between grade and rock type

Up to now, six nested structures (a nugget effect and five spherical structures) have been introduced. The first spherical structure is common for the Gaussian random fields associated with the grade (Y_0) and with the rock type (Y_1 and Y_2). The next three spherical models are common for Y_0 and Y_1, the last spherical model only pertains to Y_2, whereas the nugget effect only pertains to Y_0. In order to cross-correlate grade and rock type, we will now propose a linear model of coregionalization for Y_0, Y_1 and Y_2.

From the previous steps, some entries of the coregionalization matrices associated with the aforementioned nested structures are already specified: the diagonal entries correspond to the direct variograms of Y_0, Y_1 and Y_2, while the off-diagonal entries between Y_1 and Y_2 are equal to zero because Y_1 and Y_2 are independent. Also, the entry associated with a cross-variogram g_{ij} between Y_i and Y_j (with $i, j = 0$, 1 or 2) is zero when the entry associated with the direct variogram g_{ii} or g_{jj} is zero (Wackernagel, 2003). Accordingly, it only remains to determine four entries (a,b,c,d):

$$\begin{pmatrix} g_{00} & g_{01} & g_{02} \\ g_{01} & g_{11} & g_{12} \\ g_{02} & g_{12} & g_{22} \end{pmatrix} = \begin{pmatrix} 0.1 & 0 & 0 \\ 0 & 0 & 0 \\ 0 & 0 & 0 \end{pmatrix} \text{nugget} + \begin{pmatrix} 0.29 & a & b \\ a & 0.07 & 0 \\ b & 0 & 0.50 \end{pmatrix} sph(20,10,5)$$
$$+ \begin{pmatrix} 0.26 & c & 0 \\ c & 0.161 & 0 \\ 0 & 0 & 0 \end{pmatrix} sph(175,95,60) + \begin{pmatrix} 0.17 & d & 0 \\ d & 0.197 & 0 \\ 0 & 0 & 0 \end{pmatrix} sph(195,\infty,195)$$
$$+ \begin{pmatrix} 0.18 & e & 0 \\ e & 0.572 & 0 \\ 0 & 0 & 0 \end{pmatrix} sph(500,\infty,\infty) + \begin{pmatrix} 0 & 0 & 0 \\ 0 & 0 & 0 \\ 0 & 0 & 0.50 \end{pmatrix} sph(30,20,10). \quad (5.4)$$

For the fitting, one has to be aware of which Gaussian random field is modeling each rock type. For instance, the indicator of rock type 1 only depends on random field Y_1, while the indicators of rock types 2 and 3 depend on both random fields Y_1 and Y_2. Accordingly, the cross variogram between the transformed grade (Y_0) and the indicator of rock type 1 only depends on the cross variogram between Y_0 and Y_1, while the cross variograms between the transformed grade and the indicator of rock type 2 or rock type 3 also depend on the cross variogram between Y_0 and Y_2. Based on the previous statements, the unknown coefficients (a,c,d) are first chosen (by trial-and-error) in order to fit the cross variogram between the transformed grade and the indicator of rock type 1. Once done, the last coefficient (b) is chosen in order to fit the cross variograms between the transformed grade and the indicators of rock types 2 and 3. The following values give the best fit between sample and modeled cross variograms (Figure 5.9):

$a = 0.01$; $b = 0.2$; $c = 0.15$; $d = 0.1$; $e = 0.15$. (5.5)

In order to ensure the mathematical consistency of the proposed coregionalization model, one has to check that all the defined coregionalization matrices are positive semi-definite, i.e., that their eigenvalues are nonnegative (Wackernagel, 2003).

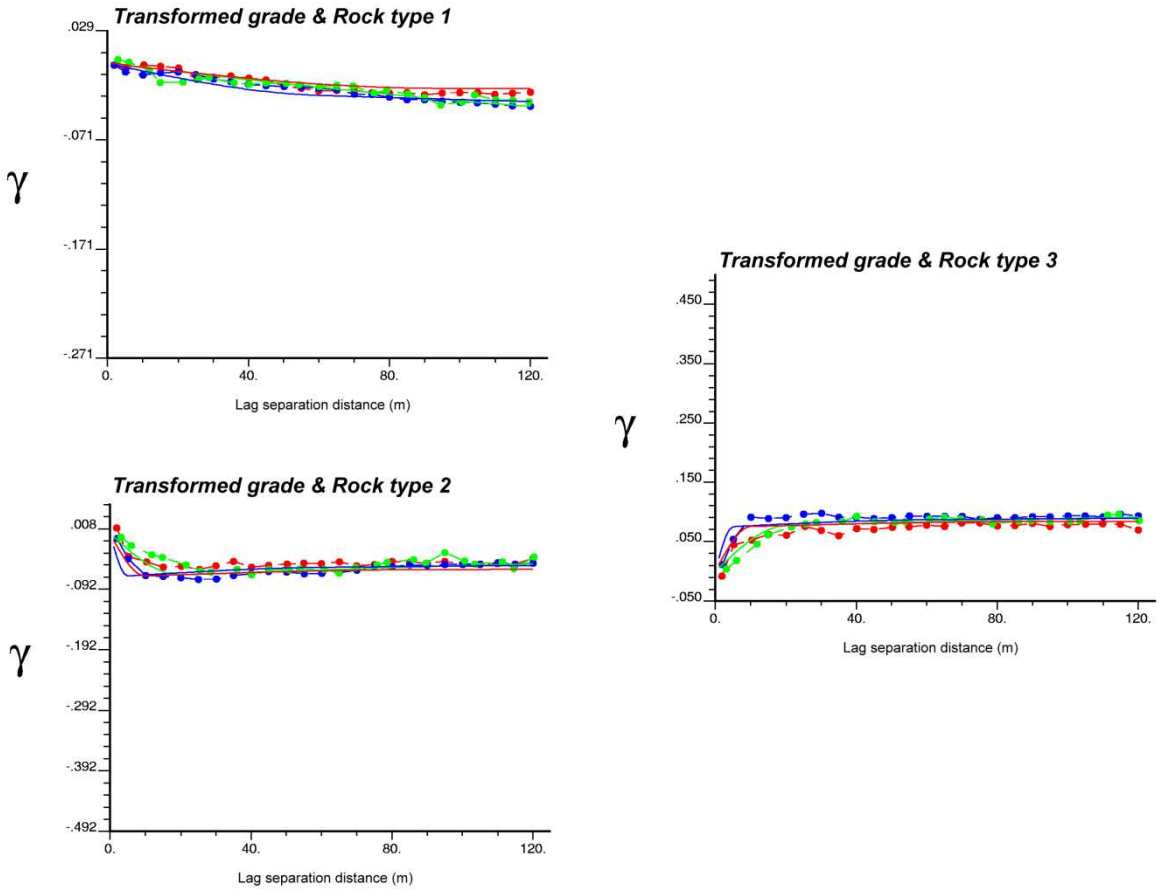

Figure 5.9: Sample (dashed lines) and modeled (solid lines) cross variograms between indicators data and transformed grade data, calculated along main anisotropy directions (green: N25°W; red: N115°E dip -60°; blue: N25°W dip -30°)

3.7. Joint simulation results

Provided with the model fitted in Sections 3.4 to 3.6, one can construct realizations of grade and rock type. The first step consists in simulating the Gaussian random fields Y_1 and Y_2 at the data locations, conditionally to the grade and rock type data, for which an iterative algorithm (Gibbs sampler) is necessary. Then, one performs a joint multi-Gaussian simulation of Y_0, Y_1 and Y_2; this is done by decomposing these random fields into spatially non-correlated factors using coregionalization analysis and by independently simulating the

factors via the turning bands method (Emery, 2008b). Figure 5.10 shows one joint realization of grade and rock type over the same cross-section as in Figure 5.2, and Figure 5.11 displays the probability of occurrence of each rock type and the expected copper grade calculated over 100 realizations. The drill hole locations are perceptible on the probability maps and correspond to the locations where the probability is close to zero or to one.

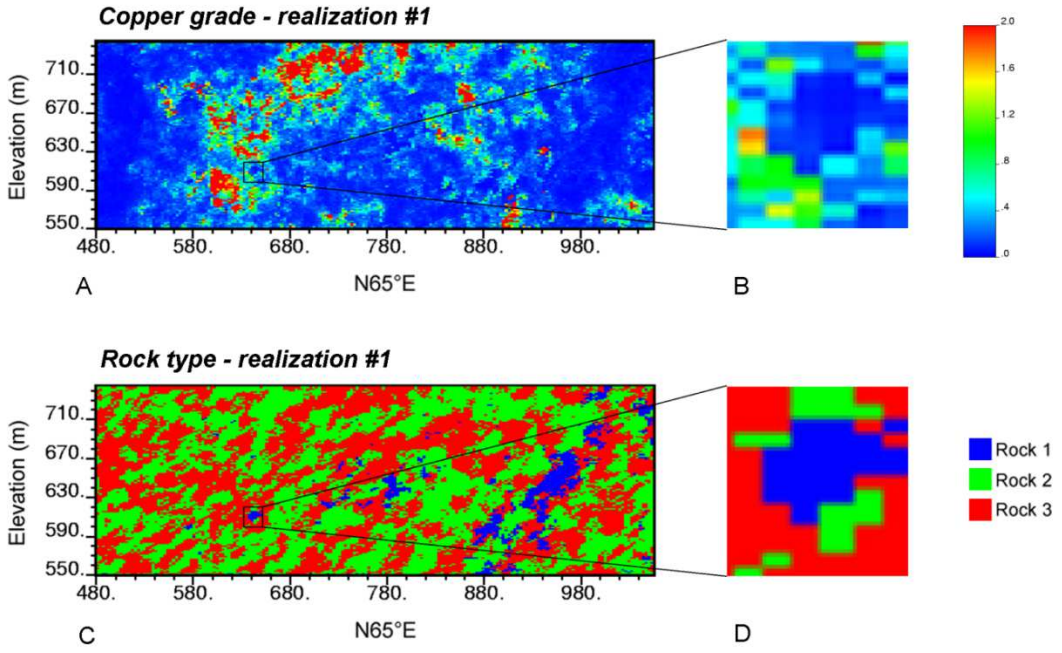

Figure 5.10: One realization of copper grade and rock type (joint simulation)

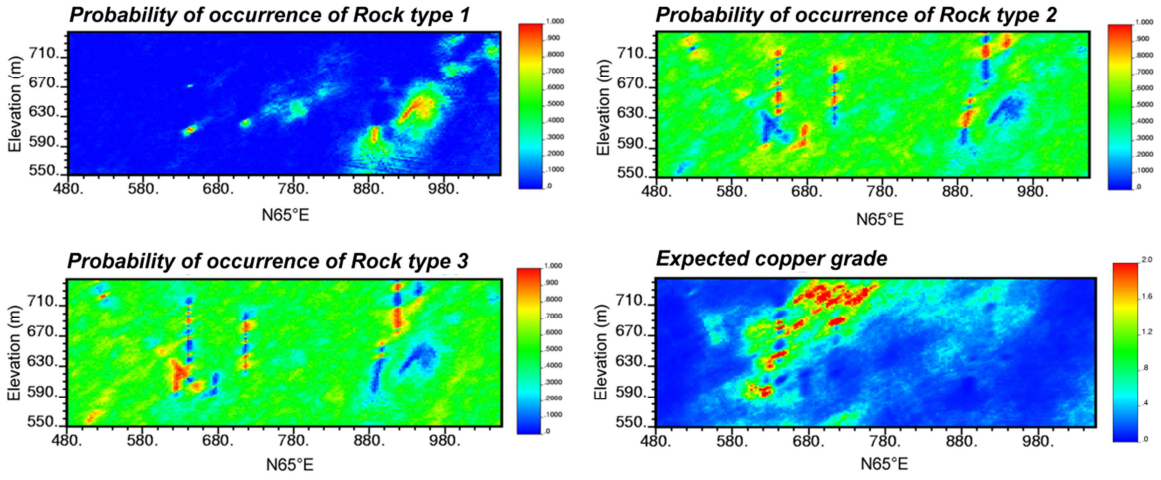

Figure 5.11: Probabilities of occurrence of each rock type and expected copper grade, calculated over 100 realizations (joint simulation)

3.8. Cascade simulation of grade and rock type

The results of the joint simulation approach will now be compared to those of the more traditional cascade approach. The cascade approach consists in first simulating the layout of the rock types, then in simulating the copper grade in each rock type separately by using only the data that pertain to the rock type under consideration. The steps are the following.

(1) For each rock type: transformation of the copper grade data into normal scores and variogram analysis of the normal scores data.

(2) Plurigaussian simulation of each rock type, using the model presented in Section 3.5.

(3) For each plurigaussian realization and each rock type
   a. Identify the nodes belonging to the rock type
   b. Simulate copper grade conditionally to the grade data belonging to the rock type. At this stage, turning bands simulation is used (Emery and Lantuéjoul, 2006).

(4) Obtain copper grade realizations by juxtaposing the simulated grades in rock types 1, 2 and 3 (a single grade realization is associated with each rock type realization).

Figures 5.12 and 5.13 illustrate the results of the cascade simulation approach. The probability maps are similar to those obtained with the joint simulation approach, which is explained because the rock type is represented by the same plurigaussian model in both approaches. In contrast, the map of expected copper grade shows stronger differences with the joint simulation approach, which can be observed by comparing Figures 5.11 and 5.13.

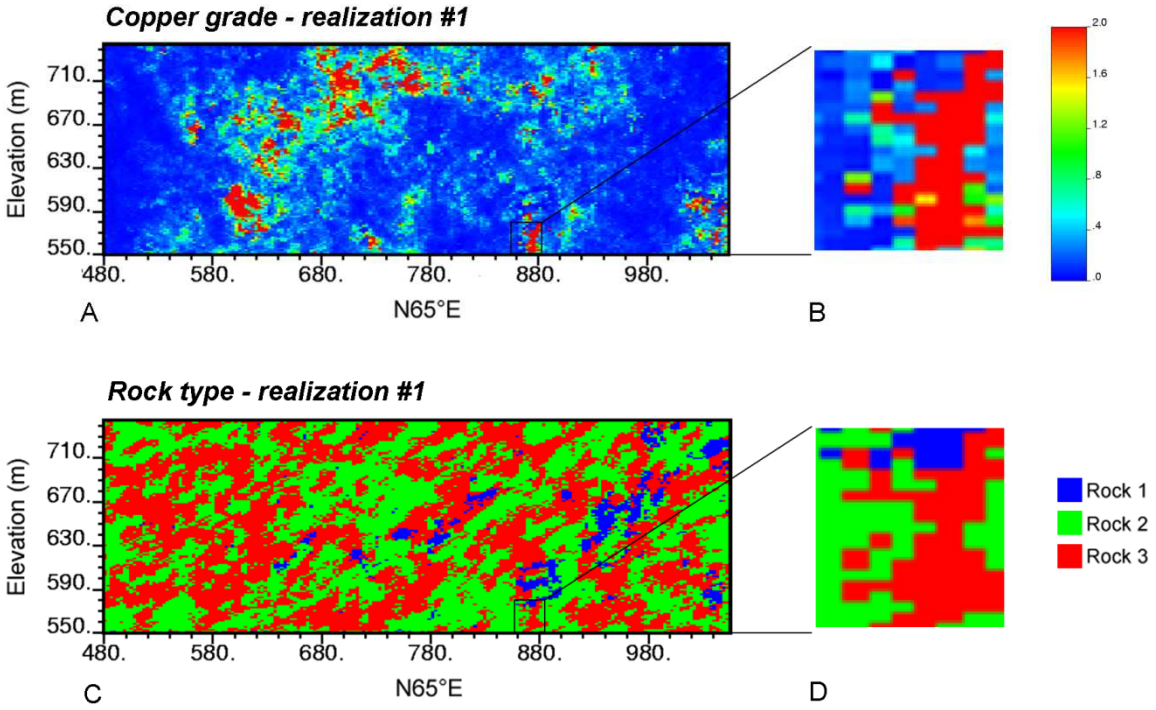

Figure 5.12: One realization of copper grade and rock type (cascade simulation)

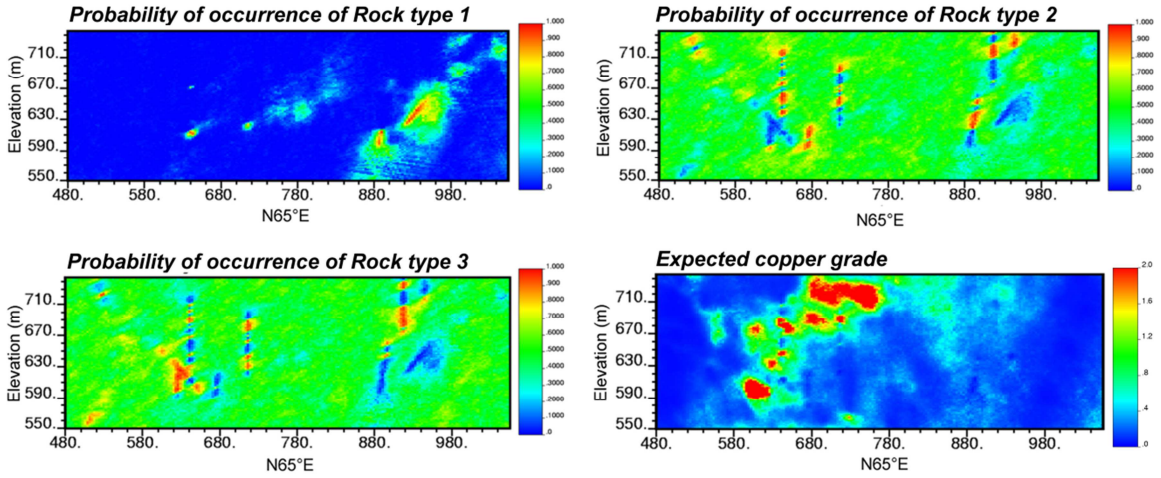

Figure 5.13: Probabilities of occurrence of each rock type and expected copper grade, calculated over 100 realizations (cascade simulation)

3.9. Comparison of results

3.9.1. Distribution of copper grade conditioned to rock type

Since it accounts for cross correlations between grade and rock type (through coefficients *a*, *b*, *c*, *d* and *e* in Equation 5.4), the joint simulation model fitted in Sections 3.4 to 3.6 yields a marginal grade distribution that differs from one rock type to another. The distribution of grade conditioned to the rock type can be assessed analytically by using expansions into Hermite polynomials (Appendix B), or numerically by co-simulating the three Gaussian random fields (Y_0, Y_1, Y_2), converting the simulated Gaussian values into grades and rock types, and finally calculating the distributions of the simulated grades after separating by rock type. The resulting distributions agree with the distributions observed on the data, within each rock type and overall (Figures 5.14A, 5.14B). Concerning the cascade approach, as the copper grade is simulated within each rock type separately, the distribution in each rock type is also well reproduced when compared to the original data (Figure 5.14A, 5.14C).

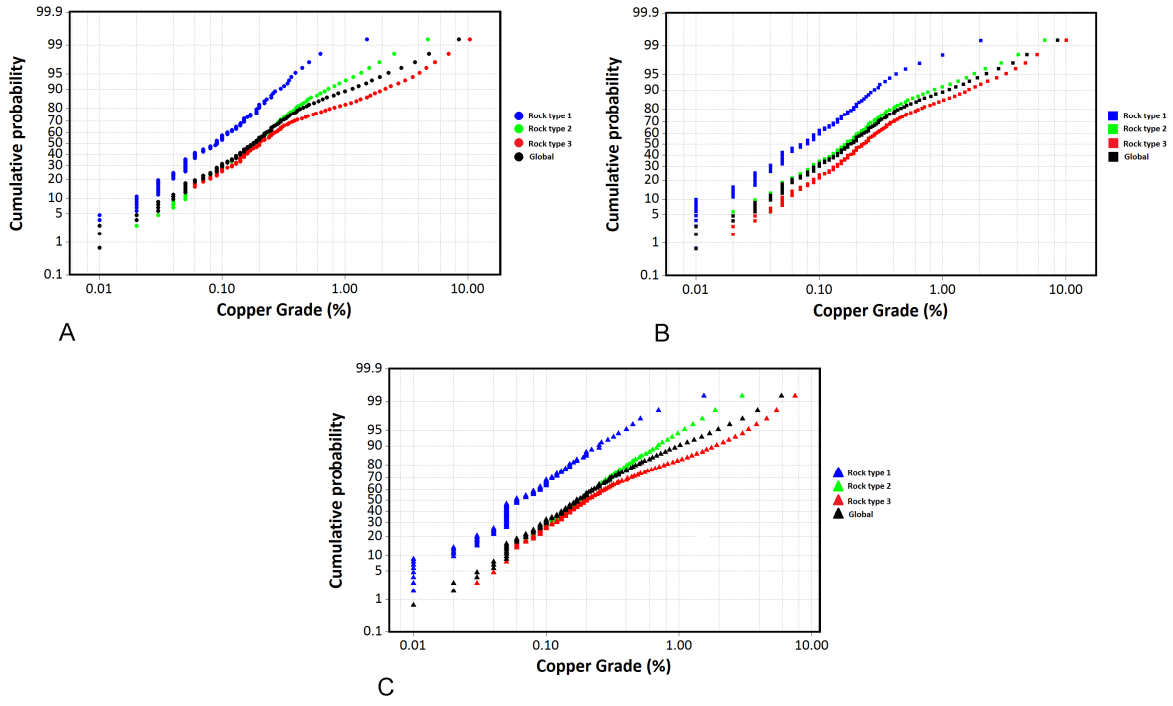

Figure 5.14: Log-probability plots showing the distributions of copper grade in each rock type and overall, for A) original drill hole data, B) joint simulation model and C) cascade simulation model

3.9.2. Spatial correlation of copper grade conditioned to rock type

In addition to marginal distributions, one can assess the spatial correlation of the simulated grade in each rock type and compare it with the experimental correlation observed in the data. It is seen (Figure 5.15) that the correlation functions are generally well reproduced with both approaches (joint and cascade simulation), with a slightly better performance of one approach in some cases and of the other approach in other cases.

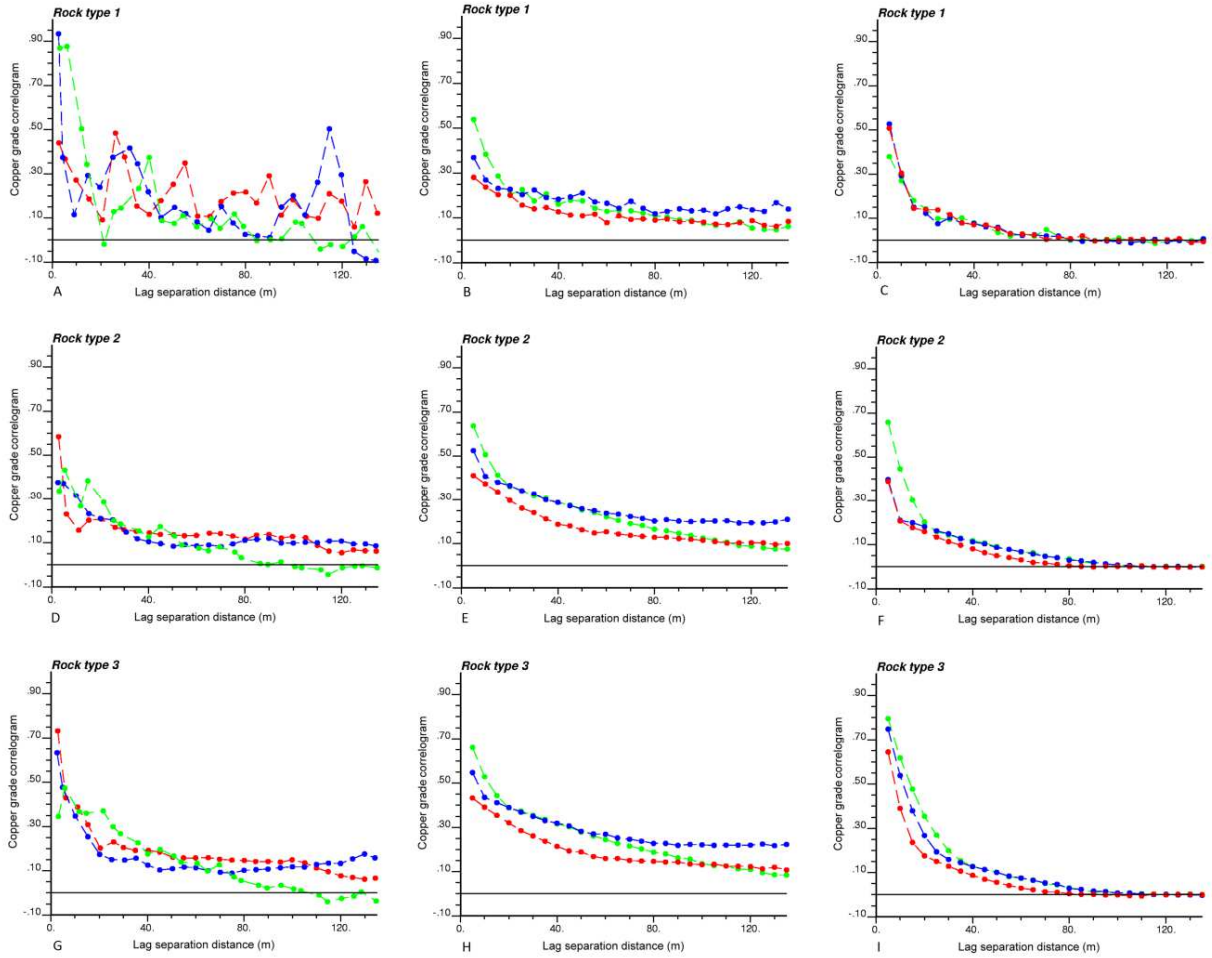

Figure 5.15: Spatial correlation of copper grades within each rock type, calculated along main anisotropy directions (green: N25°W; red: N115°E dip -60°; blue: N25°W dip -30°), for original data (A, D, G), joint simulation (B, E, H) and cascade simulation (C, F, I)

3.9.3. Rock type boundaries

The differences between the two simulation approaches are more striking when looking at the behavior of the copper grade in the vicinity of a rock type boundary. In particular, a look at the realizations indicates that the joint simulation tends to produce soft boundaries, with smooth transitions in the copper grade values (Figures 5.10B, 5.10D), while the cascade simulation tends to produce hard boundaries, with abrupt changes in copper grade (Figures 5.12B, 5.12D).

This is confirmed by examining the variations of mean grade when getting closer to a rock type boundary and by assessing the correlation of copper grade across a boundary, through mean graphs and correlation graphs similar to the ones used for contact analysis. Figures 5.16 and 5.17 show such graphs for the grades simulated with the two approaches. In the cascade approach, the mean grade shows an abrupt transition near the rock type boundaries (Figure 5.16) and the simulated grades on either side of the boundaries are practically not correlated (Figure 5.17). In contrast, with the joint simulation approach, the variations of mean grade are smoother and the simulated grades between both sides of the boundaries are correlated, as what is observed in the data (Figure 5.4) (the more irregular profile of the data curves shown in Figure 5.4 can be attributed to experimental fluctuations due to scarcity of data, rather than to a genuine behavior of the copper grade). The realizations obtained with the joint simulation approach are therefore more realistic in the neighborhood of rock type boundaries and better suited to the description of the copper grade in the deposit.

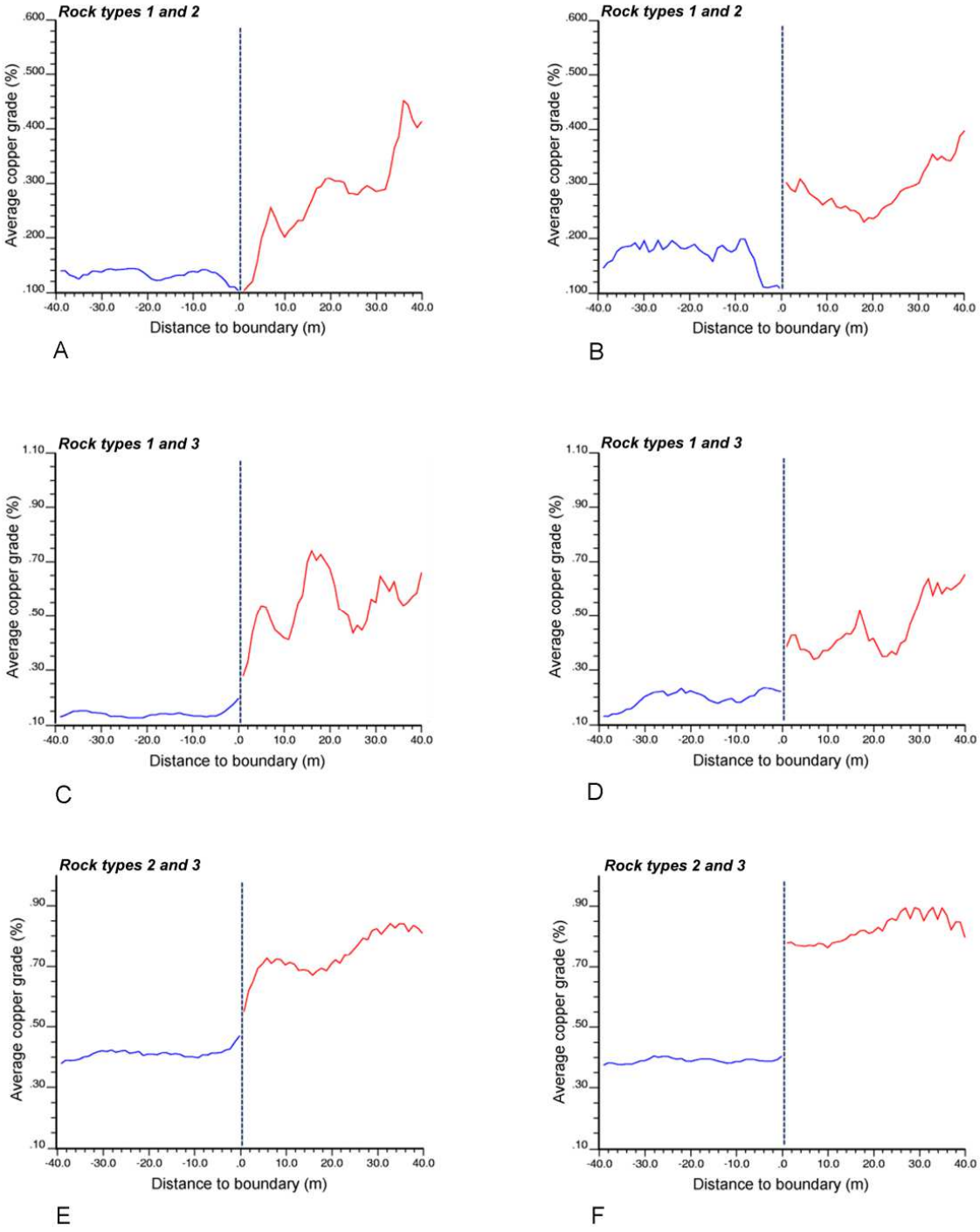

Figure 5.16: Mean grade graphs for joint simulation (A, C, E) and cascade simulation (B, D, F)

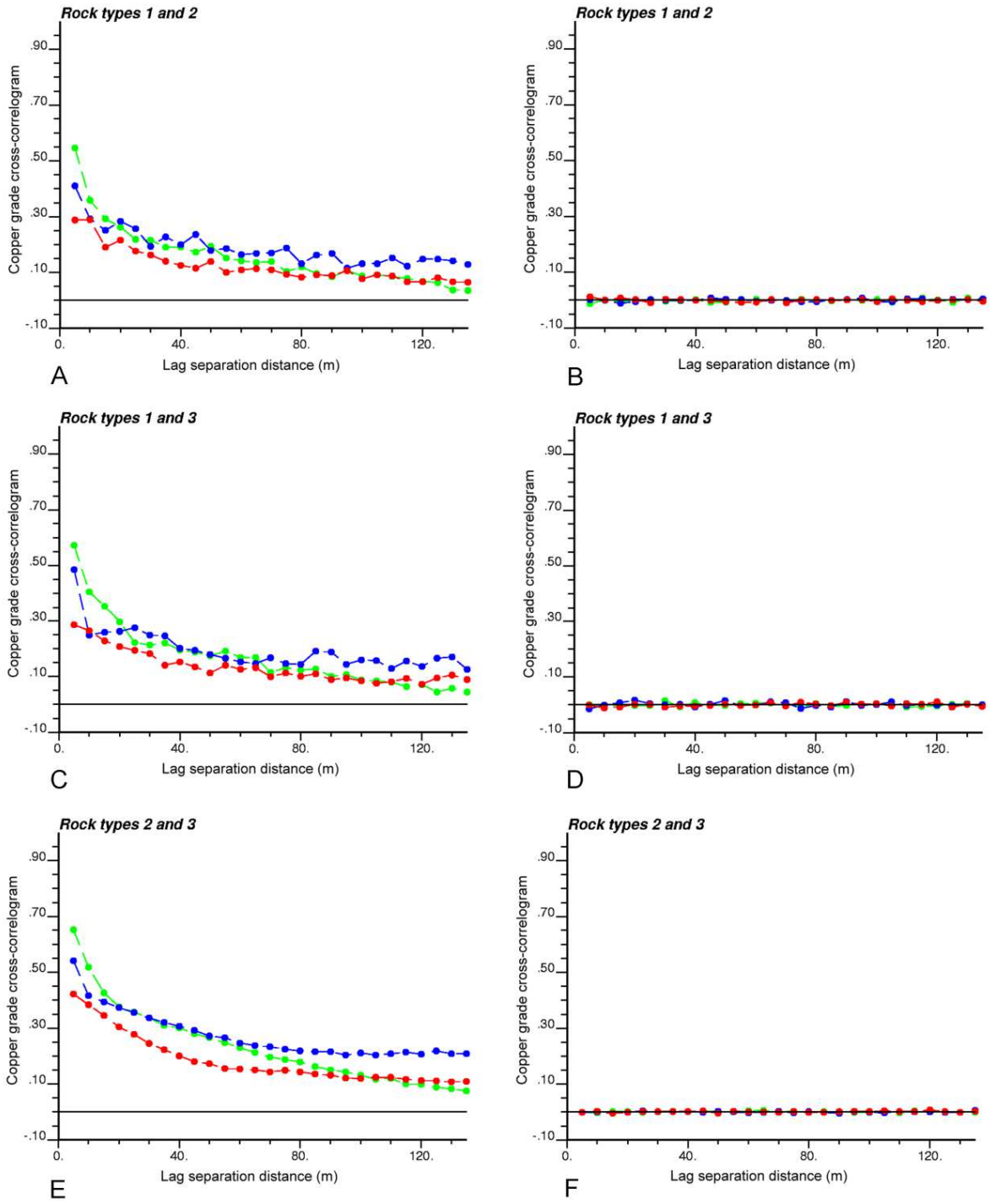

Figure 5.17: Correlation graphs for joint simulation (A, C, E) and cascade simulation (B, D, F), calculated along main anisotropy directions (green: N25°W; red: N115°E dip -60°; blue: N25°W dip -30°)

4. Conclusions

Obtaining uncertainty models is a cumbersome process when one deals with regionalized variables of different natures that are cross-correlated, such as grades and rock types. In this study, two well-known geostatistical models are combined: the multi-Gaussian model to describe grades and the plurigaussian model to describe rock types. The benefits of jointly simulating the grades and rock types with the proposed method are threefold. First, as opposed to deterministic rock type modeling, one can measure the uncertainty in the rock type layout, e.g., through probability maps. Second, the spatial dependence between grade and rock type can be reproduced. Third, the spatial correlation of grade across rock type boundaries is also reproduced, while this correlation is ignored by using the cascade simulation approach.

The co-simulation approach is suitable when grades exhibit gradual transitions across rock type boundaries. This happens in most ore deposits, in which there is no clear-cut discontinuity in the grade distribution when crossing a geological boundary, which can be explained because the physicochemical properties of the rock (pH, reduction potential, permeability, etc.) usually have transitional spatial variations. In contrast, the cascade approach consisting in simulating the rock types first, then the grades within each rock type, is adequate in the presence of hard boundaries. Such boundaries could be associated with faults or with geological gaps (vacuities or stratigraphic hiatii), among others.

5. Appendix A. Relations between indicator direct and cross variograms

In this study, three possible truncation rules that differ by the ordering of the rock types are under consideration (Figure 5.6). A simple way to determine the most suitable truncation rule is to examine the direct and cross variograms of rock type indicators (R_1, R_2 and R_3). In the model shown in Figure 5.6A, the rock type indicators are defined by truncating the Gaussian random fields Y_1 and Y_2 as follows

$$\begin{cases} R_1(\mathbf{x}) = 1_{Y_1(\mathbf{x})<y_1} \\ R_2(\mathbf{x}) = [1-1_{Y_1(\mathbf{x})<y_1}]1_{Y_2(\mathbf{x})<y_2} \\ R_3(\mathbf{x}) = [1-1_{Y_1(\mathbf{x})<y_1}][1-1_{Y_2(\mathbf{x})<y_2}]. \end{cases} \tag{5.6}$$

Let us calculate the cross variogram between R_1 and R_2 for a given lag separation vector **h**:

$$
\begin{aligned}
2\gamma_{12}(\mathbf{h}) &= E\{[R_1(\mathbf{x}+\mathbf{h}) - R_1(\mathbf{x})][R_2(\mathbf{x}+\mathbf{h}) - R_2(\mathbf{x})]\} \\
&= E\{[1_{Y_1(\mathbf{x}+\mathbf{h})<y_1} - 1_{Y_1(\mathbf{x})<y_1}][1 - 1_{Y_1(\mathbf{x}+\mathbf{h})<y_1}]1_{Y_2(\mathbf{x}+\mathbf{h})<y_2}\} \\
&\quad - E\{[1_{Y_1(\mathbf{x}+\mathbf{h})<y_1} - 1_{Y_1(\mathbf{x})<y_1}][1 - 1_{Y_1(\mathbf{x})<y_1}]1_{Y_2(\mathbf{x})<y_2}\}.
\end{aligned}
\tag{5.7}
$$

Since Y_1 and Y_2 are independent, one obtains

$$
\begin{aligned}
2\gamma_{12}(\mathbf{h}) &= E\{[1_{Y_1(\mathbf{x}+\mathbf{h})<y_1} - 1_{Y_1(\mathbf{x})<y_1}][1 - 1_{Y_1(\mathbf{x}+\mathbf{h})<y_1}]\}\, E\{1_{Y_2(\mathbf{x}+\mathbf{h})<y_2}\} \\
&\quad - E\{[1_{Y_1(\mathbf{x}+\mathbf{h})<y_1} - 1_{Y_1(\mathbf{x})<y_1}][1 - 1_{Y_1(\mathbf{x})<y_1}]\}\, E\{1_{Y_2(\mathbf{x})<y_2}\}.
\end{aligned}
\tag{5.8}
$$

Because Y_2 is stationary, $E\{1_{Y_2(\mathbf{x}+\mathbf{h})<y_2}\} = E\{1_{Y_2(\mathbf{x})<y_2}\} = G(y_2)$, where G is the standard Gaussian cumulative distribution function. Therefore

$$
\begin{aligned}
2\gamma_{12}(\mathbf{h}) &= E\{[1_{Y_1(\mathbf{x}+\mathbf{h})<y_1} - 1_{Y_1(\mathbf{x})<y_1}][1_{Y_1(\mathbf{x})<y_1} - 1_{Y_1(\mathbf{x}+\mathbf{h})<y_1}]\}\, G(y_2) \\
&= -2\, G(y_2)\, \gamma_{11}(\mathbf{h}),
\end{aligned}
\tag{5.9}
$$

where $\gamma_{11}(\mathbf{h})$ is the direct variogram of R_1 for lag separation vector $\mathbf{h}$. Similarly, one finds that the cross variogram between R_1 and R_3 is proportional to γ_{11}

$$
\gamma_{13}(\mathbf{h}) = [G(y_2) - 1]\gamma_{11}(\mathbf{h}). \tag{5.10}
$$

Accordingly, the ratios of cross-to-direct variograms, $\gamma_{12}(\mathbf{h})/\gamma_{11}(\mathbf{h})$ and $\gamma_{13}(\mathbf{h})/\gamma_{11}(\mathbf{h})$, do not depend on $\mathbf{h}$. This property implies the absence of preferential contacts (edge effects) between rock type 1 and rock type 2, and between rock type 1 and rock type 3 (Rivoirard, 1994; Séguret, 2013).

The results concerning the flags shown in Figures 5.6B and 5.6C are obtained by permuting the components of vector (R_1, R_2, R_3).

6. Appendix B. Distributions of grade conditional to rock type

In this appendix, it is of interest to determine, in the model fitted in Sections 3.4 to 3.6, the distribution of grade conditional to the rock type, i.e.

$$
\begin{aligned}
G(y_0 \mid \text{rock}\,1) &= P\{Y_0(\mathbf{x}) < y_0 \mid Y_1(\mathbf{x}) < y_1\} \\
G(y_0 \mid \text{rock}\,2) &= P\{Y_0(\mathbf{x}) < y_0 \mid Y_1(\mathbf{x}) \geq y_1, Y_2(\mathbf{x}) < y_2\} \\
G(y_0 \mid \text{rock}\,3) &= P\{Y_0(\mathbf{x}) < y_0 \mid Y_1(\mathbf{x}) \geq y_1, Y_2(\mathbf{x}) \geq y_2\}
\end{aligned}
\tag{5.11}
$$

for any real value y_0 (cut-off on the transformed copper grade).

To this end, let us expand the joint density of $\{Y_0(\mathbf{x}), Y_1(\mathbf{x})\}$ as follows (Lantuéjoul, 2002):

$$
g_{\rho_{01}}(y, y') = g(y)g(y')\sum_{p=0}^{+\infty} \frac{\rho_{01}^p}{p!} H_p(y) H_p(y'), \tag{5.12}
$$

with g the standard Gaussian probability density function, ρ_{01} the correlation coefficient between $Y_0(\mathbf{x})$ and $Y_1(\mathbf{x})$, and H_p the Hermite polynomial of degree p, defined as

$$
H_p(y) = \frac{1}{g(y)} \frac{d^p g(y)}{dy^p}. \tag{5.13}
$$

By integrating term by term, one obtains the bivariate cumulative distribution function

$$
\begin{aligned}
G_{\rho_{01}}(y_0, y_1) &= \sum_{p=0}^{+\infty} \frac{\rho_{01}^p}{p!} \int_{-\infty}^{y_0} \int_{-\infty}^{y_1} g(y)g(y') H_p(y) H_p(y')\, dy\, dy' \\
&= G(y_0)G(y_1) + g(y_0)g(y_1)\sum_{p=1}^{+\infty} \frac{\rho_{01}^p}{p!} H_{p-1}(y_0) H_{p-1}(y_1).
\end{aligned}
\tag{5.14}
$$

Likewise, the joint density of $\{Y_0(\mathbf{x}), Y_1(\mathbf{x}), Y_2(\mathbf{x})\}$ can be expanded as follows (Lantuéjoul, 2002):

$$
g_{\rho_{01},\rho_{02},\rho_{12}}(y, y', y'') = g(y)g(y')g(y'') \sum_{p,q,r=0}^{+\infty} \frac{\rho_{01}^p \rho_{02}^q \rho_{12}^r}{p!q!r!} H_{p+q}(y) H_{p+r}(y') H_{q+r}(y''). \tag{5.15}
$$

A term-by-term integration leads to the trivariate cumulative distribution function

$$
\begin{aligned}
G_{\rho_{01},\rho_{02},\rho_{12}}(y_0,y_1,y_2) = {} & G(y_0)G(y_1)G(y_2) \\
& + g(y_0)g(y_1)\sum_{p=0}^{+\infty}\frac{\rho_{01}^{q}}{q!}H_{p-1}(y_0)\,H_{p-1}(y_1) \\
& + g(y_0)g(y_2)\sum_{q=0}^{+\infty}\frac{\rho_{02}^{q}}{q!}H_{q-1}(y_0)\,H_{q-1}(y_2) \\
& + g(y_1)g(y_2)\sum_{r=0}^{+\infty}\frac{\rho_{12}^{r}}{r!}H_{r-1}(y_1)\,H_{r-1}(y_2) \\
& + \sum_{p,q,r=0}^{+\infty}\frac{\rho_{01}^{p}\,\rho_{02}^{q}\rho_{12}^{r}}{p!q!r!}g(y_0)g(y_1)g(y_2)\,H_{p+q-1}(y_0)\,H_{p+r-1}(y_1)\,H_{q+r-1}(y_2)
\end{aligned}
\tag{5.16}
$$

Accordingly, using the inclusion-exclusion principle, the distribution of grade conditional to the rock type (Equation 5.11) can be expressed as

$$
G(y_0 \mid \text{rock}\,1) = \frac{G_{\rho_{01}}(y_0,y_1)}{G(y_1)} \tag{5.17}
$$

$$
G(y_0 \mid \text{rock}\ 2) = \frac{G_{\rho_{02}}(y_0,y_2) - G_{\rho_{01},\rho_{02},\rho_{12}}(y_0,y_1,y_2)}{G(y_2) - G_{\rho_{12}}(y_1,y_2)} \tag{5.18}
$$

$$
G(y_0 \mid \text{rock}\ 3) = \frac{G(y_0) - G_{\rho_{01}}(y_0,y_1) - G_{\rho_{02}}(y_0,y_2) + G_{\rho_{01},\rho_{02},\rho_{12}}(y_0,y_1,y_2)}{1 - G(y_1) - G(y_2) + G_{\rho_{12}}(y_1,y_2)}. \tag{5.19}
$$

Chapter 6: Second Case study

1. Presentation of the case study and exploratory data analysis

The non-stationary models and algorithms presented in Chapter 3 are now applied to a second case study in mineral resources evaluation. The region under study is part of the Río Blanco – Los Bronces porphyry copper deposit, a breccia complex located in the Chilean central Andes, about 80 km northeast of Santiago.

Los Bronces is located in the western part of the deposit and is being mined by Anglo American, while the Río Blanco deposit is emplaced in the eastern part, with mineralized bodies (Río Blanco, La Unión, Central, Don Luis, Sur-Sur and La Americana) distributed over an area of six kilometers from north to south and two kilometers from east to west. La Unión, Don Luis and Sur-Sur are mined by Codelco (Andina Division) by open pit and underground operations. The Río Blanco deposit is partly hosted in the western margin of the San Francisco batholith, a multiphase intrusive containing quartz-diorite, granodiorite, quartz-monzonite, quartzmonzodiorite and granite, and partly in Miocene volcanics of the surrounding Abanico and Farellones formations, which consist of sub-horizontally dipping andesitic lavas (Warnaars et al., 1985; Stambuk et al., 1988). A geological description of the Río Blanco deposit can be found in the specialized literature (Skewes and Stern, 1995, 1996; Serrano et al., 1996; Kay et al., 1999; Vargas et al., 1999).

A set of 2376 samples from advanced exploration diamond drill holes, located in a volume of approximately 400 m × 600 m × 130 m in the Sur-Sur mineralized body, is available, with information on the rock types and total copper grades. In this deposit, the distribution of copper grade is mainly controlled by the lithology. One can actually distinguish two main rock types controlling the copper grade distribution:

- Tourmaline breccia: it is mainly located in the center of the region under study and has a high average copper grade. Tourmaline breccia has sharp and steep contacts with the host rock (Serrano et al., 1996; Frikken, 2003). The matrix is a kind of milled rock flour replaced by secondary tourmaline cement containing specular hematite, sulfide, quartz, magnetite, sulfate (anhydrite, gypsum) and biotite, with open spaces filled by tourmaline-quartz-sulfide. For lower tourmaline contents, the clasts are angular to subangular, while they become more rounded for higher tourmaline contents (Figure 6.1).

- Other rocks, with a low average copper grade. This group includes different rock types such as granodiorite and diorite in the eastern part of the region under study, whose mineralogy is mainly composed of plagioclases, orthoclase, quartz, biotite and hornblende (Figure 6.1), as well as low-graded breccias in the western part of the region under study, with a matrix of milled rock flour and a relatively low proportion of tourmaline (Frikken, 2003).

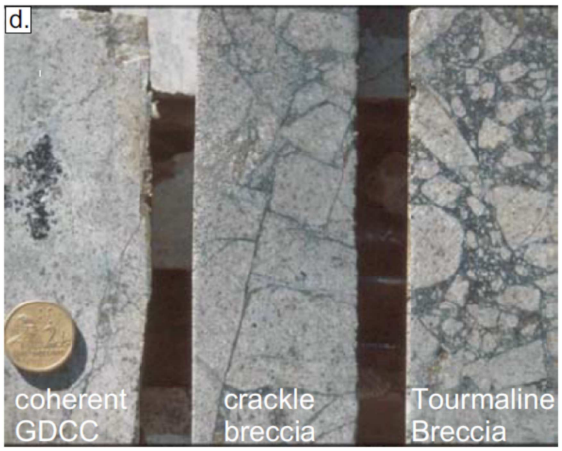

Figure 6.1: Transition from granodiorite to tourmaline breccia from drill hole samples (from Frikken (2003))

The location of the drill hole samples is displayed in Figure 6.2. One observes the clear zonation of the rock type, where the tourmaline breccia is present only in the central part of the region, while the lateral parts on the east and west sides are covered by the other rock types. A stationary model for the rock type would therefore be questionable, so that a model based on the truncation of an intrinsic random field of order k looks attractive.

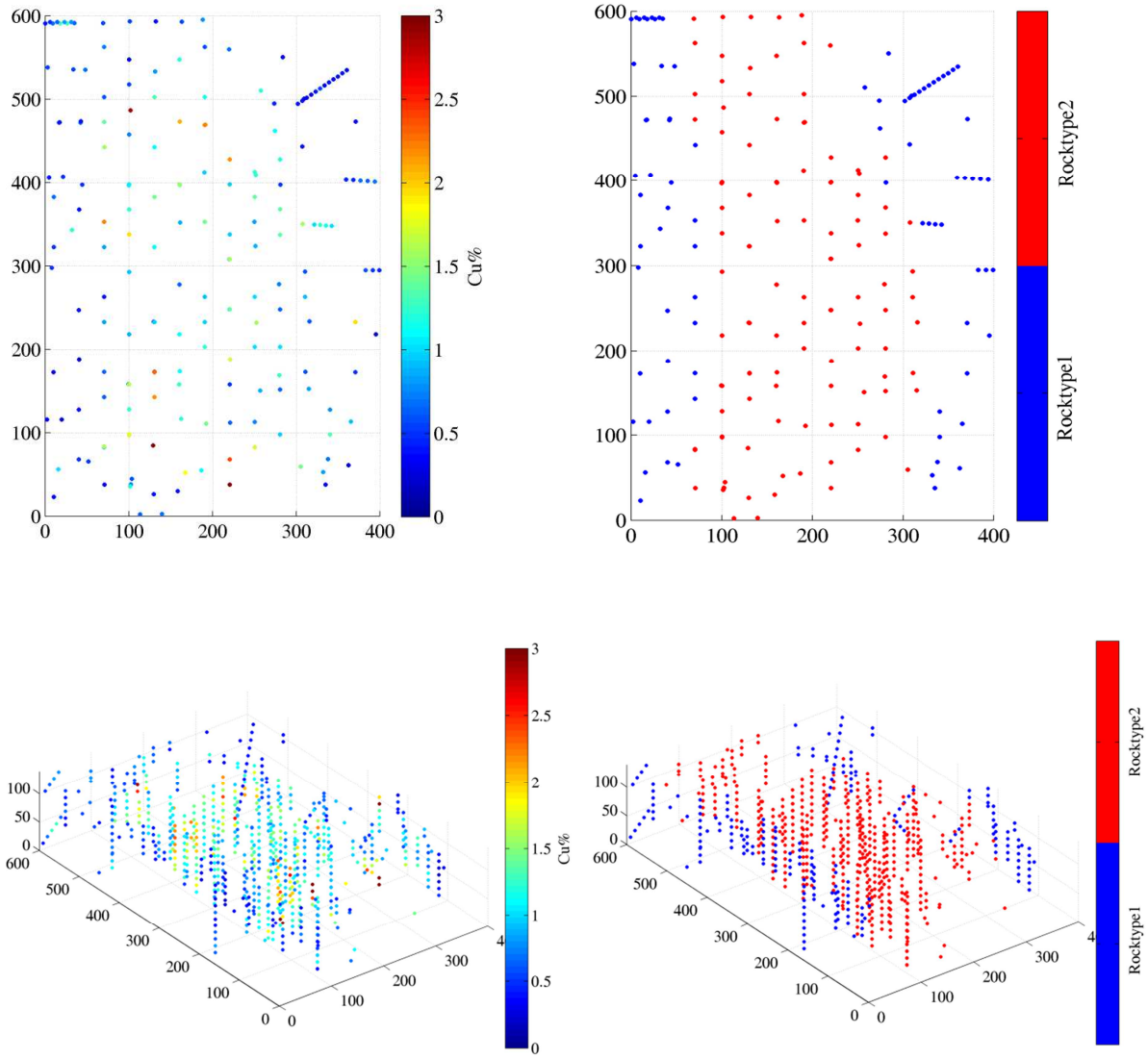

Figure 6.2: Location maps of drill hole data (top: easting-northing plan views; bottom: 3D perspective views). Colors indicate the copper grade (left) or the rock type (right) with the tourmaline breccia coded as “2” and the other rocks coded as “1”

The distribution and statistical parameters of the copper grade in the whole region and in each rock type are presented in Figure 6.3 and Table 6.1. As can be seen, the high values of copper grade are mainly located in the tourmaline breccia (rock type 2) and the low values of copper grade are mainly located in rock type 1.

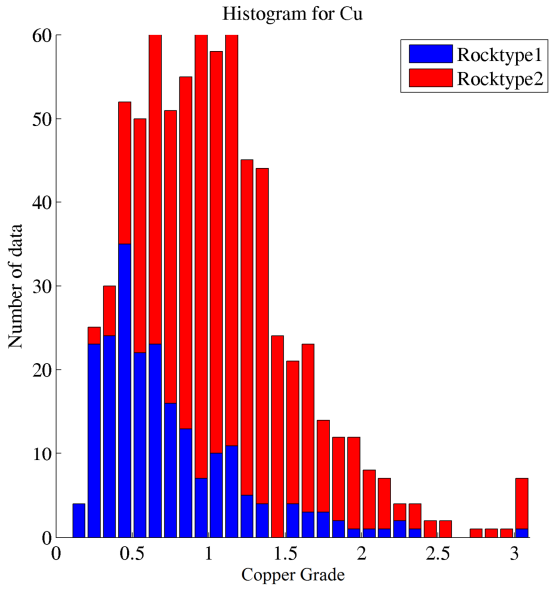

Figure 6.3: Histogram of copper grade (in percent) in different rock types

Table 6.1. Statistics of copper grade data (in percent), over the region and within each rock type

	Global	Rock type 1	Rock type 2
Number of data	737	216	521
Mean	1	0.7	1.2
Variance	0.4	0.2	0.4
Minimum	0.1	0.1	0.2
Median	1	0.6	1.1
Maximum	6.3	3.2	6.3

To determine whether or not the joint simulation approach is suited for these data, it is essential to examine the transition of copper grade between rock types, and define whether the rock type boundaries are “soft” (with gradual grade transitions) or “hard” (with abrupt grade transitions). To this end, a contact analysis between rock types was carried out. This analysis determines the behavior of the grade variable in the neighborhood of the boundary between two rock types. Specifically, one can use a “mean graph”, which shows how the mean copper grade varies when getting closer to or farther from the rock type boundaries, and a “correlation graph”, where one determines how the copper grade values between both

sides of the boundary are correlated. The results of contact analysis are displayed in Figure 6.4A (mean graphs) and Figure 6.4B (correlation graphs). In each case, one observes a soft contact between rock types, characterized by a rather smooth transition of the mean grade and correlation graphs that slowly decay to zero. So, having soft boundary incites us to use the joint simulation method instead of the conventional cascade method (recall the discussion in Chapter 1 - Section 1 and Chapter 2 - Section 3).

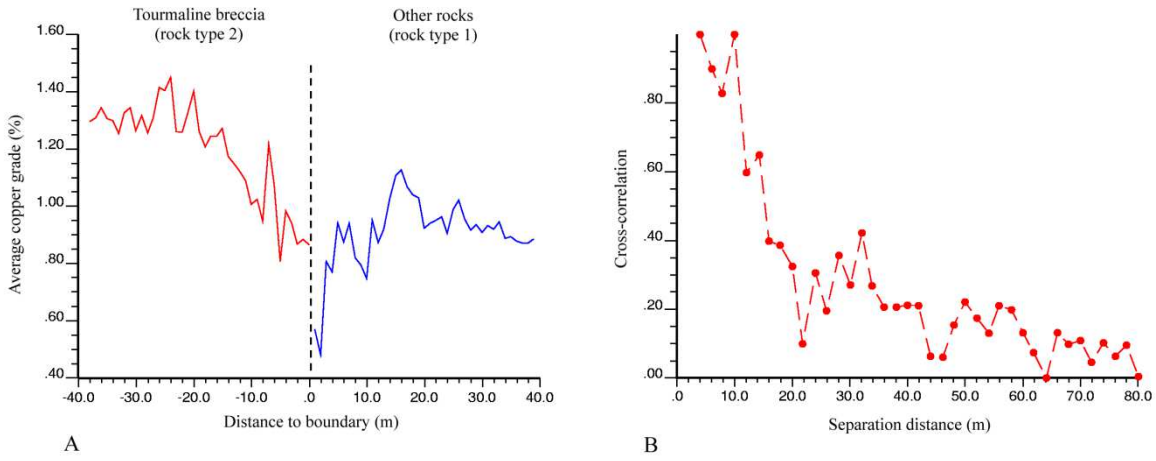

Figure 6.4: Contact analysis between rock types: A) mean grade graphs B) cross correlogram

2. Spatial structure analysis

One should define the joint spatial structure of copper grade and rock type. As explained in Chapter 4, the copper grade will be modeled by a stationary random field (transform of a Gaussian random field Y_0), while the rock type will be modeled by truncating an intrinsic random field of order *k* with Gaussian generalized increments (Y_1).

2.1. Structural analysis of copper grade

In order to identify the spatial structure of copper grade, the grade data are transformed into Gaussian data and variogram analysis is performed on the Gaussian data. The experimental variogram is calculated along the vertical and horizontal directions, which are recognized as the main anisotropy directions. The fitted model (generalized covariance K_0) comprises a nugget effect and two nested Matérn structures with shape parameters equal to 0.5, which correspond to exponential models (Figure 6.5):

$$K_0 = 0.195 \text{ nugget}$$
$$+0.29 \text{ Matérn}_{0.5}\ (30\text{m}, 75\text{m}) \qquad (5.1)$$
$$+0.45 \text{ Matérn}_{0.5}\ (100\text{m}, 250\text{m})$$

where the distances into brackets indicate the scale parameters of the Matérn models along the horizontal and vertical directions, respectively, while the scalar coefficient before each structure indicates the sill value of this structure. Recall that, for the Matérn model with shape parameter 0.5 (exponential model), one can define a practical correlation range equal to three times the scale parameter (Chilès and Delfiner, 2012).

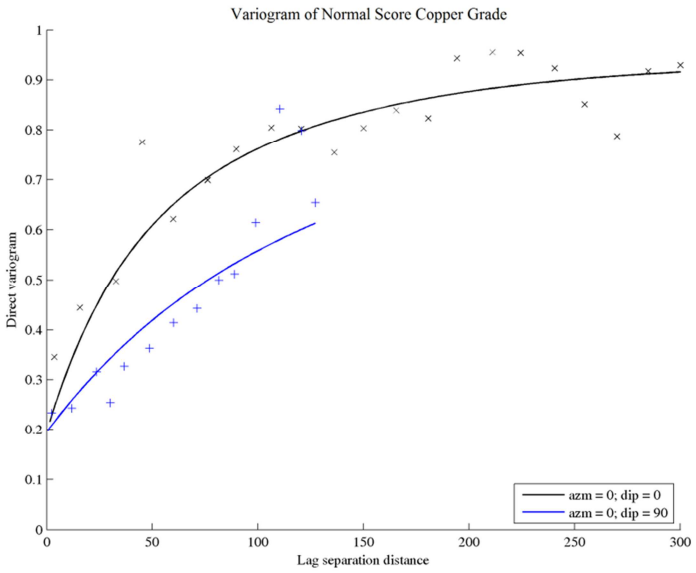

Figure 6.5: Sample and modeled variogram along main anisotropy directions (transformed copper grade)

2.2. Joint structural analysis of copper grade and rock type

In order to choose the best strategy for inferring the parameters of the rock type model, one has first to decide whether or not to represent the rock type by a stationary random field. To this end, let us calculate the experimental variogram of the tourmaline breccia indicator along the north-south and east-west directions (Figure 6.6). This indicator variogram has an apparent range of correlation that is of the order of magnitude of the region under study (400 meters along the east-west direction and 600 meters along the north-south) and, in any

case, greater than the range of correlation found for the copper grade (Figure 6.5). This observation makes questionable the use of a stationary random field model for representing the rock type, which would furthermore be complex to conciliate with the copper grade in a unified bivariate stationary model. Instead, a non-stationary model obtained by truncating an intrinsic random field of order k (denoted as Y_1) with Gaussian generalized increments, as presented in Chapter 4, seems a more convenient approach to represent the rock type.

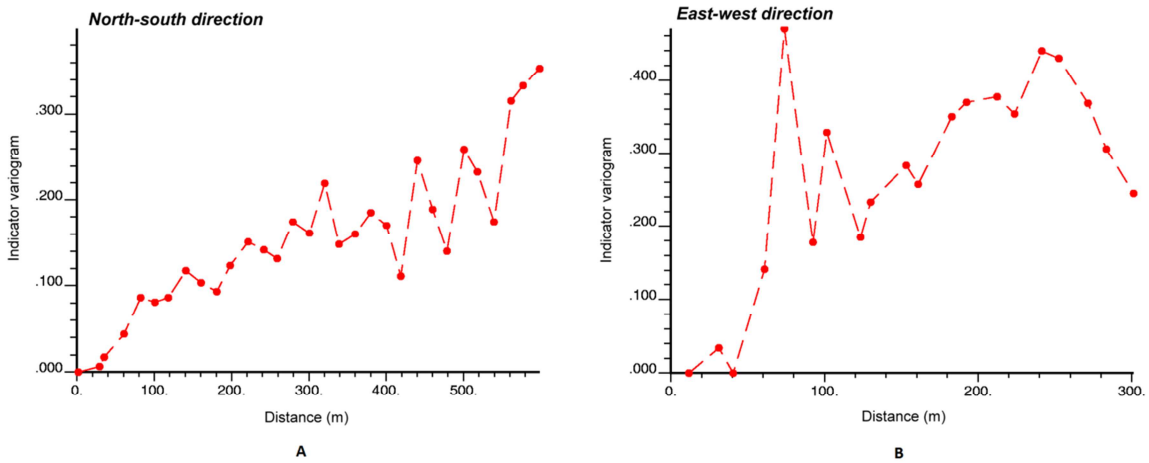

Figure 6.6: Experimental variogram of tourmaline breccia indicator along the north-south (A) and east-west (B) directions

The full spatial structure of the random fields Y_0 (associated with the copper grade) and Y_1 (associated with the rock type), i.e., their generalized direct and cross-covariances, will now be determined according to the methodology presented in Section 1.4 of Chapter 4. This methodology relies on the choice of

(1) an order k for the intrinsic random field;

(2) a set of locations for constructing an internal representation;

(3) a set of basic nested structures for the direct (K_0 and K_1) and cross (K_{10}) covariance models.

In relation to the order of the intrinsic random field, let us consider an order $k = 1$ in order to allow for a drift that could account for the rock type zonation. Once this order is chosen, the minimal number of locations needed to construct an internal representation is n = 4 (Equation 4.7); these locations are chosen randomly over the region of interest.

Concerning the nested structures, the direct covariance K_0 of the Gaussian random field Y_0 has already been fitted in the previous subsection with two Matérn models, both with shape parameters 0.5 (Equation 5.1). Under these conditions, let us assume a bivariate model for K_0, K_1 and K_{10} composed of the sum of two structures (apart from the nugget effect):

- The first structure is a bivariate Matérn model, where all the generalized direct and cross covariances are Matérn covariances. The conditions for this bivariate model to be mathematically valid have been established by Gneiting et al. (2010). For the sake of simplicity, in the following, we will set the shape parameters and the scale parameters along the horizontal and vertical directions to the same values as that found in the fitting of K_0, i.e. a shape parameter equal to 0.5 and scale parameters equal to 30 m (horizontally) and 75 m (vertically). This bivariate model actually boils down to an intrinsic correlation model where the generalized direct and cross covariances are proportional to the same exponential covariance.

- The second structure is a bivariate power-Matérn model, for which the generalized direct covariance associated with the rock type is a power model and the other direct and cross-covariances are Matérn, as presented in Section 1.5 of Chapter 4. Here again, some choices are necessary in order to reduce the number of parameters that will be determined by the least-squares fitting algorithm presented in Chapter 4. So, let us fix the exponent, shape and scale parameters of this bivariate model, in order to leave only the sills or slope to the least-squares fitting.

  - *Scale parameters*: the same scale parameters as the ones found when fitting K_0 will be used, in order to preserve the anisotropy direction and anisotropy ratio of the grade model. Consequently, the scale parameters are set to 100 m along the horizontal direction and 250 m along the vertical.

  - *Exponent*: in order to obtain an IRF-1 for the random field Y_1, the exponent of its power covariance cannot be greater than 4 (Matheron, 1973; Chilès and Delfiner, 2012). Exponents lower than 2 correspond to an IRF-0, which are not of interest here (although they can be viewed as special cases of IRF-1). Accordingly, we orient ourselves toward a power generalized covariance for Y_1 with an exponent between 2 and 4. For simplicity, let us choose a value of 3. Note that such a generalized covariance is smooth near the origin and will tend to produce smooth boundaries between the two rock types after truncating the IRF-1 (Lantuéjoul, 2002), which agrees with the geological understanding of the deposit.

  - *Shape parameter*: concerning the shape parameter of the cross-covariance between Y_0 and Y_1, the lower bound is 1, as per Equation (4.24) presented in Chapter 4. Again, for simplicity, we will take this bound as the parameter value.

The generalized direct and cross-covariances of the random fields Y_0 and Y_1 will therefore be assumed of the following form:

$$K_0 = 0.195 \text{ nugget} + 0.29 \text{ Matérn}_{0.5}(30m, 75m) + 0.45 \text{ Matérn}_{0.5}(100m, 250m)$$

$$K_1 = c_{11} \text{ Matérn}_{0.5}(30m, 75m) + c'_{11} \text{ Power}_3(100m, 250m)$$

$$K_{10} = c_{10} \text{ Matérn}_{0.5}(30m, 75m) + c'_{10} \text{ Matérn}_1(100m, 250m)$$

where the coefficients c_{11}, c'_{11}, c_{10} and c'_{10} remain to be determined. This is achieved by using the least-squares fitting algorithm presented in Chapter 4, which is aimed to obtain the smallest total sums of squared errors between the experimental and modeled covariance matrices of the indicator data and cross-covariance matrices of indicator and transformed grade data.

Also, the choice of the scale parameters, shape parameters and exponent of the bivariate model can be revised if the sum of squared errors is deemed too high. Another criterion for validating the fitted model is to construct a set of conditional realizations, to calculate the probability map for the tourmaline breccia and compare this map with the interpretation of the deposit made by the mining geologists: the closer, the better.

The final results of this process are presented in Table 6.2.

Table 6.2. Fitted generalized direct and cross covariances

	Basic structure	Sill or slope	Horizontal scale parameter (m)	Vertical scale parameter (m)	Shape parameter or exponent
Generalized direct covariance K_1	Matérn	0.030	30	75	0.5
	Power	0.098	100	250	3.0
Generalized cross-covariance K_{10}	Matérn	0.000	30	75	0.5
	Matérn	0.252	100	250	1.0

Three observations are worth being made on the fitted model:

(1) The nugget effect is only present in the grade model (covariance K_0), as the rock type variations are assumed to be continuous in space. Being absent from K_1, the nugget effect must also be absent from the cross-covariance K_{10} (Wackernagel, 2003).

(2) The sill/slope coefficients $c'_{00} = 0.45$, c'_{11} and c'_{10} of the power-Matérn model fulfill the condition presented in Equation (4.25) to be mathematically valid.

(3) The sill coefficient c_{10} of the bivariate Matérn model is zero, which means that, for this structure, there is no cross-correlation between the grade and the rock type. The cross correlation originates from the power-Matérn model, which accounts for the large scale variations and non-stationarity of the rock type distribution. In other words, the large-scale lithological zonation is responsible for the spatial dependence between the copper grade and the rock type and for the geological control exerted by the latter upon the former.

3. Conditional simulation

Provided with the spatial correlation model, one can construct realizations of the grade and rock type. The simulation first consists in simulating the intrinsic random field Y_1 at the drill hole data locations, conditionally to the grade and rock type data, by Gibbs sampling (using a mixed simple / intrinsic cokriging for determining the successive conditional distributions, as explained in Section 2.2 of Chapter 4). Then, the spectral turning bands algorithm is applied to construct non-conditional realizations over the region of interest, which are subsequently conditioned to the data (transformed grade data and output of the Gibbs sampler for the rock type data) by residual cokriging, again using a mixed simple / intrinsic cokriging. The realizations of Y_0 are back-transformed to the copper grade scale by means of the grade anamorphosis function, while the realizations of Y_1 are truncated to lead to the rock type model (tourmaline breccia / other rocks). As explained in Chapter 4, the truncation threshold can be set to zero, in both the Gibbs sampler and the truncation stages.

One hundred realizations are generated over a regular grid with a spacing of 5m × 5m × 12m along the east, north and elevation coordinates, respectively. Cokriging is made in a unique neighborhood, which theoretically ensures the convergence of the Gibbs sampler (Emery et al., 2014). The Gibbs sampler is stopped after 10,000 iterations, i.e., when the value at each drill hole data has been updated 10,000 times. Regarding the spectral - turning bands algorithm, n_D = 1000 lines are used.

Figures 6.7 and 6.8 show four conditional realizations of grade and rock type. As expected, no discontinuity is observed in the distribution of copper grade when crossing the boundary between the two rock types (soft boundaries). The maps are consistent with the data values displayed in Figure 6.2, where the tourmaline breccia is located in the center of the region under study and contains the highest copper grade.

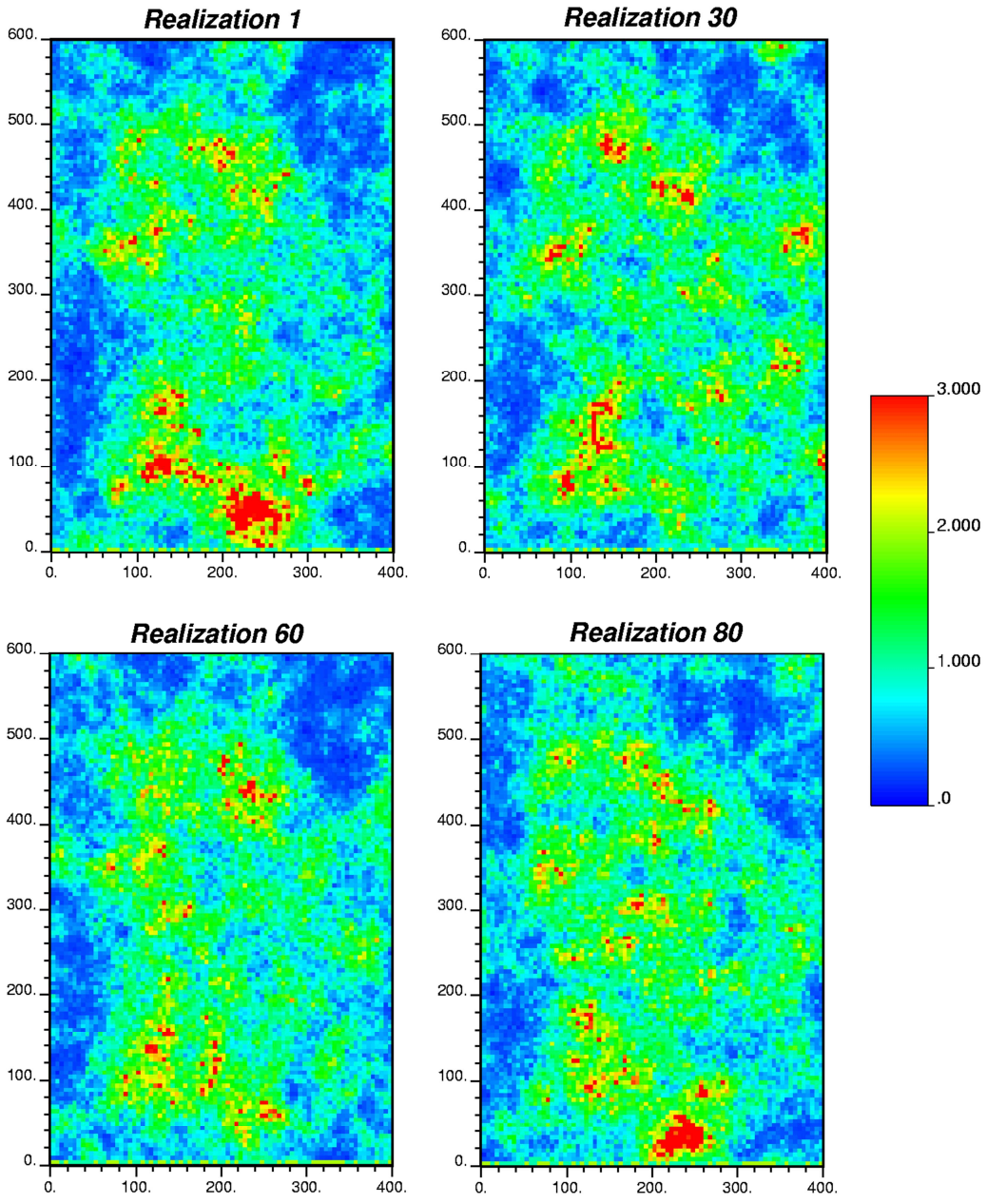

Figure 6.7: Four conditional realizations of the copper grade (easting-northing plan views) for a specific elevation

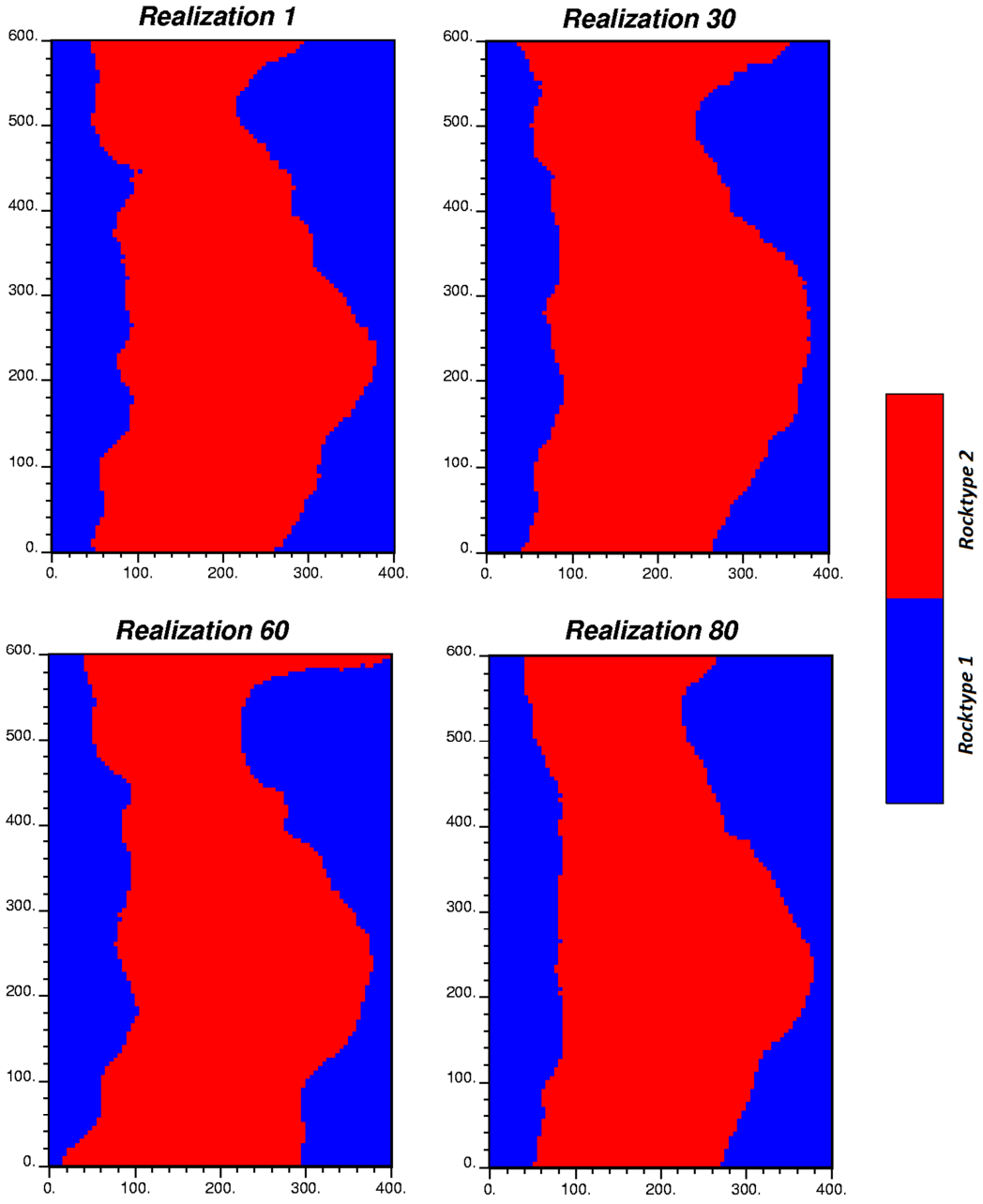

Figure 6.8: Four conditional realizations of the rock type (easting-northing plan views) for a specific elevation

4. Post-processing the realizations

4.1. Post-processing the copper grade realizations

Having constructed 100 grade realizations, several outputs can be calculated. For instance, Figure 6.9A shows the expected copper grade, identified as the average, at each location, of the 100 grade realizations (this is sometimes referred to as "conditional mean" or as "e-type"). Such an average of the realizations is actually similar to the predictor that would be obtained by simple kriging of the grade data (Figure 6.9B), except for some perceptible differences in the borders of the region under study.

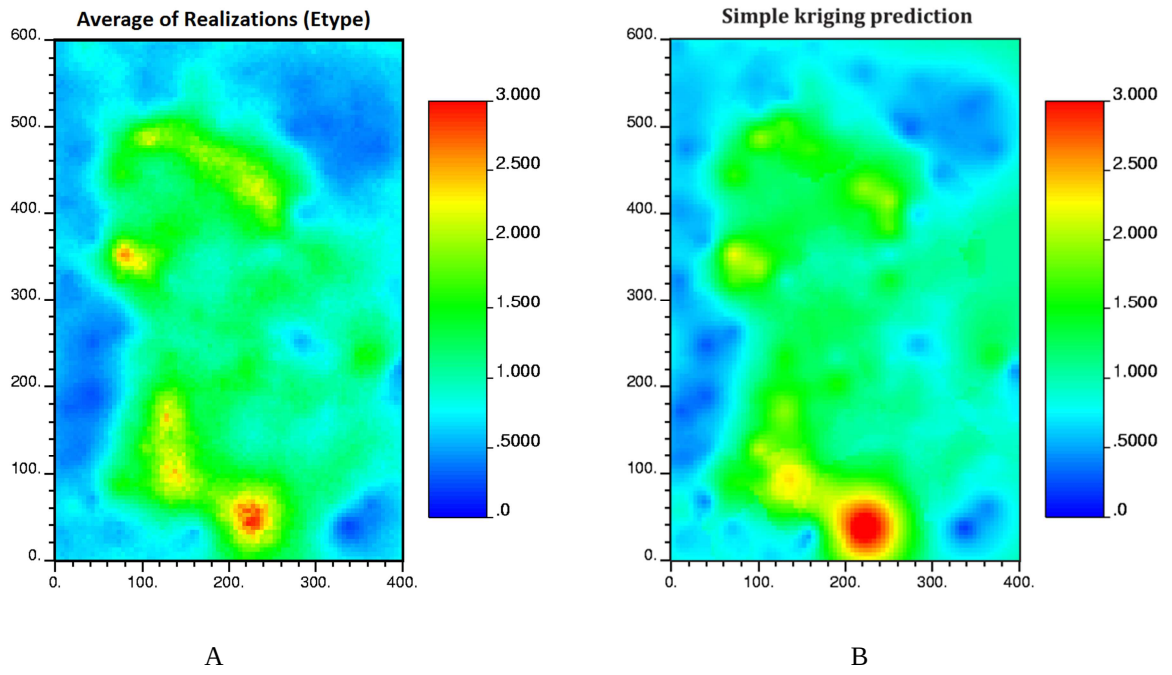

Figure 6.9: A, average of one hundred conditional realizations and B, simple kriging prediction of copper grade (easting-northing plan views) for a specific elevation

Figure 6.10 displays the conditional variance and the conditional coefficient of variation of the copper grades. The conditional variance indicates the dispersion of the simulated grade around its expected value. The conditional coefficient of variation is equal to the square root of the conditional variance divided by the conditional mean and states the local variability as a fraction of the expected value. Both the conditional variance and conditional coefficient of variation measure the uncertainty in the true (unknown) copper grades and reflect the so-called proportional effect (higher uncertainty in high-graded areas), contrarily to the kriging variance (Journel and Huijbregts, 1978).

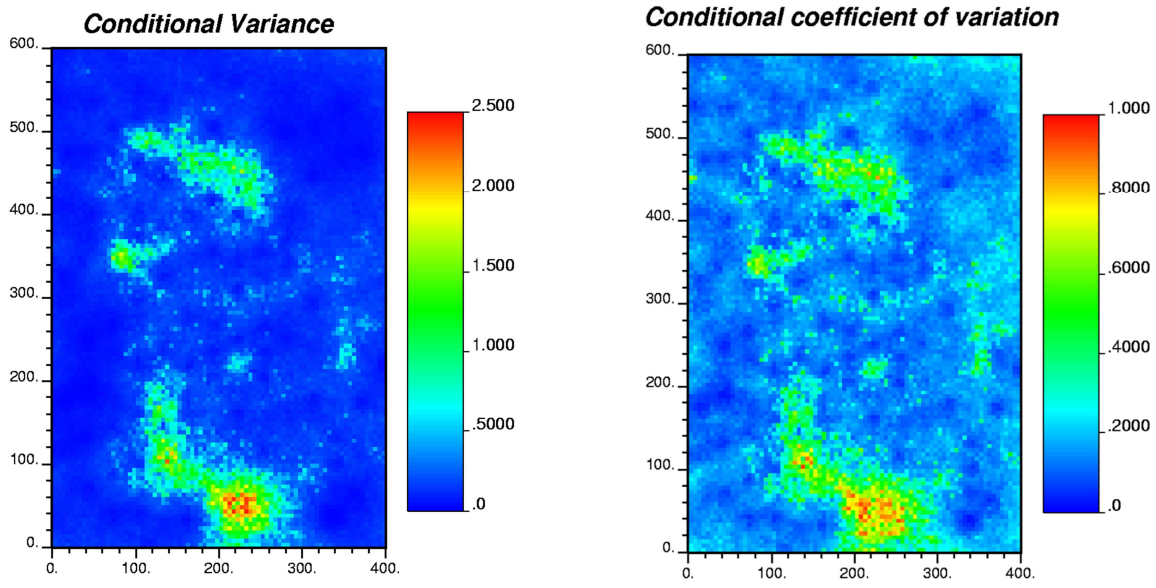

A B

Figure 6.10: A) conditional variance B) conditional coefficient of variation (easting-northing plan views) for a specific elevation

At a global scale, one can also calculate the expected mean grade and the tonnage that can be recovered for different cut-off grades (Figure 6.11). Typical cut-off grades for this kind of deposit vary between 0.3% and 0.7%, depending on technical and market conditions.

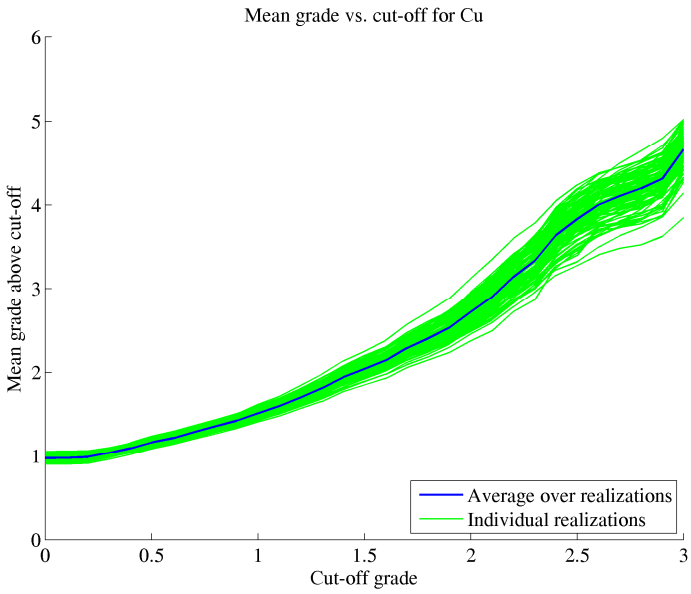

A

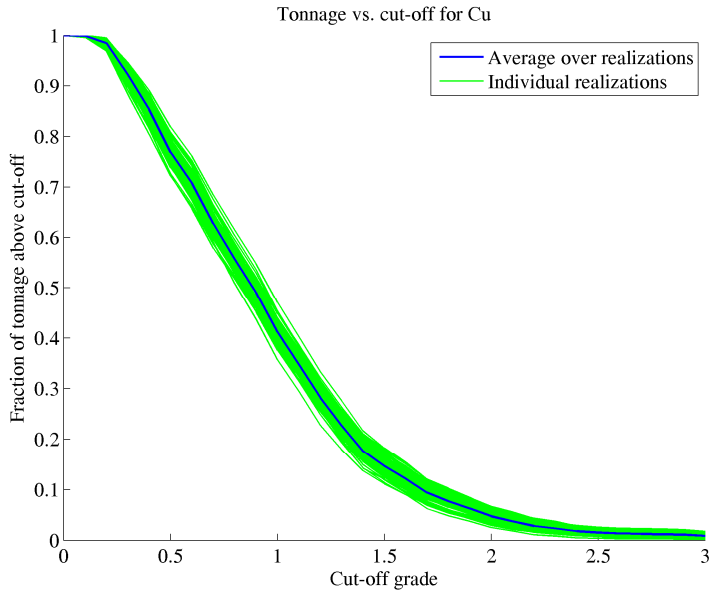

B

Figure 6.11: A) mean grade and B) tonnage above different cut-off grades

4.2. Post-processing the rock type realizations

By having one hundred realizations of the rock type, one can calculate the uncertainty in the proportions of each rock type at each target grid node, through probability maps (Figure 6.12). As can be seen from this figure, the probability of occurrence of tourmaline breccia (rock type 2) is very high in the center of the region under study and is almost zero in the eastern and western sides, while the reverse happens for the other rocks (rock type 1). This zonation is consistent with the logs observed on the drill hole data and with the geological understanding of the deposit.

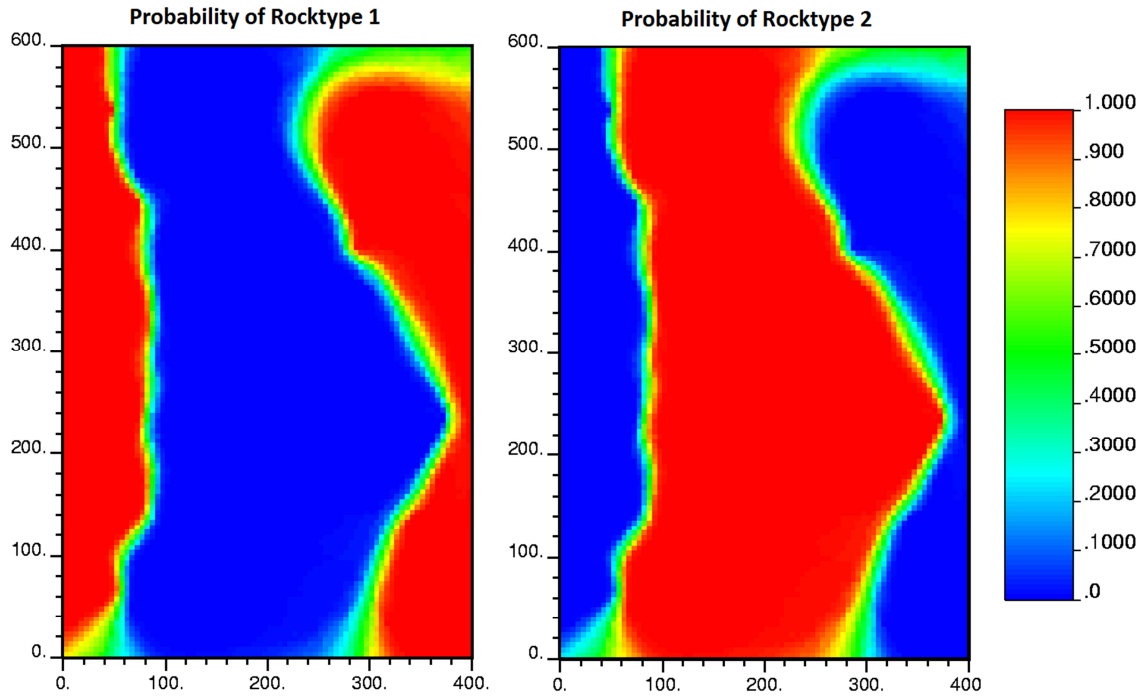

Figure 6.12: conditional probabilities of rock types 1 and 2 (easting-northing plan views) for a specific elevation

5. Model validation

5.1. Split-sample validation using drill hole data

Split-sample validation can be used to determine the accuracy and quality of the simulated values. Specifically, the original drill hole data set (2376 data) is divided into two subsets, each containing about half of the data, via a random selection. Then, one of the subsets (training subset) is used as conditioning data for simulating the grades and rock types at the locations of the other subset (testing subset). The simulated values at the testing subset, as well as their average (conditional mean, considered as the best predictor of the true values) can finally be compared to the true values.

As observed in Figure 6.13, the results of this process suggest that the proposed model is accurate for the copper grade, insofar as the grade prediction is conditionally unbiased (the regression of the true value upon the predicted value is close to the identity) and precise (the points of the scatter plot have a small dispersion)

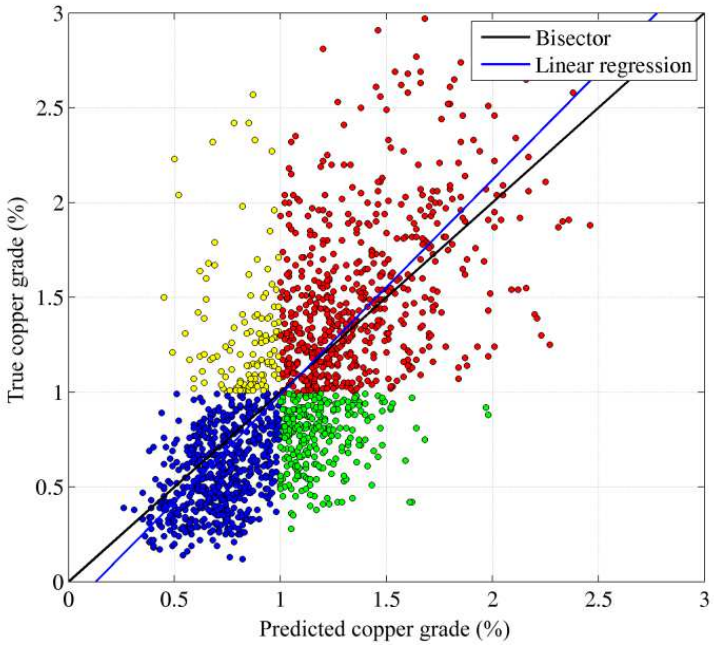

Figure 6.13: Split-sample validation of copper grade using drill hole data

For a given cut-off grade, one can classify the data into four sets: data with predicted and true grades below the cut-off (waste correctly classified as waste, blue points in Figure 6.13), data with predicted and true grades above the cut-off (ore correctly classified as ore, red points in Figure 6.13), data with predicted grade above the cut-off but true grades below the cut-off (waste misclassified as ore, green points in Figure 6.13), and data with predicted grade below the cut-off and true grade above the cut-off (ore misclassified as waste, yellow points in Figure 6.13). As a measure of accuracy, one can calculate the percentage of data that have a correct classification (waste classified as waste or ore classified as ore).

The process can be repeated by considering each grade realization individually instead of the average of the realizations. The percentages of correct classification for different cut-off grades and realizations are shown in Figure 6.14.

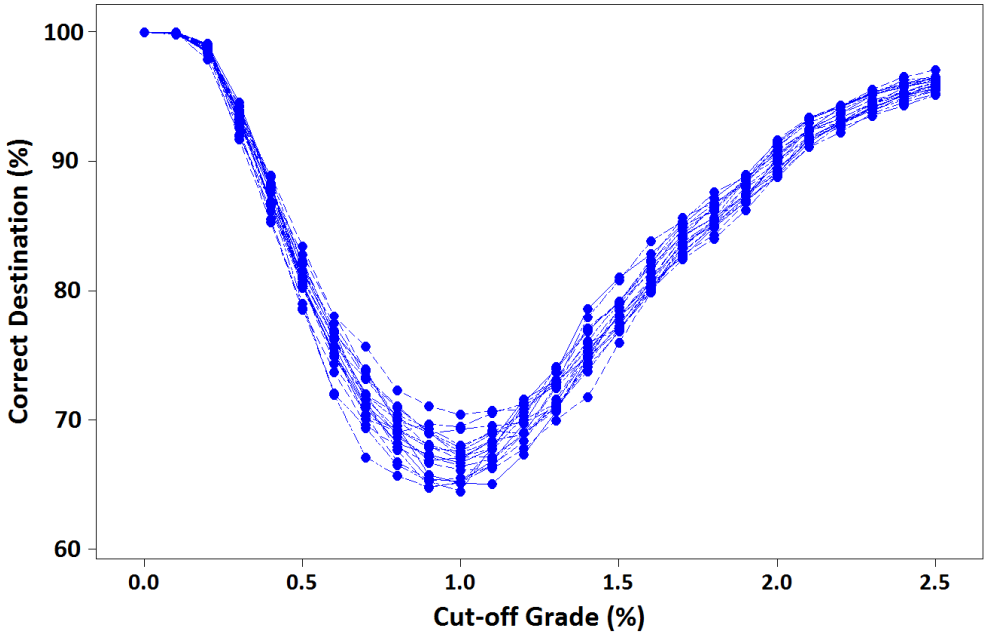

Figure 6.14: Percentage of correct classification (ore / waste) for twenty grade realizations

From the conditional realizations, one can also compute a series of symmetric p-probability intervals (PI) at each location of the testing subset. The bounds of the PI of probability p are the quantiles $(1–p)/2$ and $(1+p)/2$ of the simulated values, for instance the lower and upper quartiles if $p = 0.5$. A correct modeling of uncertainty would entail that, for example, there is a 50% probability that the actual copper grade falls into the 0.5-PI or, equivalently, that over the testing subset, approximately 50% of the 0.5-PI contain the true copper grade value (Goovaerts, 2001). As a consequence, the scatter plot of the probability p versus the proportion of testing data contained in the p-PI (known as an accuracy plot) allows one to visualize the departures between observed and expected proportions as a function of the probability p (Figure 6.15). This plot indicates an accurate modeling of the uncertainty, as the departures are small.

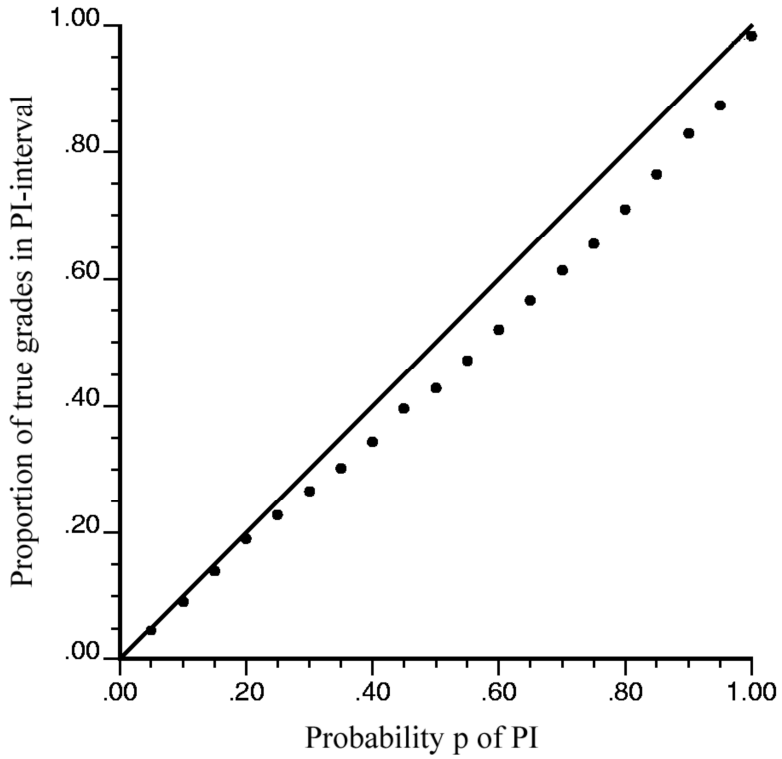

Figure 6.15: Accuracy plot calculated from 100 conditional realizations of copper grade

5.2. Validation using blast hole data

Another way to assess the accuracy of the model is to use blast hole data (if accessible). In such a case, one can simulate the copper grade at the blast hole locations and compare the simulated values with the true values. Figure 6.16 shows the locations of blast hole data in a specific horizontal bench, while Figure 6.17 shows the scatter plot of the average of 100 simulated value vs. the true value (copper grades measured at the blast hole samples). As for the split-sample validation performed on the drill hole data, the results of this process demonstrate that the model is conditionally unbiased, as the regression line is close to the bisector line, and precise, as the points of the scatter plot have a small dispersion around this bisector.

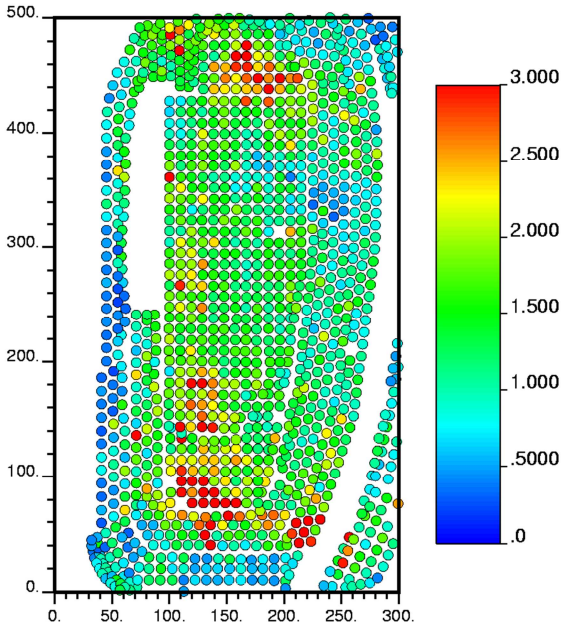

Figure 6.16: Location of blast hole data in a specific bench (color scale for copper grade)

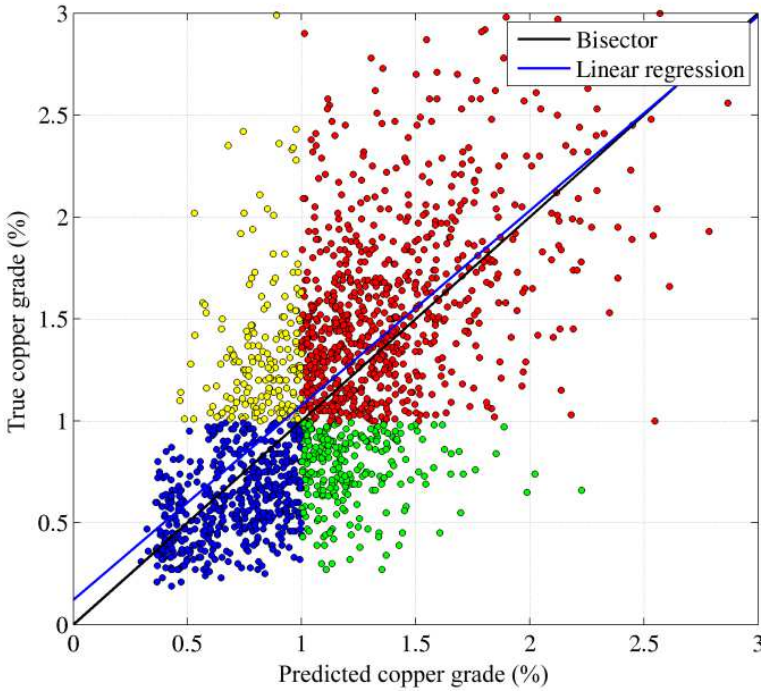

Figure 6.17: Split-sample validation of copper grade using blast hole data

6. Comparison with the cascade approach

In order to demonstrate the superiority of the joint simulation approach over the cascade approach, the copper grade has also been simulated by the cascade approach. To this end, the non-stationary rock type model obtained from the joint simulation approach is used and the copper grade is simulated in each rock type separately, according to the following steps:

For each rock type (tourmaline breccia and other rocks):

(1) Transform the copper grade data into Gaussian data
(2) Calculate the experimental variogram of the transformed data
(3) Fit a theoretical (stationary) variogram model
(4) For each rock type realization:
   - Construct a non-conditional realization of the transformed grade at the locations belonging to this rock type, by means of the stationary spectral – turning bands algorithm presented in Chapter 2, Section 1.4.
   - Condition the realization to the transformed data by simple kriging.
   - Back-transform the simulated values from the Gaussian scale to the grade scale.

This way, one obtains as many copper grade realizations as rock type realizations. In the following subsections, we compare the results of this approach with the ones obtained with the joint simulation approach.

6.1. Reproducing the nature of the rock type boundary

As shown in the first section of this chapter, the available data indicate a soft boundary between rock types 1 and 2, i.e. the transition of copper grade from rock 1 to rock type 2 is gradual. Ideally, the simulation algorithm should be capable to reproduce this soft boundary for each realization.

This can be confirmed by examining the variations of the mean grade when getting closer to a rock type boundary and by assessing the spatial correlation between the simulated copper grades across a boundary, through mean graphs and correlation graphs similar to the ones used for the available data. Figures 6.18A and 6.18B show these graphs for the joint simulation approach. It is seen that the mean grade shows a gradual transition near the rock type boundary and the simulated grades on either side of the boundaries are correlated, as what is observed in the original data (Figure 6.4). This indicates that the joint simulation approach, as was expected, reproduces the soft boundary between rock types 1 and 2. Conversely, the graphs related to the cascade approach (Figures 6.18C and 6.18D) indicate an abrupt change in the mean values of the simulated copper grades when crossing the boundary and a very weak correlation between the simulated grades on the both sides of the

boundary. This is explained because the cascade model neglects the spatial correlation of the copper grade across the boundary and therefore reproduces a hard boundary.

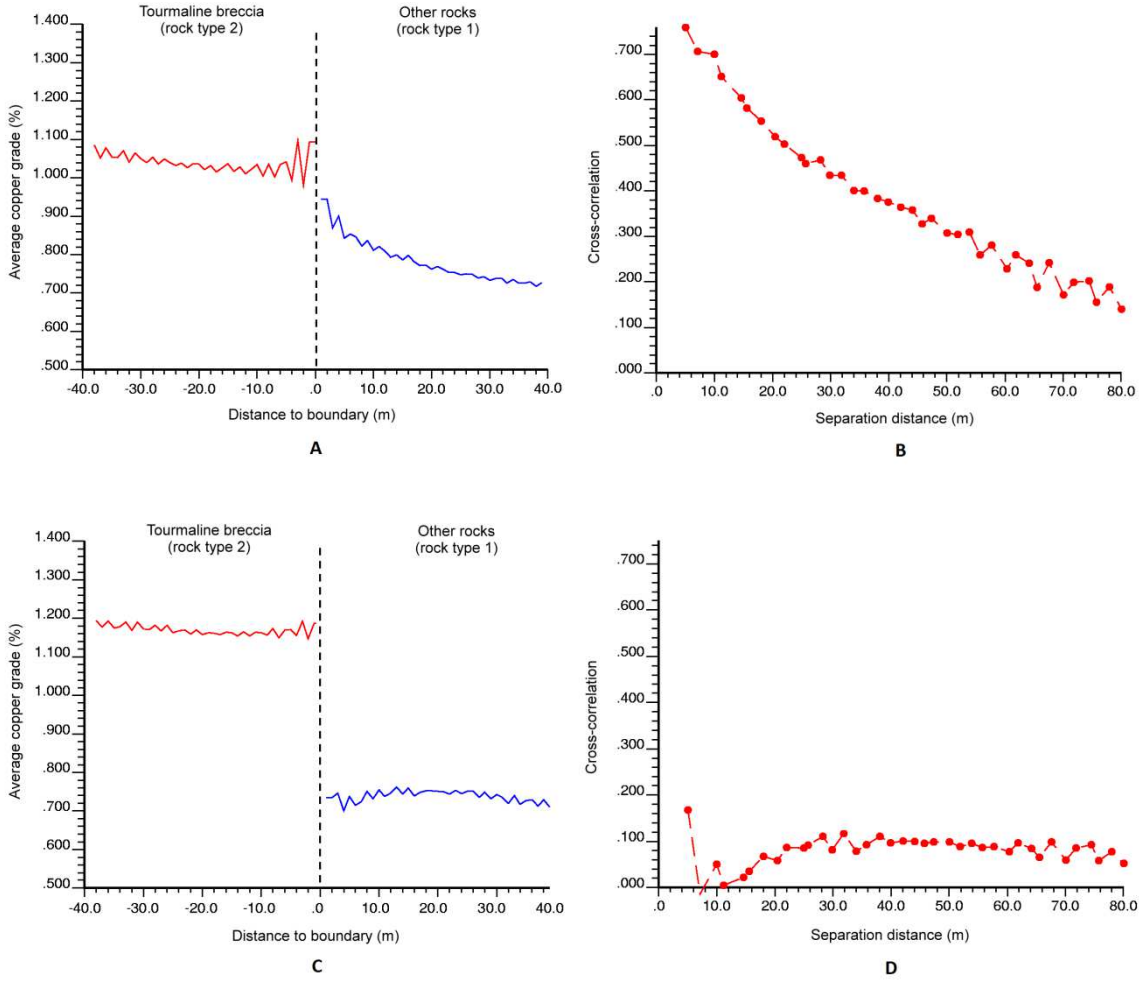

Figure 6.18: Contact analysis for results of joint simulation (A, B) and cascade (C, D) approaches

The maps of the simulated copper grades corroborate the previous statements: in the joint simulation approach, gradual variations of the grades are observed near the rock type boundary, whereas discontinuities are perceptible in the cascade approach (Figure 6.19).

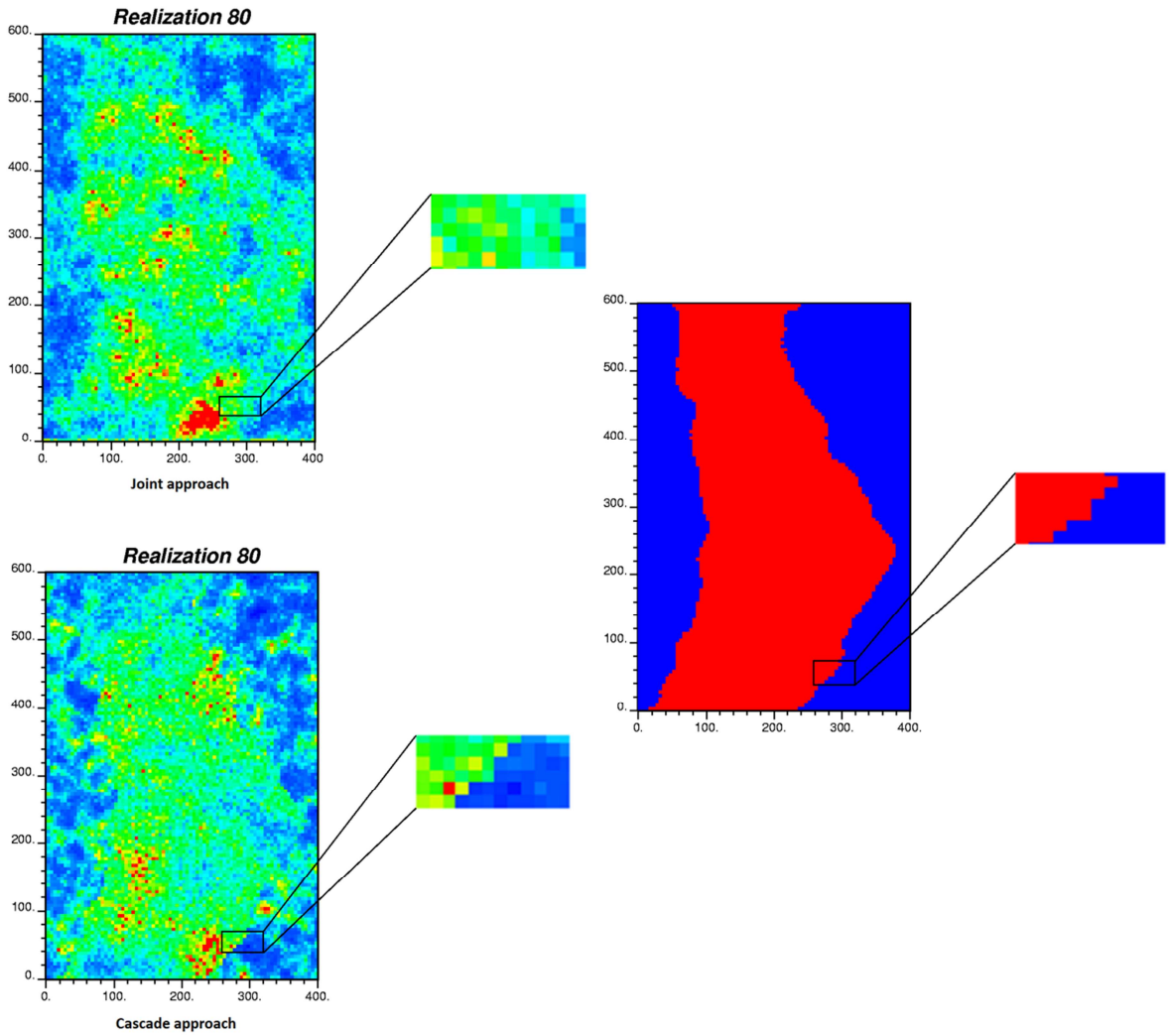

Figure 6.19: One copper grade realization generated with the joint simulation (top) and cascade (bottom) approaches, together with the corresponding rock type realization (easting-northing plan views) for a specific elevation

6.2. Prediction of copper grades

Figure 6.20 shows the average of the 100 copper grade realizations generated by the joint simulation and cascade approaches, respectively. Such an average map (conditional mean) indicates the expected copper grade and provides the prediction of the copper grade that minimizes the mean squared error.

At first glance, the joint simulation approach generates lower values of the copper grade in the edges of the region under study (corresponding to rock type 1) in comparison with the cascade approach. This can be explained because, in the joint simulation, the copper grade is positively correlated with the IRF-1 associated with the rock type, which is likely to take

large negative values in the outer locations. In contrast, in the cascade approach, the grade in rock type 2 is modeled as a stationary field with a constant mean value, so the variations in the conditional mean are only due to the effect of the conditioning data (these data are not so abundant in this rock type, so their effect is moderate).

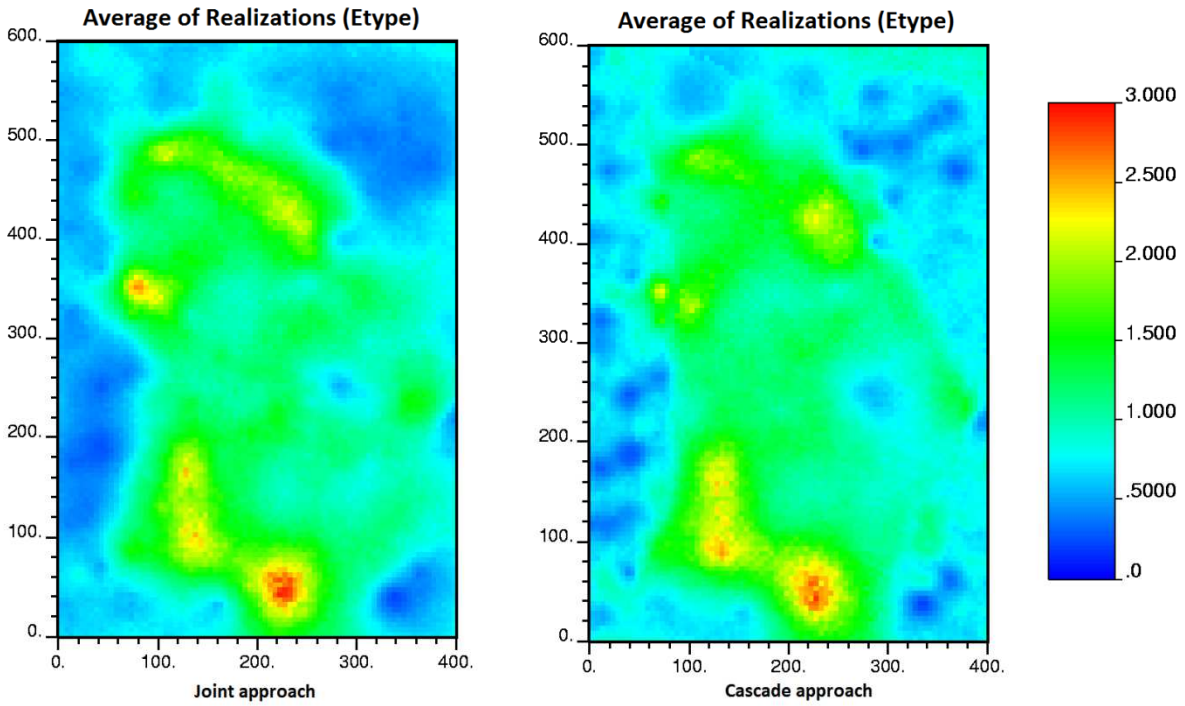

Figure 6.20: Average of one hundred realizations of the copper grade generated by the joint simulation (left) and cascade (right) approaches (easting-northing plan views) for a specific elevation

6.3. Quantification of grade uncertainty

Nowadays, uncertainty is a fundamental parameter that is widely used for classifying mineral resources into measured, indicated and inferred resources. Among many possible measures of uncertainty, the conditional variance (CV) and the conditional coefficient of variation (CCV) are sometimes considered as criteria for classifying the resources (Dimitrakopoulos et al., 2010; Maleki-Tehrani et al., 2013). As seen in Figures 6.10 and 6.21, both the CV and CCV are significantly smaller when using the joint simulation approach in comparison with the cascade approach, which is explained because the latter uses fewer conditioning data when simulating the grades in each rock type separately (tourmaline breccia data are neglected when simulating the other rock type, and vice-versa, which leads to a greater uncertainty).

As a result, if one uses these measures as criteria for classifying the mineral resources, the amount of the ore tonnage located in the measured class is likely to considerably increase by using the joint simulation approach, while the cascade approach will tend to provide more ore tonnage in inferred resources, thus a more conservative resource classification. In other words, by using the joint simulation approach, the uncertainty in the obtained model is reduced significantly by a more judicious use of the information conveyed by the drill hole data.

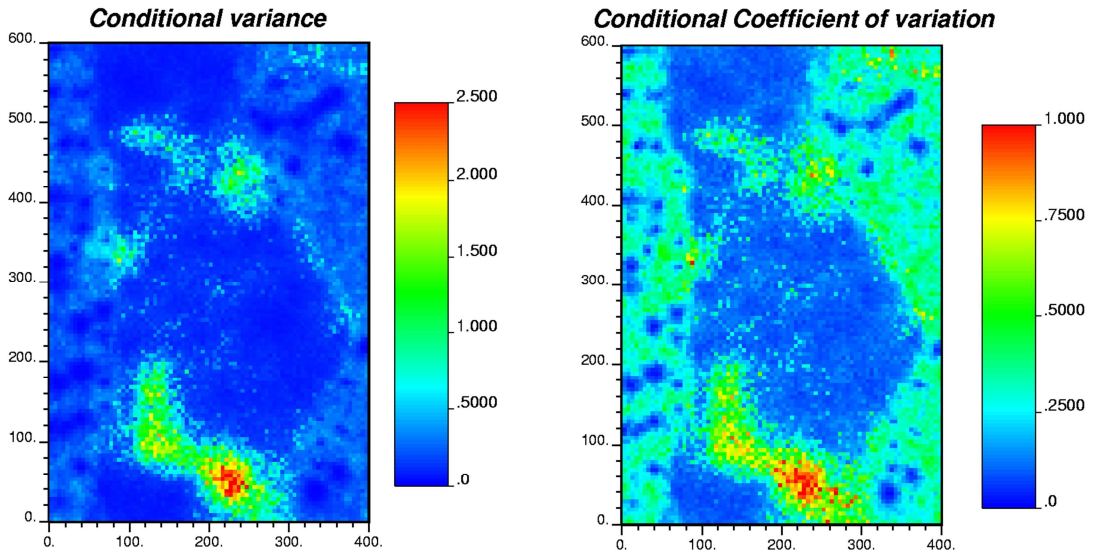

A B

Figure 6.21: A) Conditional variance and B) conditional coefficient of variation for the copper grade, obtained by the cascade approach (easting-northing plan views) for a specific elevation

Chapter 7: Discussion and conclusions

1. General discussion

In this thesis we have generalized an algorithm established in the stationary framework for jointly simulating categorical (rock type) and continuous (grade) variables. In the proposed generalization, the continuous variable is the transform of a stationary Gaussian random field and the categorical variable is obtained by truncating an intrinsic random function of order *k* with Gaussian generalized increments (instead of a stationary Gaussian random field). This algorithm is very useful as, in practice, geological domains such as rock types, mineralization or alteration domains often exhibit spatial trends, so that the probability of occurrence of a given domain is not constant in space. Using a non-stationary model therefore seems consistent with the existence of geological zonations. The second case study has proven the applicability and capability of the proposed model and algorithms to perform joint simulation of stationary and non-stationary random fields and to reproduce their spatial correlation and spatial trends.

From a methodological viewpoint, one does not have access to an experimental covariance or variogram to which a theoretical model can be fitted graphically, as happens in the stationary case. Therefore, in practice, the main difficulty of the proposed algorithm is the inference of the generalized covariance associated with the non-stationary field and the generalized cross covariance with the stationary field. A semi-automated fitting procedure has been designed, based on the calculation of the indicator covariance and cross covariance between all the pairs of data locations, followed by a least-square optimization to determine the parameters of the generalized covariance and cross covariance functions to be modeled. Also, some bivariate models for the generalized direct and cross covariances of a stationary and a non-stationary random field have been developed, and conditions on their parameters have been established to guarantee their mathematical validity.

Another difficulty that has been solved relates to the processes of converting a non-conditional simulation into a conditional one and of converting categorical data into continuous ones via Gibbs sampling. For a stationary Gaussian random field, these processes rely on the use of simple kriging or, when simulating two or more cross-correlated random fields, simple cokriging. In the present thesis however, we dealt with two Gaussian random fields, one of which was stationary and the other one was an IRF-*k* (non-stationary). As a consequence, a specific type of cokriging, called mixed simple / intrinsic cokriging, has been designed for the purpose of conditioning the realizations and Gibbs sampling. Concerning the practical implementation of cokriging, a unique neighborhood has been used to ensure the convergence of the Gibbs sampler to the desired distribution.

2. Conclusions

In mining applications, one is generally interested in modeling the uncertainty in the outcome of continuous variables (such as metal grades), conditionally to the data on these variables and a correlated categorical variable representing geological domains. As these variables have a different nature, their joint modeling is often complex and cumbersome. Most often, this problem is by-passed by resorting to a hierarchical or cascade approach, in which the categorical variable is modeled first, then the continuous variables are modeled within each category, which tends to produce discontinuities when crossing the boundaries between categories.

To address this issue, approaches mixing the multigaussian and plurigaussian models have been proposed in the past years, but were restricted to a stationary setting, while the spatial layout of rock types, mineralization or alteration domains often exhibits spatial trends and zonations, making the stationarity assumption questionable.

In this context, the objective of this thesis was to extend the joint simulation of continuous and categorical random fields to a non-stationary setting, by assuming that the categorical field is obtained through the truncation of an intrinsic random field of order k. To reach this objective, some essential tools and algorithms have been developed for inferring the model parameters (essentially, the spatial correlation structure, represented by generalized direct and cross covariance functions) and for constructing realizations conditioned to existing data. Then, the proposed tools and algorithms have been applied and validated through a real case study (Rio-Blanco Los Bronces porphyry copper deposit), where copper grade and rock type have been jointly simulated conditionally to the information available at a set of drill hole samples from advanced exploration campaigns.

The methodological proposals presented in this thesis may be the basis for future works, in particular:

1) A straightforward generalization to simulate more than two rock types would be to use the plurigaussian model instead of the truncated Gaussian model, following the work of Madaniesfahani (2016).

2) Improvements in the identification of the spatial correlation structure (generalized direct and cross covariances) and in the Gibbs sampler when the available data are numerous are challenging issues. Indeed, the algorithms proposed in this thesis are still limited by the number n of input data, as the inference of generalized direct and cross covariances relies on the fitting of data-to-data covariance matrices (i.e., matrices of size $n \times n$), while Gibbs sampling is performed with a unique neighborhood implementation.

Chapter 8: Bibliography

[1] Alabert, F.G. (1987) Stochastic imaging of spatial distributions using hard and soft information. Master's Thesis, Stanford University, Stanford, California.

[2] Alabert, F.G., Massonnat, G.J. (1990) Heterogeneity in a complex turbiditic reservoir: stochastic modelling of facies and petrophysical variability. In: 65th annual technical conference and exhibition of the Society of Petroleum Engineers, SPE-20604, pp. 775-790.

[3] Armstrong, M., Galli, A., Beucher, H., Le Loc'h, G., Renard, D., Doligez, B., Eschard, R., Geffroy, F. (2011) Plurigaussian Simulations in Geosciences. Springer, Berlin.

[4] Armstrong, M., Jabin, R. (1981) Variogram models must be positive-definite. Mathematical Geology 13(5): 455-459.

[5] Arroyo, D., Emery, X. (2015) Simulation of intrinsic random fields of order k with Gaussian generalized increments by Gibbs sampling. Mathematical Geosciences 47(8): 955-974.

[6] Arroyo, D., Emery, X. (2016a) Spectral simulation of multivariate fractional Brownian surfaces in d-dimensional Euclidean spaces. Stochastic Environmental Research and Risk Assessment, in press. DOI: 10.1007/s00477-016-1225-7.

[7] Arroyo, D., Emery, X. (2016b) A spectral-turning bands algorithm to jointly simulate stationary and intrinsic Gaussian random fields in d-dimensional Euclidean spaces. In: Tenth International Geostatistics Congress, Valencia, Spain.

[8] Arroyo, D., Emery, X., Peláez, M. (2012) An enhanced Gibbs sampler algorithm for nonconditional simulation of Gaussian random vectors. Computers & Geosciences 46:138-148.

[9] Bahar, A., Kelkar, M. (2000) Journey from well logs/cores to integrated geological and petrophysical properties simulation: a methodology and application. SPE Reservoir Evaluation and Engineering 3(5): 444-456.

[10] Bernstein, D. (2005). Matrix Mathematics. Princeton University Press.

[11] Beucher, H., Galli, A., Le Loc'h, G., Ravenne, C. (1993) Including a regional trend in reservoir modeling using the truncated Gaussian method. In: Soares, A. (ed.) Geostatistics Tróia'92. Kluwer Academic, Dordrecht, pp. 555-566.

[12] Biver, P., Haas, A., Bacquet, C. (2002) Uncertainties in facies proportion estimation II: application to geostatistical simulation of facies and assessment of volumetric uncertainties. Mathematical Geology 34(6): 703-714.

[13] Bochner, S. (1933) Monotone Funktionen, Stieljessche Integrale und harmonische Analyse. Mathematische Annalen 108: 378-410.

[14] Boucher, A., Dimitrakopoulos, R. (2012) Multivariate block-support simulation of the Yandi iron ore deposit, Western Australia. Mathematical Geosciences 44(4): 449-468.

[15] Boulanger, F. (1990) Modélisation et simulation de variables régionalisées, par des fonctions aléatoires stables. Doctoral dissertation, Ecole Nationale Supérieure des Mines de Paris, Fontainebleau.

[16] Box, G.E.P, Jenkins, G.M. (1976) Time Series Analysis: Forecasting and Control. Holden Day, Oakland.

[17] Brooker, P.I. (1985) Two-dimensional simulation by turning bands. Mathematical Geology 17(1): 81-90.

[18] Bruno, R., Raspa, G. (1993) Towards a direct structural analysis of an IRF-k. In: Soares, A. (ed.) Geostatistics Tróia'92. Kluwer, Dordrecht, pp. 49-59.

[19] Cáceres, A., Emery, X. (2010) Conditional co-simulation of copper grades and lithofacies in the Rio Blanco-Los Bronces copper deposit. In: Castro, R., Emery, X., Kuyvenhoven, R. (eds.) Proceedings of the IV international conference on mining innovation MININ 2010. Gecamin Ltd, Santiago, Chile, pp. 311-320.

[20] Cáceres, A., Emery, X., Aedo, L., Galvez, O. (2011) Stochastic geological modeling using implicit boundary simulation. Proceedings of the 2th International seminar geology for mining industry. Gecamin Ltda., Santiago, Chile.

[21] Cassiani, G., Christakos, G. (1998) Analysis and estimation of natural processes with nonhomogeneous spatial variation using secondary information. Mathematical Geology 30(1): 57-76.

[22] Chan, K.S. (1993) Asymptotic behavior of the Gibbs sampler. Journal of the American Statistical Association 88(421): 320-326.

[23] Chessa, A.G., Martinius, A.W. (1992) Object-based modelling of the spatial distribution of fluvial sandstone deposits. In: Christie, M.A., Da Silva, F.V., Farmer, C.L., Guillon, O., Heinemann, Z.E., Lemonnier, P., Regtien J.M.M., van Spronsen, E. (eds.) Proceedings of the 3rd European Conference on the Mathematics of Oil Recovery, Delft University Press, pp. 5-14.

[24] Chiasson, P., Soulie, M. (1997) Nonparametric estimation of generalized covariances by modeling on-line data. Mathematical Geology 29(1): 153-172.

[25] Chilès, J.P. (1977) Géostatistique des phénomènes non-stationnaires (dans le plan). Doctoral dissertation, Université de Nancy-I, France.

[26] Chilès, J.P. (1995) Quelques méthodes de simulation de fonctions aléatoires intrinsèques. In: Cahiers de Géostatistique 5: 97-112. Ecole Nationale Supérieure des Mines de Paris, Fontainebleau, France.

[27] Chilès, J.P., Delfiner, P. (1997) Discrete exact simulation by the Fourier method. In: Baafi, E.Y., Schofield, N.A. (eds.), Geostatistics Wollongong '96. Kluwer Academic, Dordrecht, pp. 258-269.

[28] Chilès, J.P., Delfiner, P. (2012) Geostatistics: Modeling Spatial Uncertainty. Wiley, New York, 699 pp.

[29] Chilès, J.P., Gable, R. (1984) Three-dimensional modelling of a geothermal field. In: Verly, G., David, M., Journel, A.G., Maréchal, A. (eds.) Geostatistics for Natural Resources Characterization. Reidel, Dordrecht, pp. 587-598.

[30] Chilès, J.P., Gentier, S. (1993) Geostatistical modelling of a single fracture. In: Soares, A. (ed.) Geostatistics Tróia'92. Kluwer, Dordrecht, pp. 95-108.

[31] Cown, E.J. (2003) Practical implicit geological modeling. In: Proceedings of Fifth International Mining Geology Conference. The Australasian Institute of Mining and Metallurgy, Melbourne, pp. 1-3.

[32] Cressie, N. (1987) A nonparametric view of generalized covariances for kriging. Mathematical Geology 19(5): 563-586.

[33] Daly, C., Caers, J. (2010) Multi-point geostatistics - an introductory overview. First Break 28(9): 39-47.

[34] Davis, M. (1987) Production of conditional simulations via the LU triangular decomposition of the covariance matrix. Mathematical Geology 19(2): 91-98.

[35] Delfiner, P. (1976) Linear estimation of nonstationary spatial phenomena. In: Guarascio, M., David, M., Huijbregts, C.J. (eds.) Advanced Geostatistics in the Mining Industry. Reidel, Dordrecht, pp. 49-68.

[36] De Marsily, G. (1986) Quantitative Hydrogeology: Groundwater Hydrology for Engineers. Academic, San Diego.

[37] Deutsch, C.V., Journel, A, G. (1998) GSLIB: Geostatistical software library and user's guide. Oxford University Press, New York, 369 pp.

[38] Dietrich, C.R., Newsam, G.N. (1993) A fast and exact method for multidimensional Gaussian stochastic simulations. Water Resources Research 29 (8): 2861-2869.

[39] Dimitrakopoulos, R. (1990) Conditional simulation of intrinsic random functions of order k. Mathematical Geology 22(3): 361-380.

[40] Dimitrakopoulos, R., Godoy, M., Chou, C.L. (2010) Resource/reserve classification with integrated geometric and local grade variability measures. In: Dimitrakopoulos, R. (ed.), Advances in Ore Body Modelling and Strategic Mine Planning. Australasian Institute of Mining and Metallurgy, Melbourne, pp. 207-214.

[41] Dong, A. (1990) Estimation géostatistique des phénomènes régis par des équations aux dérivées partielles. Doctoral thesis, Ecole des Mines de Paris, Paris.

[42] Dowd, P.A. (1994) Geological controls in the geostatistical simulation of hydrocarbon reservoirs. Arabian Journal for Science and Engineering 19(2B): 237-247.

[43] Dowd, P.A. (1997) Structural controls in the geostatistical simulation of mineral deposits. In: Baafi, E.Y., Schofield, N.A. (eds.), Geostatistics Wollongong'96. Kluwer Academic, Dordrecht, pp. 647-657.

[44] Dowd, P.A., Pardo-Igúzquiza, E., Xu, C. (2003) Plurigau: a computer program for simulating spatial facies using the truncated plurigaussian method. Computers & Geosciences 29(2): 123-141.

[45] Duke, J.H., Hanna, P.J. (2001) Geological interpretation for resource modelling and estimation. In: Edwards, A.C. (ed.) Mineral Resource and Ore Reserve Estimation - The AusIMM Guide to Good Practice. The Australasian Institute of Mining and Metallurgy, Melbourne, pp. 147-156.

[46] Emery, X. (2007a) Using the Gibbs sampler for conditional simulation of Gaussian-based random fields. Computers & Geosciences 33(4): 522-537.

[47] Emery, X. (2007b) Simulation of geological domains using the plurigaussian model: New developments and computer programs. Computers & Geosciences 33(9): 1189-1201.

[48] Emery, X. (2008a) Statistical tests for validating geostatistical simulation algorithms. Computers & Geosciences 34(11): 1610-1620.

[49] Emery, X. (2008b) A turning bands program for conditional co-simulation of cross-correlated Gaussian random fields. Computers & Geosciences 34(12): 1850-1862.

[50] Emery, X., Arroyo, D., Peláez, M. (2014) Simulating large Gaussian vectors subject to inequality constraints by Gibbs sampling. Mathematical Geosciences 46: 265-283.

[51] Emery, X., Arroyo, D., Porcu, E. (2016) An improved spectral turning-bands algorithm for simulating stationary vector Gaussian random fields. Stochastic Environmental Research and Risk Assessment 30(7): 1863-1873.

[52] Emery X., Lantuéjoul, C. (2006) TBSIM: a computer program for conditional simulation of three-dimensional Gaussian random fields via the turning bands method. Computers & Geosciences 32(10): 1615-1628.

[53] Emery, X., Lantuéjoul, C. (2008) A spectral approach to simulating intrinsic random fields with power and spline generalized covariances. Computational Geosciences 12(1): 121-132.

[54] Emery, X., Peláez, M. (2011) Assessing the accuracy of sequential Gaussian simulation and cosimulation. Computational Geosciences 15(4): 673-689.

[55] Emery, X., Silva, D.A. (2009) Conditional co-simulation of continuous and categorical variables for geostatistical applications. Computers & Geosciences 35(6): 1234-1246.

[56] Freulon, X. (1992) Conditionnement du modèle Gaussien par des inégalités ou des randomisées. Doctoral dissertation, Ecole Nationale Supérieure des Mines de Paris, Fontainebleau.

[57] Freulon, X., de Fouquet, C., Rivoirard, J. (1990) Simulation of the geometry and grades of a uranium deposit using a geological variable. In: Proceedings of the XXII International Symposium on Applications of Computers and Operations Research in the Mineral Industry. Technische Universität Berlin, Berlin, pp. 649-659.

[58] Frikken, P. (2003) Breccia-hosted copper-molybdenum mineralisation at Rio Blanco, Chile. PhD thesis, University of Tasmania, Australia.

[59] Galli, A., Beucher, H., Le Loc'h, G., Doligez, B. (1994) The pros and cons of the truncated Gaussian method. In: Armstrong, M., Dowd, P.A. (eds.) Geostatistical Simulation. Kluwer, Dordrecht, pp. 217-233.

[60] Glacken, I.M., Snowden, D.V. (2001) Mineral resource estimation. In: Edwards, A.C. (ed.) Mineral Resource and Ore Reserve Estimation - The AusIMM Guide to Good Practice. The Australasian Institute of Mining and Metallurgy, Melbourne, pp. 189-198.

[61] Gneiting, T., Kleiber, W., Schlather, M. (2010) Matérn cross-covariance functions for multivariate random fields. Journal of the American Statistical Association 105(491): 1167-1177.

[62] Gómez-Hernández, J.J., Cassiraga, E.F. (1994) Theory and practice of sequential simulation. In: Armstrong, M., Dowd, P.A. (eds.), Geostatistical Simulations, Kluwer Academic Publishers, Dordrecht, pp. 111-124.

[63] Goovaerts, P. (1997) Geostatistics for Natural Resources Evaluation. Oxford University Press, New York.

[64] Goovaerts, P. (2001) Geostatistical modelling of uncertainty in soil science. Geoderma 103: 3-26.

[65] Guardiano, F., Srivastava, M. (1993) Multivariate geostatistics: beyond bivariate moments. In: Soares, A. (ed.) Geostatistics Tróia '92. Kluwer Academic, Dordrecht, pp. 133-144.

[66] Guyon, X. (1995) Random Fields on a Network – Modeling, Statistics and Applications. Springer, New York.

[67] Huang, C.F., Yao, Y.G., Cressie, N., Hsing, T.L. (2009) Multivariate intrinsic random functions for cokriging. Mathematical Geosciences 41(8): 887-904.

[68] Jones, P., Douglas, I., Jewbali, A. (2013) Modeling combined geological and grade uncertainty: application of multiple-point simulation at the Apensu gold deposit, Ghana. Mathematical Geosciences 45(8): 949-965.

[69] Journel, A.G. (1983) Nonparametric estimation of spatial distribution. Mathematical Geology 15(3): 445-468.

[70] Journel, A.G. (1989) Fundamentals of geostatistics in five lessons. Short Course in Geology, vol. 8. American Geophysical Union.

[71] Journel, A.G., Alabert, F.G. (1988) Focusing on spatial connectivity of extreme valued attributes: stochastic indicator models of reservoir heterogeneities, SPE Paper 18324.

[72] Journel, A.G., Alabert, F.G. (1990) New method for reservoir mapping. Journal of Petroleum Technology 42(2): 212-218.

[73] Journel, A.G., Huijbregts, C.J. (1978) Mining Geostatistics. Academic Press, London.

[74] Journel, A.G., Isaaks, E.H. (1984) Conditional indicator simulation: application to a Saskatchewan uranium deposit. Mathematical Geology 16(7): 685-718.

[75] Kay, S.M., Mpodozis, C., Coira, B. (1999) Neogene magmatism, tectonism and mineral deposits of the central Andes. In: Skinner, B.J. (ed.) Geology and ore deposits of the Central Andes. Special Publication No. 7. Society of Economic Geologists, Littleton, pp. 7-59.

[76] Kim, H.M., Mallick, B.K., Holmes, C.C. (2005) Analyzing nonstationary spatial data using piecewise Gaussian processes. Journal of the American Statistical Association 100(470): 653-668.

[77] Kitanidis, P.K. (1983) Statistical estimation of polynomial generalized covariance functions and hydrologic applications. Water Resources Research 19(4): 909-921.

[78] Kitanidis, P.K. (1985) Minimum-variance unbiased quadratic estimation of covariances of regionalized variables. Mathematical Geology 17(2): 195-208.

[79] Kitanidis, P.K. (1999) Generalized covariance functions associated with the Laplace equation and their use in interpolation and inverse problems. Water Resources Research 35 (5): 1361-1367.

[80] Kunsch, H.R., Papritz, A., Bassi, F. (1997) Generalized cross-covariances and their estimation. Mathematical Geology 29(6): 779-799.

[81] Kyriakidis, P.C., Deutsch, C.V., Grant, M. L. (1999) Calculation of the normal scores variogram for truncated Gaussian simulation: theory and FORTRAN code. Computers & Geosciences 25(2): 161-169.

[82] Lantuéjoul, C. (1994) Non-conditional simulation of stationary isotropic multigaussian random functions. In: Armstrong, M., Dowd, P.A. (eds.) Geostatistical Simulations. Kluwer Academic, Dordrecht, pp. 147-177.

[83] Lantuéjoul, C. (2002) Geostatistical simulation, models and algorithms. Springer-Verlag, Berlin, 256 p.

[84] Lantuéjoul, C., Desassis, N. (2012) Simulation of a Gaussian random vector: a propagative version of the Gibbs sampler. In: Ninth International Geostatistics Congress, Oslo.

[85] Larrondo, P., Leuangthong, O., Deutsch, C.V. (2004) Grade estimation in multiple rock types using a linear model of coregionalization for soft boundaries. In: Magri, E., Ortiz, J., Knights, P., Henríquez, F., Vera, M., Barahona, C. (eds.) Proceedings of the 1st international conference on mining innovation. Gecamin Ltd, Santiago, Chile, pp. 187-196.

[86] Le Cointe, P. (2006) Kriging with partial differential equations in hydrogeology. Master's thesis, Université Pierre et Marie Curie, Ecole des Mines de Paris & Ecole Nationale du Génie Rural des Eaux et Forêts, Paris.

[87] Le Loc'h, G., Beucher, H., Galli, A., Doligez, B. (1994) Improvement in the truncated Gaussian method: combining several Gaussian functions. In: Proceedings of the Fourth European Conference on the Mathematics of Oil Recovery ECMOR IV, Roros, Norway, 13 p.

[88] Le Loc'h, G., Galli, A. (1997) Truncated plurigaussian method: theoretical and practical points of view. In: Baafi, E.Y., Schofield, N.A. (eds.), Geostatistics Wollongong'96. Kluwer Academic, Dordrecht, pp. 211-222.

[89] Mackenzie, D.H., Wilson, G.I. (2001) Geological interpretation and geological modeling. In: Edwards, A.C. (ed.) Mineral Resource and Ore Reserve Estimation - The AusIMM Guide to Good Practice. The Australasian Institute of Mining and Metallurgy, Melbourne, pp. 111-118.

[90] Madaniesfahani, N. (2016). Plurigaussian simulation of non-stationary categorical variables and its application to ore body modeling. Ph.D. thesis in Mining Engineering, University of Chile.

[91] Maleki, M., Emery, X. (2015) Joint simulation of grade and rock type in a stratabound copper deposit. Mathematical Geosciences 47: 471-495.

[92] Maleki-Tehrani, M., Asghari, O., Emery, X. (2013) Simulation of mineral grades and classification of mineral resources by using hard and soft conditioning data: application to Sungun porphyry copper deposit. Arabian Journal of Geosciences 6: 3773-3781.

[93] Mantoglou, A. (1987) Digital simulation of multivariate two-and three-dimensional stochastic processes with a spectral turning bands method. Mathematical Geology 19(2): 129-149.

[94] Mantoglou, A., Wilson, J.L. (1982) The turning bands method for simulation of random fields using line generation by a spectral method. Water Resources Research 18: 1379-1394.

[95] Marcotte D (2015) TASC3D: A program to test the admissibility in 3D of non-linear models of coregionalization. Computers & Geosciences 83: 168-175

[96] Mariethoz, G., Caers, J. (2014) Multiple-point geostatistics: stochastic modeling with training images. Wiley-Blackwell, 384 p.

[97] Marshall, R.J., Mardia, K.V. (1985) Minimum norm quadratic estimation of components of spatial covariance. Mathematical Geology 17(5): 517-525.

[98] Matheron, G. (1971) The theory of regionalized variables and its applications. Ecole Nationale Supérieure des Mines de Paris, Fontainebleau, 212 p.

[99] Matheron, G. (1973) The intrinsic random functions and their applications. Advances in Applied Probability 5: 439-468.

[100] Matheron, G. (1975) Compléments sur les modèles isofactoriels. Internal Report, Note Géostatistique 132, Centre de Géostatistique, Ecole Nationale Supérieure des Mines de Paris, Fontainebleau.

[101] Matheron, G. (1989) Estimating and Choosing: an Essay on Probability in Practice. Springer, Berlin, 141 p.

[102] Matheron, G., Beucher, H., De Fouquet, C., Galli, A., Guérillot, D., Ravenne, C. (1987) Conditional simulation of a fluvio-deltaic reservoir. SPE paper 16753, 62nd Annual Technical Conference and Exhibition of the Society of Petroleum Engineers, pp. 591-599.

[103] Mignolet, M.P., Spanos, P.D. (1992) Simulation of homogeneous two-dimensional random fields: Part I – AR and ARMA models. Journal of Applied Mechanics 59(2): 260-269.

[104] Oliveros, V., Trsitá-Aguilera, D., Féraud, G., Morata, D., Aguirre, L., Kojima, S., Ferraris, F. (2008) Time relationships between volcanism–plutonism–alteration–mineralization in Cu-stratabound ore deposits from the Michilla mining district, northern Chile: a 40Ar/39Ar geochronological approach. Mineralium Deposita 43(1): 61-78.

[105] Ortiz, J.M. (2003) Characterization of high order correlation for enhanced indicator simulation. Ph.D. Dissertation, University of Alberta.

[106] Ortiz, J.M., Deutsch, C.V. (2004) Indicator simulation accounting for multiple-point statistics. Mathematical Geology 36(5): 545-565.

[107] Ortiz, J.M., Emery, X. (2006) Geostatistical estimation of mineral resources with soft geological boundaries: a comparative study. Journal of the South African Institute of Mining and Metallurgy 106(8): 577-584.

[108] Pardo-Igúzquiza, E. (1997) GCINFE: a computer program for inference of polynomial generalized covariance functions. Computers & Geosciences 23(2): 163-174.

[109] Pardo-Igúzquiza, E., Chica-Olmo, M. (1993) The Fourier integral method - an efficient spectral method for simulation of random fields. Mathematical Geology 25(2): 177-217.

[110] Ravenne, C., Galli, A., Doligez, B., Beucher, H., Eschard, R. (2002) Quantification of facies relationships via proportion curves. In: Armstrong, M., Bettini, C., Champigny, N., Galli, A., Remacre, A. (eds.) Geostatistics Rio 2000. Kluwer, Dordrecht, pp. 19-40.

[111] Renard, D. (1989) Automatic structure recognition. In: Armstrong, M. (ed.) Geostatistics. Kluwer, Dordrecht, pp. 579-590.

[112] Ripley, B.D. (1987) Stochastic Simulation. Wiley, New York, 256 p.

[113] Rivoirard, J. (1994) Introduction to Disjunctive Kriging and Non-Linear Geostatistics. Oxford University Press, New York.

[114] Roldão, D., Ribeiro, D., Cunha, E., Noronha, R., Madsen, A., Masetti, L. (2012) Combined use of lithological and grade simulations for risk analysis in iron ore, Brazil. In: Abrahamsen, P., Hauge, R., Kolbjørnsen, O. (eds.) Geostatistics Oslo 2012. Springer, Berlin, pp. 423-434.

[115] Rossi, M.E., Deutsch, C.V. (2014) Mineral resource estimation. Springer, Dordrecht

[116] Séguret, S.A. (2013) Analysis and estimation of multi-unit deposits: application to a porphyry copper deposit. Mathematical Geosciences 45(8): 927-947.

[117] Serrano, L., Vargas, R., Stambuk, V., Aguilar, C., Galeb, M., Holmgren, C., Contreras, A., Godoy, S., Vela, I., Skewes, M.A., Stern, C.R. (1996) The late Miocene to early Pliocene Río Blanco-Los Bronces copper deposit, Central Chilean Andes. In: Camus, F., Sillitoe, R.H., Petersen, R. (eds.) Andean copper deposits: new discoveries, mineralization, styles and metallogeny. Special Publication No. 5. Society of Economic Geologists, Littleton, pp. 119-130.

[118] Shinozuka, M. (1971) Simulation of multivariate and multidimensional random processes. The Journal of the Acoustical Society of America, 49(1B): 357-367.

[119] Shinozuka, M., Jan, C.M. (1972) Digital simulation of random processes and its applications. Journal of Sound and Vibrations 25(1): 111-128.

[120] Skewes, M.A., Stern, C.R. (1995) Genesis of the late Miocene to Pliocene copper deposits of central Chile in the context of Andean magmatic and tectonic evolution. International Geology Review 37(10): 893-909.

[121] Skewes, M.A., Stern, C.R. (1996) Late Miocene mineralized breccias in the Andes of central Chile: Sr and Nd isotopic evidence for multiple magmatic sources. In: Camus, F., Sillitoe, R.H., Petersen, R. (eds.) Andean copper deposits: new discoveries, mineralization, styles and metallogeny. Special Publication No. 5. Society of Economic Geologists, Littleton, pp. 119-130.

[122] Spanos, P.D., Mignolet, M.P. (1992) Simulation of homogeneous two-dimensional random fields: Part II – MA and ARMA models. Journal of Applied Mechanics 59(2): 270-277.

[123] Stambuk, V., Aguilar, C., Blondel, J., Galeb, M., Serrano, L., Vargas, R. (1988) Geología del yacimiento Río Blanco. Technical Report. Codelco-Chile, División Andina.

[124] Stein, M.L. (1986) A modification of minimum norm quadratic estimation of a generalized covariance function for use with large data sets. Mathematical Geology 18(7): 625-633.

[125] Stein, M.L. (2001) Local stationarity and simulation of self-affine intrinsic random functions. IEEE Transactions on Information Theory 47(4): 1385-1390.

[126] Stein, M.L. (2002) Fast and exact simulation of fractional Brownian surfaces. Journal of Computational and Graphical Statistics 11(3): 587-599.

[127] Stoyan, D., Kendall, W.S., Mecke, J. (1996) Stochastic Geometry and Its Applications, second ed. Wiley, New York.

[128] Strebelle, S. (2002) Conditional simulation of complex geological structures using multiple-point statistics. Mathematical Geology 34(1): 1-22.

[129] Strebelle, S., Journel, A.G. (2000) Sequential simulation drawing structures from training images. In: Kleingeld, W.J., Krige, D.G. (eds.) Geostats 2000 Cape Town. Geostatistical Association of Southern Africa, Johannesburg.

[130] Suárez Arriaga, M.C., Samaniego, F. (1998) Intrinsic random functions of high order and their application to the modeling of non-stationary geothermal parameters. In: Proceedings of the Twenty-third Workshop on Geothermal Reservoir Engineering, pp. 169–175. Technical report SGP-TR-158, Stanford University, Stanford.

[131] Talebi, H., Asghari, O., Emery, X. (2013) Simulation of the lately injected dykes in an Iranian porphyry copper deposit using the plurigaussian model. Arabian Journal of Geosciences 7: 2771-2780.

[132] Vargas-Guzmán, J.A. (2008) Transitive geostatistics for stepwise modeling across boundaries between rock regions. Mathematical Geosciences 40(8): 861-873.

[133] Vargas, R., Gustafson, L.B., Vukasovic, M., Tidy, E., Skewes, M.A. (1999) Ore breccias in the Río Blanco-Los Bronces copper deposit, Chile. In: Skinner, B.J. (ed.) Geology and ore deposits of the Central Andes. Special Publication No. 7. Society of Economic Geologists, Littleton, pp. 281-297.

[134] Verly, G. (1983) The multigaussian approach and its applications to the estimation of local reserves. Mathematical Geology 15(2): 259-286.

[135] Viseur, S. (1999) Stochastic Boolean simulation of fluvial deposits: a new approach combining accuracy with efficiency. In: Proceedings of the 1999 SPE Annual Technical Conference and Exhibition, Houston. Society of Petroleum Engineers, SPE 56688.

[136] Wackernagel, H. (2003) Multivariate Geostatistics: An Introduction with Applications. Springer-Verlag, Berlin.

[137] Warnaars, F., Holgrem, C., Barassi, S. (1985) Porphyry copper and tourmaline breccias at Los Bronces-Río Blanco, Chile. Economic Geology 80: 1544-1565.

[138] Wilde, B.J., Deutsch, C.V. (2012) Kriging and simulation in presence of stationary domains: developments in boundary modeling. In: Abrahamsen, P., Hauge, R., Kolbjørnsen, O. (eds.) Geostatistics Oslo 2012. Springer, Berlin, pp. 289-300.

[139] Yaglom, A.M. (1987) Correlation Theory of Stationary and Related Random Functions. Springer, New York.

[140] Zimmerman, D.L. (1989) Computationally efficient restricted maximum likelihood estimation of generalized covariance functions. Mathematical Geology 21(7): 655-672.